COUPLING STOKES-DARCY FLOW WITH TRANSPORT ON IRREGULAR GEOMETRIES

by

Pu Song

B.S. in Mathematics, ChongQing University, 2005

M.S. in Mathematics, ChongQing University, 2008

M.S. in Mathematics, Clemson University, 2010

Submitted to the Graduate Faculty of

the Kenneth P. Dietrich School of Arts and Sciences in partial fulfillment

of the requirements for the degree of

Doctor of Philosophy in Mathematics

University of Pittsburgh

2017

UNIVERSITY OF PITTSBURGH

DIETRICH SCHOOL OF ARTS AND SCIENCES

This dissertation was presented

by

Pu Song

It was defended on

August 1, 2017

and approved by

Ivan Yotov, Dietrich School of Arts and Sciences, University of Pittsburgh

William Layton, Dietrich School of Arts and Sciences, University of Pittsburgh

Michael Neilan, Dietrich School of Arts and Sciences, University of Pittsburgh

Paolo Zunino, Department of Mathematics, Polytechnic University of Milan

Dissertation Director: Ivan Yotov, Dietrich School of Arts and Sciences, University of Pittsburgh

COUPLING STOKES-DARCY FLOW WITH TRANSPORT ON IRREGULAR GEOMETRIES

Pu Song, PhD

University of Pittsburgh, 2017

This thesis studies a mathematical model, in which Stokes-Darcy flow system is coupled with a transport equation. The objective is to develop stable and convergent numerical schemes that could be used in environmental applications. Special attention is given to discretization methods which can handle irregular geometry.

First, we will use a multiscale mortar finite element method to discretize coupled Stokes-Darcy flows on irregular domains. Especially, we will utilize a special discretization method called multi-point flux mixed finite element method to handle Darcy flow. This method is accurate for rough grids and rough full tensor coefficients, and reduces to a cell-centered pressure scheme. On quadrilaterals and hexahedra the method can be formulated either on the physical space or on the reference space, leading to a non-symmetric or symmetric scheme, respectively. While Stokes region is discretized by standard inf-sup stable elements. The mortar space can be coarser and it is used to approximate the normal stress on the interface and to impose weakly continuity of normal flux. The interfaces can be curved and matching conditions are imposed via appropriate mappings from physical grids to reference grids with flat interfaces.

Another approach that we use to deal with the flow equations is based on non-overlapping domain decomposition. Domain decomposition enables us to solve the coupled Stokes-Darcy flow problem in parallel by partitioning the computational domain into subdomains, upon which families of coupled local problems of lower complexity are formulated. The coupling of the subdomain problems is removed through an iterative procedure. We investigate the

properties of this method and derive estimates for the condition number of the associated algebraic system.

To discretize the transport equation we develop a local discontinuous Galerkin mortar method. In the method, the subdomain grids need not match and the mortar grid may be much coarser, giving a two-scale method. We weakly impose the boundary condition on the inflow part of the interface and the Dirichlet boundary condition on the elliptic part of the interface via Lagrange multipliers. We develop stability for the concentration and the diffusive flux in the transport equation.

Keywords: Stokes-Darcy flows, mortar finite element, mixed finite element, multiscale finite element, multipoint flux approximation, curved interface,non-overlapping domain decomposition.

TABLE OF CONTENTS

LIST OF TABLES

LIST OF FIGURES

ACKNOWLEDGEMENTS

I would like to express my deep gratitude to Prof. Ivan Yotov for giving me the exciting opportunity to be in his active research group. The confidence he has had in me over these years and his invaluable guidance enabled me to carry out this thesis.

A very special thank to Prof. William Layton for his stimulating and enthusiastic lectures, which gave me an insightful understanding of various topics in numerical analysis.

I would also like to thank Prof. Michael Neilan and Prof. Paolo Zunino for your time to review my thesis and to be my committee members.

Finally, I wish to dedicate this dissertation to my wife Mia. I owe her everything for sacrificing with me these past years as a graduate student. I look forward to our future of infinite possibilities together.

1.0 INTRODUCTION

The coupled Stokes-Darcy model has been thoroughly investigated in recent years due to its broad applications: interaction between surface and subsurface flows, fuel cells, flow in fractured porous media, blood flow in vessels and industrial filtration. The mathematical model is based on the experimentally derived Beavers–Joseph–Saffman interface condition [5, 45] and other continuity conditions of flux and normal stress. In [36, 17], the existence and uniqueness of a weak solution has been proved. Lots of numerical discretizations for this model has been developed in [36, 16, 17, 44, 21, 34, 18, 39, 23, 24, 47].

In this thesis we assume the interaction between surface water and groundwater flows as the physical interpretation of the model. Fresh water is essential to human and other lifeforms. It is estimated that nearly 69 percent of the total fresh water on Earth is frozen in glaciers and permanent ice covers in the Antarctic and the Arctic regions. About 96 percent of the total unfrozen fresh water in the world is groundwater, which resides in the pores of the soil or the rocks. A geologic formation containing water that can be withdrawn at wells or springs is called an aquifer. One serious problem today is contamination of groundwater. Many aquifers have been invaded by pollutants resulting from leaky underground storage tanks, chemical spills and other human activities. Coupling the Stokes-Darcy equations with a transport equation offers an effective tool for predicting the spread of the pollution and assesing the danger to the fresh water resources.

In our model we consider a fluid region as a Stokes Region Ω_s and a saturated porous medium region as a Darcy Region Ω_d (1.0.1). These are separated by an interface Γ_{sd}, through which the fluid can flow in both directions. Both Ω_s and Ω_d are bounded domains with Lipschitz continuous boundaries.The outward unit normal vector exterior to Ω_s or Ω_d is denoted by $\boldsymbol{n}_s$ or $\boldsymbol{n}_d$. We let $\mathbf{u}_s$, p_s, respectively $\mathbf{u}_d$, p_d, be the velocity and pressure in

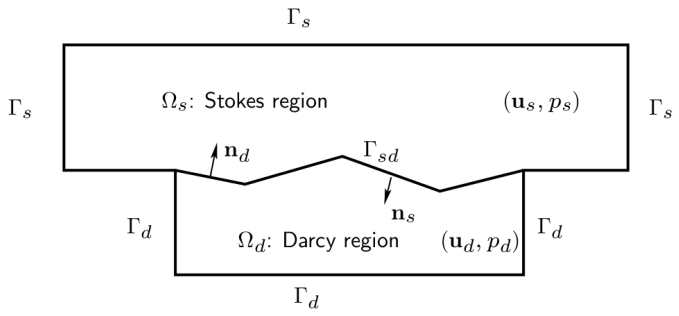

Figure 1.0.1: Stokes-Darcy domain

the Stokes region and the Darcy region respectively.

1.1 FLOW EQUATIONS

1.1.1 Stokes equations

Two important variables in the characterization of fluid motion are the deformation (or strain) rate tensor, which is defined as the symmetric part of the velocity gradient $\mathbf{D}(\mathbf{u}_s) := \frac{1}{2}(\nabla \mathbf{u}_s + (\nabla \mathbf{u}_s)^T)$ and the Cauchy stress tensor $\mathbf{T}$, which represents the forces exerted by the fluid per unit infinitesimal area. For a Newtonian fluid, like water, $\mathbf{T}$ and $\mathbf{D}(\mathbf{u}_s)$ are linearly related. Assuming that the fluid is incompressible,

$$\nabla \cdot \mathbf{u}_s = 0$$

and the stress-strain rate relation, also known as the Stokes law, is

$$\mathbf{T}(\mathbf{u}_s, p_s) := -p_s \mathbf{I} + 2\nu_s \mathbf{D}(\mathbf{u}_s)$$

where ν_s is the fluid viscosity. The resulting Stokes equations are suitable to describe the creeping flow in a surface basin, e.g. lake:

$$
\begin{aligned}
-\nabla \cdot \mathbf{T} \equiv -2\nu_s \nabla \cdot \mathbf{D}(\mathbf{u_s}) + \nabla p_s &= \mathbf{f}_s \quad \text{in } \Omega_s, && (1.1.1)\\
\nabla \cdot \mathbf{u_s} &= 0 \quad \text{in } \Omega_s, && (1.1.2)\\
\mathbf{u_s} &= \mathbf{0} \quad \text{on } \Gamma_s. && (1.1.3)
\end{aligned}
$$

1.1.2 Darcy equations

Darcy's experiments revealed a proportionality between the rate of unidirectional flow and the applied pressure in a uniform porous medium. In three dimensions using modern notation this relationship is expressed by

$$\mathbf{u}_d = -\frac{\mathbf{K}}{\nu_d} \nabla p_d$$

Here $\mathbf{u}_d$ is the seepage velocity, which is the average velocity respective to a representative volume incorporating both solid and fluid material, and $\mathbf{K}$ is a symmetric and positive definite tensor representing the permeability. The permeability tensor can be brought into diagonal form

$$\mathbf{K} = diag\{K_1, K_2, K_3\}$$

by introducing three mutually orthogonal axes called axes of principal directions of anisotropy. It is well known that Darcys law can be obtained by averaging of the equations for incompressible flow through porous medium.

1.1.3 Coupled Stokes-Darcy equations with interface and boundary conditions

In order to couple the flow equations in the free fluid region Ω_s with the equations governing the flow in the porous medium region Ω_d appropriate conditions must be specified on the interface Γ_{sd}. This is a challenging problem from both physical and mathematical point of view. One difficulty stems from the fact that the definitions of the variables differ in the two regions. Also there are no velocity derivatives involved in the Darcy's law while the Stokes

equation is of second order for the velocity. Another question to consider is whether the interface conditions are compatible with the boundary conditions at $\Gamma_{sd} \cap \partial\Omega$.

The first interface condition comes from mass conservation and can be written as follows

$$\mathbf{u}_s \cdot \mathbf{n}_s + \mathbf{u}_d \cdot \mathbf{n}_d = 0 \quad \text{on } \Gamma_{sd}. \tag{1.1.4}$$

Another condition is obtained by balancing the normal forces acting on the interface in each region. The force exerted by the free fluid in Ω_s on the boundary $\partial\Omega_s$ is equal to $-\mathbf{n}\cdot\mathbf{T}$. Since the only force acting on Γ_{sd} from Ω_d is the Darcy pressure p_d, the second interface condition which also means continuity of normal stress on Γ_{sd} is

$$-(\mathbf{T}\mathbf{n}_s)\cdot\mathbf{n}_s \equiv p_s - 2\nu_s(\mathbf{D}(\mathbf{u}_s)\mathbf{n}_s)\cdot\mathbf{n}_s = p_d \quad \text{on } \Gamma_{sd}. \tag{1.1.5}$$

The last interface condition is the well-known Beavers-Joseph-Saffman law [5, 45] for the slip with friction interface condition, where $\alpha > 0$ is an experimentally determined dimensionless constant

$$-(\mathbf{T}\mathbf{n}_s)\cdot\boldsymbol{\tau}_j \equiv -2\nu_s(\mathbf{D}(\mathbf{u}_s)\mathbf{n}_s)\cdot\boldsymbol{\tau}_j = \frac{\nu_s\alpha}{\sqrt{K_j}}\mathbf{u}_s\cdot\boldsymbol{\tau}_j, \quad j = 1, d-1, \quad \text{on} \quad \Gamma_{sd}, \tag{1.1.6}$$

Depending on the particular flow problem in Ω_s there are different choices of possible boundary conditions on Γ_s. To facilitate the notation in the flow problem formulation we will use no slip boundary condition $\mathbf{u}_s = 0$ on Γ_s, but computational results with combinations of Dirichlet (prescribed velocity) and Neumann (prescribed normal and tangential stresses) boundary data will be presented. For the Darcys equation we specify no flow boundary condition $\mathbf{u}_d \cdot \mathbf{n}_d = 0$ on Ω_d, which corresponds to an impermeable rock surrounding the aquifer.

Now the coupled Stokes-Darcy model can be presented as follows: Then the flow equations in Darcy region with no flow boundary condition are:

$$\nu_d\mathbf{K}^{-1}\mathbf{u}_d + \nabla p_d = \mathbf{f}_d \quad \text{in } \Omega_d, \tag{1.1.7}$$

$$\operatorname{div}\mathbf{u}_d = q_d \quad \text{in } \Omega_d, \tag{1.1.8}$$

$$\mathbf{u}_d \cdot \mathbf{n} = 0 \quad \text{on } \Gamma_d. \tag{1.1.9}$$

where q_d denotes an external source or sink term in Ω_d and is assumed to satisfy solvability condition

$$\int_{\Omega_d} q_d \, d\boldsymbol{x} = 0. \tag{1.1.10}$$

1.2 TRANSPORT EUQATION

The transport equation can be considered as a advection-diffusion equation:

$$\phi c_t + \nabla \cdot (c\mathbf{u} - \boldsymbol{D}\nabla c) = \phi s \quad \forall (\mathbf{x}, t) \in \Omega \times (0, T), \tag{1.2.1}$$

where $c(\mathbf{x}, t)$ is the concentration of some chemical component, $0 < \phi_* \leq \phi(\mathbf{x}) \leq \phi^*$ is the porosity of the medium in Ω_2, $\mathbf{D}(\mathbf{x}, t)$ is the diffusion/dispersion tensor assumed to be symmetric and positive definite with smallest and largest eigenvalues D_* and D^*, respectively, $s(\mathbf{x}, t)$ is a source term, and $\mathbf{u}$ is the velocity feild defined by $\mathbf{u}|_{\Omega_s} = \mathbf{u}_s$, and $\mathbf{u}|_{\Omega_d} = \mathbf{u}_d$. The model is completed by the initial condition

$$c(\mathbf{x}, 0) = c^0(\mathbf{x}), \quad \forall \mathbf{x} \in \Omega \tag{1.2.2}$$

and the boundary conditions

$$(c\mathbf{u} + \boldsymbol{z}) \cdot \mathbf{n} = (c_{in}\mathbf{u}) \cdot \mathbf{n} \quad \text{on} \quad \Gamma_{in}, \tag{1.2.3}$$

$$\boldsymbol{z} \cdot \mathbf{n} = 0 \quad \text{on} \quad \Gamma_{out}, \tag{1.2.4}$$

Here, $\Gamma_{in} := \{\mathbf{x} \in \partial\Omega : \mathbf{u} \cdot \mathbf{n} < 0\}$, $\Gamma_{out} := \{\mathbf{x} \in \partial\Omega : \mathbf{u} \cdot \mathbf{n} \geq 0\}$, and $\mathbf{n}$ is the unit outward normal vector to $\partial\Omega$.

1.3 MULTISCALE MORTAR MIXED FINITE ELEMENT METHOD

The use of Mixed Finite Element (MFE) methods is advantageous for its simultaneous high-order approximation of both the primary variable and a second variable of physical interest. Since the 1970's, a robust theory has been developed to produce stable schemes for subsurface ow, as well as applications in surface flow, electromagnetism, and elasticity. Moreover these methods provide physical fidelity via the element-wise conservation of mass, a property that standard Galerkin finite element methods do not possess. However, difficulties arise in porous media flow applications, where the domain is quite large and the permeability tensor varies on a fine scale. Resolving the solution on the fine scale is often computationally infeasible, necessitating the use of multiscale approximations.

In this thesis we use a new multiscale mortar mixed method that uses the multipoint flux mixed finite element (MFMFE) [57, 30] for Darcy subdomain discretization. The MFMFE method was motivated by the multipoint flux approximation (MPFA) method.The latter method was originally developed as a non-variational finite volume method. It is locally mass conservative, accurate for rough grids and coefficients, and reduces to a cell-centered system for the pressures. In that sense it combines the advantages of MFE and several MFE-related methods.

MFE methods are commonly used for flow in porous media, as they provide accurate and locally mass conservative velocities and handle well rough coefficients. However, the resulting algebraic system is of saddle point type and involves both the pressure and the velocity. Various modifications have been developed to alleviate this problem, including the hybrid MFE method that reduces to a symmetric positive definite face-centered pressure system, as well as more efficient cell-centered formulations [57, 4, 3] based on numerical quadrature for the velocity mass matrix in the lowest order Raviart-Thomas [31] (RT_0) case.

The MPFA method handles accurately very general grids and discontinuous full tensor coefficients and at the same time reduces to a positive definite cell-centered algebraic system for the pressure. The analysis of the MPFA method has been done by formulating it as a MFE method with a special quadrature, see [57] and [30] for the symmetric version on $O(h^2)$-perturbations of parallelograms and parallelepipeds, respectively, as well as [56] for

the non-symmetric version on general quadrilaterals and hexahedra, respectively. A non-symmetric MFD method on polyhedral elements that reduces to a cell-centered pressure system using a MPFA-type velocity elimination is developed and analyzed in [37].

1.4 THESIS OUTLINE

The rest of this thesis is organized as follows: In Chapter 2, we will apply multi-scale mortar multipoint flux mixed finite element method into Stokes-Darcy Model and show the stability and error analysis for this method. Implementation on curved interfaces and simulation with irregular geometry grids will also be presented. In Chapter 3, we will present a non-overlapping domain decomposition method for Stokes-Darcy model with curved interfaces. Condition number analysis and numerical results will also be presented. In Chapter 4, we will formulate a Local Discontinous Galerkin (LDG) mortar method for transport equation coupled Stokes-Darcy flow. Stability analysis and interesting numerical simulations will also be presented.

2.0 MULTISCALE MORTAR FINITE ELEMENT METHODS FOR COUPLED STOKES-DARCY FLOWS WITH CURVED INTERFACES

Coupled Stokes-Darcy model has been thoroughly investigated in recent years due to its broad applications: interaction between surface and subsurface flows, industrial contaminants filtration, fuel cells and vascular flows. The mathematical model is based on the experimentally derived Beavers–Joseph–Saffman interface condition [5, 45] and other continuity conditions of flux and normal stresses. In [36, 17], the existence and uniqueness of a weak solution has been proved. Lots of numerical discretizations for this model hase been developed in [36, 17, 44, 21, 34, 18, 39, 23, 24, 47].

In this thesis, we extend the method in [27] to handle irregular geometries where both boundaries and interfaces are curved. We utilize multipoint flux mixed finite element (MFMFE) [55, 29] to discretize Darcy subdomains and conforming Stokes elements for Stokes subdomains on a fine scale. Both type subdomain grids are not necessarily matching on their interfaces. Mortar finite element space on a coarse scale is used to impose weakly continuity conditions between different type interfaces. In [36, 44, 21, 8], the mortar finite element space has different physical meanings in different subdomains: it represents the pressure for Darcy flow, respectively, normal stress for the Stokes flow. Mortar mixed finite element method for the single Darcy region has been studied in [58, 1, 42, 2] and for the single Stokes region has been investigated in [6, 7]. The former allows for mortar grids to be different from the traces of subdomain grids with appropriate assumption on the mortar finite element space.

The MFMFE method was motivated by the multipoint flux approxmation (MPFA) method. It handles accurately irregular girds and discontinuous full tensor coefficients and reduces to a positive definite cell-centered algebraic system for the pressure with special finite element spaces and numerical quadrature rule.

Since we use a multi-domain discretization, then we should consider three type interfaces condition: On the Stokes-Stokes interfaces, the continuity of the whole velocity are weakly imposed by the mortar functions which represents the entire stress vector. On the Stokes-Darcy and Darcy-Darcy interfaces, we imposed weak continuity condition for the normal velocity by the mortar funcions which represents pressure or lagrange multiplier in the Darcy region and normal stress in the Stokes region. The mortar spaces are assumed to satisfy suitable inf-sup conditions, allowing for very general subdomain and mortar grid configurations.

To implement our method on the curved interfaces with non-mathcing grids, we employ two type transformations based on three types interfaces conditions to map subdomain and mortar grids into reference grids with flat interfaces. On Stokes-Darcy and Darcy-Darcy interfaces, we employ Piola transformation which preserves the normal component of velocity while on the Stokes-Stokes interfaces, the standard change of variables is used for the mapping.

The error analysis relies on the construction of a bounded global interpolant in the space of weakly continuous velocities that also preserves the velocity divergence in the usual discrete sense and RT_0 projections of the BDM_1 or BDDF_1 space. This is done in two steps, starting from suitable local interpolants and correcting them to satisfy the interface matching conditions. The correction step requires the existence of bounded mortar interpolants. This is a very general condition that can be easily satisfied in practice. We present two examples in $2-D$ and one example in $3-D$ that satisfy this solvability condition. Our error analysis shows that the global velocity and pressure errors are bounded by the fine scale local approximation error and the coarse scale non-conforming error. Since the polynomial degrees on subdomains and interfaces may differ, one can choose higher order mortar polynomials to balance the fine scale and the coarse scale error terms and obtain fine scale asymptotic convergence. The dependence of the stability and convergence constants on the subdomain size is explicitly determined. In particular, the stability and fine scale convergence constants do not depend on the size of subdomains, while the coarse scale non-conforming error constants deteriorate when the subdomain size goes to zero. This is to be expected, as the relative effect of the non-conforming error becomes more significant in such regime. However, this dependence

can be made negligible by choosing higher order mortar polynomials.

Throughout this paper, we use for simplicity $X \lesssim (\gtrsim) Y$ to denote that there exists a constant C, independent of mesh sizes h and H, such that $X \leq (\geq) CY$. The notation $X \eqsim Y$ means that both $X \lesssim Y$ and $X \gtrsim Y$ hold.

2.1 NOTATION AND PRELIMINARIES

Let Ω be a bounded, connected Lipschitz domain of $\mathbb{R}^n$, $n = 2, 3$, with boundary $\partial\Omega$ and exterior unit normal vector $\boldsymbol{n}$, and let Γ be a part of $\partial\Omega$ with positive $n-1$ measure: $|\Gamma| > 0$. We do not assume that Γ is connected, but if it is not connected, we assume that it has a finite number of connected components. In the case when $n = 3$, we also assume that Γ is itself Lipschitz. Let

$$H^1_{0,\Gamma}(\Omega) = \{v \in H^1(\Omega)\,;\, v|_\Gamma = 0\}.$$

Poincaré's inequality in $H^1_{0,\Gamma}(\Omega)$ reads: There exists a constant $\mathcal{P}_\Gamma$ depending only on Ω and Γ such that

$$\forall v \in H^1_{0,\Gamma}(\Omega)\,,\ \|v\|_{L^2(\Omega)} \leq \mathcal{P}_\Gamma |v|_{H^1(\Omega)}. \tag{2.1.1}$$

The norms and spaces are made precise later on. The formula (2.1.1) is a particular case of a more general result (cf. [40, 9]):

Proposition 2.1.1. *Let Ω be a bounded, connected Lipschitz domain of $\mathbb{R}^n$ and let Φ be a seminorm on $H^1(\Omega)$ satisfying:*

1) *there exists a constant P_1 such that*

$$\forall v \in H^1(\Omega)\,,\ \Phi(v) \leq P_1 \|v\|_{H^1(\Omega)}, \tag{2.1.2}$$

2) *the condition $\Phi(c) = 0$ for a constant function c holds if and only if $c = 0$.*

Then there exists a constant P_2 depending only on Ω, such that

$$\forall v \in H^1(\Omega)\,,\ \|v\|_{L^2(\Omega)} \leq P_2\big(|v|^2_{H^1(\Omega)} + \Phi(v)^2\big)^{1/2}. \tag{2.1.3}$$

We recall Korn's first inequality: There exists a constant C_1 depending only on Ω and Γ such that

$$\forall \boldsymbol{v} \in H^1_{0,\Gamma}(\Omega)^n\,,\ |\boldsymbol{v}|_{H^1(\Omega)} \leq C_1 \|\boldsymbol{D}(\boldsymbol{v})\|_{L^2(\Omega)}, \tag{2.1.4}$$

where $\boldsymbol{D}(\boldsymbol{v})$ is the deformation rate tensor, also called the symmetric gradient tensor:

$$\boldsymbol{D}(\boldsymbol{v}) = \frac{1}{2}\big(\nabla\, \boldsymbol{v} + \nabla\, \boldsymbol{v}^T\big).$$

We shall use the Hilbert space

$$H(\mathrm{div};\Omega) = \left\{\boldsymbol{v} \in L^2(\Omega)^n\,;\ \mathrm{div}\, \boldsymbol{v} \in L^2(\Omega)\right\},$$

equipped with the graph norm

$$\|\boldsymbol{v}\|_{H(\mathrm{div};\Omega)} = \Big(\|\boldsymbol{v}\|^2_{L^2(\Omega)} + \|\mathrm{div}\, \boldsymbol{v}\|^2_{L^2(\Omega)}\Big)^{1/2}.$$

The normal trace $\boldsymbol{v}\cdot\boldsymbol{n}$ of a function $\boldsymbol{v}$ of $H(\mathrm{div},\Omega)$ on $\partial\Omega$ belongs to $H^{-1/2}(\partial\Omega)$ (cf. [25]). The same result holds when Γ is a part of $\partial\Omega$ and is a closed surface. But if Γ is not a closed surface, then $\boldsymbol{v}\cdot\boldsymbol{n}$ belongs to the dual of $H^{1/2}_{00}(\Gamma)$. When $\boldsymbol{v}\cdot\boldsymbol{n} = 0$ on $\partial\Omega$, we use the space

$$H_0(\mathrm{div};\Omega) = \{\boldsymbol{v} \in H(\mathrm{div};\Omega)\,;\ \boldsymbol{v}\cdot\boldsymbol{n} = 0 \text{ on } \partial\Omega\}\,.$$

2.2 NON-OVERLAPPING DOMAIN DECOMPOSITION WEAK FORMULATION

Let Ω_s, respectively Ω_d, be decomposed into M_s, respectively M_d, *non-overlapping*, open Lipschitz subdomains:

$$\overline{\Omega}_s = \cup_{i=1}^{M_s} \overline{\Omega}_{s,i} \ , \ \overline{\Omega}_d = \cup_{i=1}^{M_d} \overline{\Omega}_{d,i}.$$

Set $M = M_d + M_s$; according to convenience we can also number the subdomains with a single index i, $1 \leq i \leq M$, the Darcy subdomains running from $M_s + 1$ to M. Let $\boldsymbol{n}_i$ denote the outward unit normal vector on $\partial\Omega_i$. For $1 \leq i \leq M$, let the boundary interfaces be denoted by Γ_i, with possibly zero measure:

$$\Gamma_i = \partial\Omega_i \cap \partial\Omega,$$

and for $1 \leq i < j \leq M$, let the interfaces between subdomains be denoted by Γ_{ij}, again with possibly zero measure:

$$\Gamma_{ij} = \partial\Omega_i \cap \partial\Omega_j.$$

In addition to Γ_{sd}, let Γ_{dd}, respectively Γ_{ss}, denote the set of interfaces between subdomains of Ω_d, respectively Ω_s. Then, assuming that the solution $(\boldsymbol{u}, p)$ of (1.1.7)–(1.1.6) is slightly smoother, we can obtain an equivalent formulation by writing individually (1.1.7)–(1.1.6) in each subdomain Ω_i, $1 \leq i \leq M$, and complementing these systems with the following interface conditions

$$[\boldsymbol{u}_d \cdot \boldsymbol{n}] = 0 \quad , \quad [p_d] = 0 \quad \text{on } \Gamma_{dd}, \tag{2.2.1}$$

$$[\boldsymbol{u}_s] = \boldsymbol{0} \quad , \quad [\boldsymbol{\sigma}(\boldsymbol{u}_s, p_s)\boldsymbol{n}] = \boldsymbol{0} \quad \text{on } \Gamma_{ss}, \tag{2.2.2}$$

where the jumps on an interface Γ_{ij}, $1 \leq i < j \leq M$, are defined as

$$[\boldsymbol{v} \cdot \boldsymbol{n}] = \boldsymbol{v}_i \cdot \boldsymbol{n}_i + \boldsymbol{v}_j \cdot \boldsymbol{n}_j, \quad [\boldsymbol{\sigma}\boldsymbol{n}] = \boldsymbol{\sigma}_i\boldsymbol{n}_i + \boldsymbol{\sigma}_j\boldsymbol{n}_j, \quad [v] = (v_i - v_j)|_{\Gamma_{ij}},$$

using the notation $v_i = v|_{\Omega_i}$. The smoothness requirement on the solution is meant to ensure that the jumps $[\boldsymbol{u}_d \cdot \boldsymbol{n}]$, respectively $[\boldsymbol{\sigma}(\boldsymbol{u}_s, p_s)\boldsymbol{n}]$, are well-defined on each interface of Γ_{dd}, respectively Γ_{ss}.

Finally, let us prescribe weakly the interface conditions (2.2.1), (3.1.1), and (1.1.4) by means of Lagrange multipliers, usually called *mortars*. For this, it is convenient to attribute a unit normal vector $\boldsymbol{n}_{ij}$ to each interface Γ_{ij} of positive measure, directed from Ω_i to Ω_j (recall that $i<j$). The basic velocity spaces are:

$$\begin{aligned} X_d = \{&\boldsymbol{v}\in L^2(\Omega_d)^n\,;\,\boldsymbol{v}_{d,i}:=\boldsymbol{v}|_{\Omega_{d,i}}\in H(\mathrm{div};\Omega_{d,i}),1\le i\le M_d,\\ &\boldsymbol{v}\cdot\boldsymbol{n}_{ij}\in H^{-1/2}(\Gamma_{ij}),\Gamma_{ij}\in\Gamma_{dd}\cup\Gamma_{sd},\boldsymbol{v}\cdot\boldsymbol{n}=0\text{ on }\Gamma_d\},\\ X_s = \{&\boldsymbol{v}\in L^2(\Omega_s)^n\,;\,\boldsymbol{v}_{s,i}:=\boldsymbol{v}|_{\Omega_{s,i}}\in H^1(\Omega_{s,i})^n,1\le i\le M_s,\boldsymbol{v}=\boldsymbol{0}\text{ on }\Gamma_s\}, \end{aligned} \tag{2.2.3}$$

and the mortar spaces are:

$$\begin{aligned} \forall\Gamma_{ij}\in\Gamma_{ss}\,,\ \Lambda_{ij}&=\big(H^{-1/2}(\Gamma_{ij})\big)^n,\\ \forall\Gamma_{ij}\in\Gamma_{sd}\cup\Gamma_{dd}\,,\ \Lambda_{ij}&=H^{1/2}(\Gamma_{ij}). \end{aligned} \tag{2.2.4}$$

Then we define the gobal velocity space by

$$X=\{\boldsymbol{v}\in L^2(\Omega)^n\,;\,\boldsymbol{v}_d:=\boldsymbol{v}|_{\Omega_d}\in X_d,\boldsymbol{v}_s:=\boldsymbol{v}|_{\Omega_s}\in X_s\}, \tag{2.2.5}$$

we keep $W=L^2_0(\Omega)$ for the pressure, and we define the mortar spaces

$$\begin{aligned} \Lambda_s&=\{\boldsymbol{\lambda}\in\big(\mathcal{D}'(\Gamma_{ss})\big)^n\,;\,\boldsymbol{\lambda}|_{\Gamma_{ij}}\in\big(H^{-1/2}(\Gamma_{ij})\big)^n\text{ for all }\Gamma_{ij}\in\Gamma_{ss}\},\\ \Lambda_{sd}&=\{\lambda\in L^2(\Gamma_{sd})\,;\,\lambda|_{\Gamma_{ij}}\in H^{1/2}(\Gamma_{ij})\text{ for all }\Gamma_{ij}\in\Gamma_{sd}\},\\ \Lambda_d&=\{\lambda\in L^2(\Gamma_{dd})\,;\,\lambda|_{\Gamma_{ij}}\in H^{1/2}(\Gamma_{ij})\text{ for all }\Gamma_{ij}\in\Gamma_{dd}\}. \end{aligned} \tag{2.2.6}$$

We equip these spaces with broken norms:

$$|||\boldsymbol{v}|||_{X_d}=\Big(\sum_{i=1}^{M_d}\|\boldsymbol{v}\|^2_{H(\mathrm{div};\Omega_{d,i})}\Big)^{1/2},\ |||\boldsymbol{v}|||_{X_s}=\Big(\sum_{i=1}^{M_s}\|\boldsymbol{v}\|^2_{H^1(\Omega_{s,i})}\Big)^{1/2},\ |||\boldsymbol{v}|||_{X}=\Big(|||\boldsymbol{v}|||^2_{X_d}+|||\boldsymbol{v}|||^2_{X_s}\Big)^{1/2},$$

$$|||\boldsymbol{\lambda}|||_{\Lambda_s}=\Big(\sum_{\Gamma_{ij}\in\Gamma_{ss}}\|\boldsymbol{\lambda}\|^2_{H^{-1/2}(\Gamma_{ij})}\Big)^{1/2},\ |||\lambda|||_{\Lambda_{sd}}=\Big(\sum_{\Gamma_{ij}\in\Gamma_{sd}}\|\lambda\|^2_{H^{1/2}(\Gamma_{ij})}\Big)^{1/2},$$

$$|||\lambda|||_{\Lambda_d}=\Big(\sum_{\Gamma_{ij}\in\Gamma_{dd}}\|\lambda\|^2_{H^{1/2}(\Gamma_{ij})}\Big)^{1/2}.$$

Note that in most geometrical situations, X_d (and hence X) is not complete for the above norm, but none of the subsequent proofs require its completeness.

The matching condition between subdomains is weakly enforced through the following bilinear forms:

$$\begin{aligned}
\forall \boldsymbol{v} \in X_s, \forall \boldsymbol{\mu} \in \Lambda_s \,,\, b_s(\boldsymbol{v}, \boldsymbol{\mu}) &= \sum_{\Gamma_{ij} \in \Gamma_{ss}} \langle [\boldsymbol{v}], \boldsymbol{\mu} \rangle_{\Gamma_{ij}}, \\
\forall \boldsymbol{v} \in X_d, \forall \mu \in \Lambda_d \,,\, b_d(\boldsymbol{v}, \mu) &= \sum_{\Gamma_{ij} \in \Gamma_{dd}} \langle [\boldsymbol{v} \cdot \boldsymbol{n}], \mu \rangle_{\Gamma_{ij}}, \\
\forall \boldsymbol{v} \in X, \forall \mu \in \Lambda_{sd} \,,\, b_{sd}(\boldsymbol{v}, \mu) &= \sum_{\Gamma_{ij} \in \Gamma_{sd}} \langle [\boldsymbol{v} \cdot \boldsymbol{n}], \mu \rangle_{\Gamma_{ij}}.
\end{aligned} \tag{2.2.7}$$

For the velocity and pressure in the Darcy and Stokes regions, we use the following bilinear forms:

$$\begin{aligned}
\forall (\boldsymbol{u}, \boldsymbol{v}) \in X_s \times X_s \,,\, a_{s,i}(\boldsymbol{u}, \boldsymbol{v}) &= 2\,\nu_s \int_{\Omega_{s,i}} \boldsymbol{D}(\boldsymbol{u}_{s,i}) : \boldsymbol{D}(\boldsymbol{v}_{s,i}) \\
&\quad + \sum_{l=1}^{n-1} \int_{\partial\Omega_{s,i} \cap \Gamma_{sd}} \frac{\nu_s \alpha}{\sqrt{K_l}} (\boldsymbol{u}_s \cdot \boldsymbol{\tau}_l)(\boldsymbol{v}_s \cdot \boldsymbol{\tau}_l) \;,\; 1 \le i \le M_s, \\
\forall (\boldsymbol{u}, \boldsymbol{v}) \in X_d \times X_d \,,\, a_{d,i}(\boldsymbol{u}, \boldsymbol{v}) &= \nu_d \int_{\Omega_{d,i}} \boldsymbol{K}^{-1} \boldsymbol{u}_{d,i} \cdot \boldsymbol{v}_{d,i} \;,\; 1 \le i \le M_d, \\
\forall \boldsymbol{v} \in X, \forall w \in L^2(\Omega) \,,\, b_i(\boldsymbol{v}, w) &= -\int_{\Omega_i} w \mathrm{div}\, \boldsymbol{v}_i \;,\; 1 \le i \le M.
\end{aligned} \tag{2.2.8}$$

Then we set

$$\forall (\boldsymbol{u}, \boldsymbol{v}) \in X \times X \,,\, a(\boldsymbol{u}, \boldsymbol{v}) = \sum_{i=1}^{M_s} a_{s,i}(\boldsymbol{u}, \boldsymbol{v}) + \sum_{i=1}^{M_d} a_{d,i}(\boldsymbol{u}, \boldsymbol{v}),$$

$$\forall (\boldsymbol{v}, w) \in X \times L^2(\Omega) \,,\, b(\boldsymbol{v}, w) = \sum_{i=1}^{M} b_i(\boldsymbol{v}, w).$$

The second variational formulation reads: Find $(\boldsymbol{u}, p, \lambda_{sd}, \lambda_d, \boldsymbol{\lambda}_s) \in X \times W \times \Lambda_{sd} \times \Lambda_d \times \Lambda_s$ such that

$$\begin{aligned}
\forall \boldsymbol{v} \in X \,,\, a(\boldsymbol{u}, \boldsymbol{v}) + b(\boldsymbol{v}, p) + b_{sd}(\boldsymbol{v}, \lambda_{sd}) + b_d(\boldsymbol{v}, \lambda_d) + b_s(\boldsymbol{v}, \boldsymbol{\lambda}_s) &= \int_\Omega \boldsymbol{f} \cdot \boldsymbol{v}, \\
\forall w \in W \,,\, b(\boldsymbol{u}, w) &= -\int_{\Omega_d} w\, q_d, \\
\forall \mu \in \Lambda_{sd} \,,\, b_{sd}(\boldsymbol{u}, \mu) &= 0, \\
\forall \mu \in \Lambda_d \,,\, b_d(\boldsymbol{u}, \mu) &= 0, \\
\forall \boldsymbol{\mu} \in \Lambda_s \,,\, b_s(\boldsymbol{u}, \boldsymbol{\mu}) &= 0.
\end{aligned} \tag{2.2.9}$$

It remains to prove that (2.2.9) is equivalent to (1.1.7)–(1.1.6) when the solution is sufficiently smooth. Since we know from Theorem 2.1 in [27] that (1.1.7)–(1.1.6) has a unique solution, equivalence will also establish that (2.2.9) is uniquely solvable.

Theorem 2.2.1 ([27], Theorem 2.2)**.** *Assume that the solution* $(\boldsymbol{u}, p)$ *of* (1.1.7)–(1.1.6) *satisfies*

$$\forall \Gamma_{ij} \in \Gamma_{dd} \cup \Gamma_{sd}\,,\ (\boldsymbol{u}_d \cdot \boldsymbol{n}_d)|_{\Gamma_{ij}} \in H^{-1/2}(\Gamma_{ij})\ ,\ \forall \Gamma_{ij} \in \Gamma_{ss}\,,\ (\boldsymbol{\sigma}(\boldsymbol{u}_s, p_s)\boldsymbol{n}_s)|_{\Gamma_{ij}} \in H^{-1/2}(\Gamma_{ij})^n.$$

Then (2.2.9) *is equivalent to* (1.1.7)–(1.1.6)*.*

Remark 2.2.1. *From above theorem, we can easily get the well posedness of* (2.2.9)*, since the exsitence and uniqueness of the solution to* (1.1.7)–(1.1.6) *has been proposed in [27]*

2.3 FINITE ELEMENT DISCRETIZATION

In this section, we will discuss finite element discretization for both Stokes and Darcy regions. In Stokes region, we used standard conforming finite element while in Darcy region, we employ a multipoint flux mixed finite element method to handle irregular geometries which is base on ased on the lowest order BDM_1 or BDDF_1 elements with a quadrature rule, which allows for local velocity elimination and reduction to a cell-centered scheme for the pressure. The method is presented for simplices and general quadrilaterals and hexahedra. Thus, let us first introduce this method for Darcy flow.

2.3.1 Finite element mappings in Darcy flow

Let $\mathcal{T}_{d,i}^h$ be a conforming, shape-regular, quasi-uniform partition of $\Omega_{d,i}$, $1 \le i \le M_d$. Then we denote $\mathcal{T}_d^h = \cup_{i=1}^{M_d} \mathcal{T}_{d,i}^h$ to be the partition of the whole Darcy domain. The elements considered are two and three dimensional simplexes, convex quadrilaterals in two dimensions, and hexahedra in three dimensions. The hexahedra can have non-planar faces. For any element $E \in \mathcal{T}_{d,i}^h$, there exists a bijection mapping $F_E : \hat{E} \to E$, where $\hat{E}$ is a reference element. Denote the Jacobian matrix by DF_E and let $J_E = \det(DF_E)$ where we assume that

$\text{sign}(J_E) > 0$. Denote the inverse mapping by F_E^{-1}, its Jacobian matrix by DF_E^{-1}, and let $J_{F_E^{-1}} = \det(DF_E^{-1})$. We have that

$$DF_E^{-1}(x) = (DF_E)^{-1}(\hat{x}), \quad J_{F_E^{-1}}(x) = \frac{1}{J_E(\hat{x})}.$$

In the case of convex hexahedra, $\hat{E}$ is the unit cube with vertices $\hat{\mathbf{r}}_1 = (0,0,0)^T$, $\hat{\mathbf{r}}_2 = (1,0,0)^T$, $\hat{\mathbf{r}}_3 = (1,1,0)^T$, $\hat{\mathbf{r}}_4 = (0,1,0)^T$, $\hat{\mathbf{r}}_5 = (0,0,1)^T$, $\hat{\mathbf{r}}_6 = (1,0,1)^T$, $\hat{\mathbf{r}}_7 = (1,1,1)^T$, and $\hat{\mathbf{r}}_8 = (0,1,1)^T$. Denote by $\mathbf{r}_i = (x_i, y_i, z_i)^T, i = 1, \ldots, 8$, the eight corresponding vertices of element E as shown in Figure 1 in [54]. We note that the element can have non-planar faces. The outward unit normal vectors to the faces of E and $\hat{E}$ are denoted by $\boldsymbol{n}_i$ and $\hat{\boldsymbol{n}}_i$, $i = 1, \ldots, 6$, respectively. In this case F_E is a trilinear mapping given by

$$\begin{aligned} F_E(\hat{\mathbf{r}}) &= \mathbf{r}_1(1-\hat{x})(1-\hat{y})(1-\hat{z}) + \mathbf{r}_2\hat{x}(1-\hat{y})(1-\hat{z}) + \mathbf{r}_3\hat{x}\hat{y}(1-\hat{z}) + \mathbf{r}_4(1-\hat{x})\hat{y}(1-\hat{z}) \\ &\quad + \mathbf{r}_5(1-\hat{x})(1-\hat{y})\hat{z} + \mathbf{r}_6\hat{x}(1-\hat{y})\hat{z} + \mathbf{r}_7\hat{x}\hat{y}\hat{z} + \mathbf{r}_8(1-\hat{x})\hat{y}\hat{z} \\ &= \mathbf{r}_1 + \mathbf{r}_{21}\hat{x} + \mathbf{r}_{41}\hat{y} + \mathbf{r}_{51}\hat{z} + (\mathbf{r}_{34} - \mathbf{r}_{21})\hat{x}\hat{y} + (\mathbf{r}_{65} - \mathbf{r}_{21})\hat{x}\hat{z} + (\mathbf{r}_{85} - \mathbf{r}_{41})\hat{y}\hat{z} \\ &\quad + (\mathbf{r}_{21} - \mathbf{r}_{34} - \mathbf{r}_{65} + \mathbf{r}_{78})\hat{x}\hat{y}\hat{z}, \end{aligned} \tag{2.3.1}$$

where $\mathbf{r}_{ij} = \mathbf{r}_i - \mathbf{r}_j$. It is easy to see that each component of DF_E is a bilinear function of two space variables:

$$\begin{aligned} DF_E(\hat{\mathbf{r}}) = [&\mathbf{r}_{21} + (\mathbf{r}_{34} - \mathbf{r}_{21})\hat{y} + (\mathbf{r}_{65} - \mathbf{r}_{21})\hat{z} + (\mathbf{r}_{21} - \mathbf{r}_{34} - \mathbf{r}_{65} + \mathbf{r}_{78})\hat{y}\hat{z}, \\ &\mathbf{r}_{41} + (\mathbf{r}_{34} - \mathbf{r}_{21})\hat{x} + (\mathbf{r}_{85} - \mathbf{r}_{41})\hat{z} + (\mathbf{r}_{21} - \mathbf{r}_{34} - \mathbf{r}_{65} + \mathbf{r}_{78})\hat{x}\hat{z}, \\ &\mathbf{r}_{51} + (\mathbf{r}_{65} - \mathbf{r}_{21})\hat{x} + (\mathbf{r}_{85} - \mathbf{r}_{41})\hat{y} + (\mathbf{r}_{21} - \mathbf{r}_{34} - \mathbf{r}_{65} + \mathbf{r}_{78})\hat{x}\hat{y}]. \end{aligned} \tag{2.3.2}$$

In the case of tetrahedra, $\hat{E}$ is the reference tetrahedron with vertices $\hat{\mathbf{r}}_1 = (0,0,0)^T$, $\hat{\mathbf{r}}_2 = (1,0,0)^T$, $\hat{\mathbf{r}}_3 = (0,1,0)^T$, and $\hat{\mathbf{r}}_4 = (0,0,1)^T$. Let $\mathbf{r}_i, i = 1, \ldots, 4$, be the corresponding vertices of E. The linear mapping for tetrahedra has the form

$$F_E(\hat{\mathbf{r}}) = \mathbf{r}_1(1 - \hat{x} - \hat{y} - \hat{z}) + \mathbf{r}_2\hat{x} + \mathbf{r}_3\hat{y} + \mathbf{r}_4\hat{z} \tag{2.3.3}$$

with respective Jacobian matrix and its determinant

$$DF_E = [\mathbf{r}_{21}, \mathbf{r}_{31}, \mathbf{r}_{41}] \quad \text{and} \quad J_E = 2|E|, \tag{2.3.4}$$

where $|E|$ is the area of element E.

The mappings in the cases of quadrilaterals and triangles are described similarly to the cases of hexahedra and tetrahedra, respectively. Note that in the case of simplicial elements the mapping is affine and the Jacobian matrix and its determinant are constants. This is not the case for quadrilaterals and hexahedra.

Using the above mapping definitions and the classical formula $\nabla\phi = DF_E^{-T}\hat{\nabla}\hat{\phi}$, for $\phi(\mathbf{r}) = \hat{\phi}(\hat{\mathbf{r}})$, it is easy to see that for any face or edge $e_i \subset E$,

$$\boldsymbol{n}_i = \frac{DF_E^{-T}\hat{\boldsymbol{n}}_i}{|DF_E^{-T}\hat{\boldsymbol{n}}_i|}. \tag{2.3.5}$$

Also, the shape regularity and quasi-uniformity of the grids imply that for all elements $E \in \mathcal{T}_d^h$,

$$\|DF_E\|_{0,\infty,\hat{E}} \lesssim h, \quad \|J_E\|_{0,\infty,\hat{E}} \eqsim h^d, \quad \|DF_E^{-1}\|_{0,\infty,E} \lesssim h^{-1}, \quad \|J_{F_E^{-1}}\|_{0,\infty,\hat{E}} \eqsim h^{-d}. \tag{2.3.6}$$

2.3.2 Mixed finite element spaces in Darcy flow

We introduce four finite element spaces with respect to the four types of elements considered in this paper. Let $\hat{\boldsymbol{X}}_d(\hat{E})$ and $\hat{W}_d(\hat{E})$ denote the finite element spaces on the reference element $\hat{E}$.

For simplicial elements, we employ BDM_1 [19] on triangles and BDDF_1 [20] on tetrahedra:

$$\hat{\boldsymbol{X}}_d(\hat{E}) = (P_1(\hat{E}))^d, \quad \hat{W}_d(\hat{E}) = P_0(\hat{E}), \tag{2.3.7}$$

where P_k denotes the space of polynomials of degree $\leq k$.

On the unit square, we employ BDM_1 [19]:

$$\hat{\boldsymbol{X}}_d(\hat{E}) = (P_1(\hat{E}))^2 + r\ \mathrm{curl}(\hat{x}^2\hat{y}) + s\ \mathrm{curl}(\hat{x}\hat{y}^2), \quad \hat{W}_d(\hat{E}) = P_0(\hat{E}), \tag{2.3.8}$$

where r and s are real constants.

On the unit cube, we employ the enhanced BDDF_1 space [29]:

$$\begin{aligned}\hat{\boldsymbol{X}}_d(\hat{E}) = \mathrm{BDDF}_1(\hat{E}) &+ r_2\mathrm{curl}(0,0,\hat{x}^2\hat{z})^T + r_3\mathrm{curl}(0,0,\hat{x}^2\hat{y}\hat{z})^T + s_2\mathrm{curl}(\hat{x}\hat{y}^2,0,0)^T \\ &+ s_3\mathrm{curl}(\hat{x}\hat{y}^2\hat{z},0,0)^T + t_2\mathrm{curl}(0,\hat{y}\hat{z}^2,0)^T + t_3\mathrm{curl}(0,\hat{x}\hat{y}\hat{z}^2,0)^T, \\ \hat{W}_d(\hat{E}) = P_0(\hat{E}),\end{aligned} \tag{2.3.9}$$

where the BDDF_1 space on unit cube [20] is defined as

$$\begin{aligned}\mathrm{BDDF}_1(\hat{E}) = (P_1(\hat{E}))^3 + r_0\mathrm{curl}(0,0,\hat{x}\hat{y}\hat{z})^T + r_1\mathrm{curl}(0,0,\hat{x}\hat{y}^2)^T + s_0\mathrm{curl}(\hat{x}\hat{y}\hat{z},0,0)^T \\ + s_1\mathrm{curl}(\hat{y}\hat{z}^2,0,0)^T + t_0\mathrm{curl}(0,\hat{x}\hat{y}\hat{z},0)^T + t_1\mathrm{curl}(0,\hat{x}^2\hat{z},0)^T,\end{aligned}$$

where $r_i, s_i, t_i, i = 0, \ldots 3$, are real constants.

Note that in all four cases

$$\hat{\nabla}\cdot\hat{\boldsymbol{X}}_d(\hat{E}) = \hat{W}_d(\hat{E}). \tag{2.3.10}$$

On any face (edge in 2D) $\hat{e} \in \hat{E}$, for all $\hat{\boldsymbol{v}} \in \hat{\boldsymbol{X}}_d(\hat{E})$, $\hat{\boldsymbol{v}}\cdot\hat{\boldsymbol{n}}_{\hat{e}} \in P_1(\hat{e})$ on the reference square or simplex, and $\hat{\boldsymbol{v}}\cdot\hat{\boldsymbol{n}}_{\hat{e}} \in Q_1(\hat{e})$ on the reference cube, where $Q_1(\hat{e})$ is the space of bilinear functions on $\hat{e}$.

The degrees of freedom for $\hat{\boldsymbol{X}}_d(\hat{E})$ are chosen to be the values of $\hat{\boldsymbol{v}}\cdot\hat{\boldsymbol{n}}_{\hat{e}}$ at the vertices of $\hat{e}$, for each face (edge) $\hat{e}$. This choice gives certain orthogonalities for the quadrature rule introduced in the next section and leads to a cell-centered pressure scheme.

The spaces $\boldsymbol{X}_d(E)$ and $W_d(E)$ on any physical element $E \in \mathcal{T}_d^h$ are defined, respectively, via the Piola transformation

$$\boldsymbol{v} \leftrightarrow \hat{\boldsymbol{v}} : \boldsymbol{v} = \frac{1}{J_E} DF_E\hat{\boldsymbol{v}} \circ F_E^{-1}$$

and standard scalar transformation

$$w \leftrightarrow \hat{w} : w = \hat{w} \circ F_E^{-1}.$$

Under these transformations, the divergence and the normal components of the velocity vectors on the faces (edges) are preserved [11]:

$$(\nabla\cdot\boldsymbol{v}, w)_E = (\hat{\nabla}\cdot\hat{\boldsymbol{v}}, \hat{w})_{\hat{E}} \quad \text{and} \quad \langle\boldsymbol{v}\cdot\boldsymbol{n}_e, w\rangle_e = \langle\hat{\boldsymbol{v}}\cdot\hat{\boldsymbol{n}}_{\hat{e}}, \hat{w}\rangle_{\hat{e}}. \tag{2.3.11}$$

In addition, (2.3.5) implies that

$$\boldsymbol{v}\cdot\boldsymbol{n}_e = \frac{1}{|J_E DF_E^{-T}\hat{\boldsymbol{n}}_{\hat{e}}|}\hat{\boldsymbol{v}}\cdot\hat{\boldsymbol{n}}_{\hat{e}}, \tag{2.3.12}$$

and (2.3.11) implies that

$$\nabla\cdot\boldsymbol{v} = \left(\frac{1}{J_E}\hat{\nabla}\cdot\hat{\boldsymbol{v}}\right) \circ F_E^{-1}(\boldsymbol{x}). \tag{2.3.13}$$

On quadrilaterals or hexahedra, $\nabla\cdot\boldsymbol{v} \neq$ constant since J_E is not constant.

The finite element spaces $\boldsymbol{X}_{d,i}^h$ and $W_{d,i}^h$ on subdomain $\Omega_{d,i}$ are given by

$$\begin{aligned}\boldsymbol{X}_{d,i}^h &= \left\{\boldsymbol{v} \in \boldsymbol{X}_d : \quad \boldsymbol{v}|_E \leftrightarrow \hat{\boldsymbol{v}},\ \hat{\boldsymbol{v}} \in \hat{\boldsymbol{X}}_d(\hat{E}), \quad \forall E \in \mathcal{T}_{d,i}^h\right\},\\ W_{d,i}^h &= \left\{w \in W_d : \quad w|_E \leftrightarrow \hat{w},\ \hat{w} \in \hat{W}_d(\hat{E}), \quad \forall E \in \mathcal{T}_{d,i}^h\right\}.\end{aligned} \tag{2.3.14}$$

The global mixed finite element spaces in Darcy flow are defined as

$$\boldsymbol{X}_d^h = \bigoplus_{i=1}^n \boldsymbol{X}_{d,i}^h, \quad W_d^h = \bigoplus_{i=1}^n W_{d,i}^h.$$

We recall the projection operator in the space $\boldsymbol{X}_{d,i}^h$. The operator $\hat{R}_d^h : (H^1(\hat{E}))^d \to \hat{\boldsymbol{X}}_d(\hat{E})$ is defined locally on each element by

$$\langle (\hat{R}_d^h \hat{\mathbf{q}} - \hat{\mathbf{q}}) \cdot \hat{\boldsymbol{n}}_{\hat{e}}, \hat{q}_1 \rangle_{\hat{e}} = 0, \quad \forall \hat{e} \subset \partial \hat{E}, \tag{2.3.15}$$

where $\hat{q}_1 \in P_1(\hat{e})$ when $\hat{E}$ is the unit square or simplicial element, and $\hat{q}_1 \in Q_1(\hat{e})$ when $\hat{E}$ is the unit cube. The global operator in Darcy flow $R_d^h : \boldsymbol{X}_d \cap (H^1(\Omega))^d \to \boldsymbol{X}_d^h$ on each element E is defined via the Piola transformation:

$$R_d^h \mathbf{q} \leftrightarrow \widehat{R_d^h \mathbf{q}}, \quad \widehat{R_d^h \mathbf{q}} = \hat{R}_d \hat{\mathbf{q}}. \tag{2.3.16}$$

Furthermore, (2.3.11), (2.3.15), and (2.3.16) imply that $R_d^h \mathbf{q} \cdot \boldsymbol{n}$ is continuous across element interfaces, which gives $R_d^h \mathbf{q} \in \boldsymbol{X}_{d,i}^h$, and that

$$(\nabla \cdot (R_d^h \mathbf{q} - \mathbf{q}), w)_{\Omega_{d,i}} = 0, \quad \forall w \in W_{h,i}. \tag{2.3.17}$$

In the analysis, we also need similar projection operators onto the lowest order Raviart-Thomas [41, 31] spaces. The RT_0 spaces are defined on the reference cube and the reference tetrahedron, respectively, as

$$\hat{\boldsymbol{X}}_d^{RT}(\hat{E}) = \begin{pmatrix} r_1 + s_1 \hat{x} \\ r_2 + s_2 \hat{y} \\ r_3 + s_3 \hat{z} \end{pmatrix}, \qquad \hat{W}_d^{RT}(\hat{E}) = P_0(\hat{E}), \tag{2.3.18}$$

and

$$\hat{\boldsymbol{X}}_d^{RT}(\hat{E}) = \begin{pmatrix} r_1 + s \hat{x} \\ r_2 + s \hat{y} \\ r_3 + s \hat{z} \end{pmatrix}, \qquad \hat{W}_d^{RT}(\hat{E}) = P_0(\hat{E}), \tag{2.3.19}$$

with similar definitions in two dimensions, where s, r_i, s_i (i=1,2,3) are constants.

In all cases $\hat{\nabla}\cdot\hat{\boldsymbol{X}}_d^{RT} = \hat{W}_d^{RT}(\hat{E})$ and $\hat{\boldsymbol{v}}\cdot\hat{\boldsymbol{n}}_e \in P_0(\hat{e})$. The degrees of freedom of $\hat{\boldsymbol{X}}_d^{RT}(\hat{E})$ are chosen to be the values of $\hat{\boldsymbol{v}}\cdot\hat{\boldsymbol{n}}_{\hat{e}}$ at the midpoints of all faces (edges) of $\hat{E}$. The projection operator $\hat{R}_d^{RT} : (H^1(\hat{E}))^d \to \hat{\boldsymbol{X}}_d^{RT}(\hat{E})$ satisfies

$$\langle(\hat{R}_d^{RT}\hat{\mathbf{q}} - \hat{\mathbf{q}})\cdot\hat{\boldsymbol{n}}_{\hat{e}}, \hat{q}_0\rangle_{\hat{e}} = 0, \quad \forall \hat{e} \subset \partial\hat{E}, \quad \forall q_0 \in P_0(\hat{E}). \tag{2.3.20}$$

The spaces $\boldsymbol{X}_d^{RT}$ and W_d^{RT} on Ω and the projection operator $R_d^{RT} : (H^1(\Omega))^d \to \boldsymbol{X}_{d,h}^{RT}$ are defined similarly to the case of $\boldsymbol{X}^h$ and W^h. By definition, we have

$$\boldsymbol{X}_{d,i}^{RT} \subset \boldsymbol{X}_{d,i}^h \qquad W_{d,i}^{RT} = W_{d,i}^h. \tag{2.3.21}$$

The projection operator R_d^{RT} satisfies

$$(\nabla\cdot(R_d^{RT}\mathbf{q} - \mathbf{q}), w)_{\Omega_{d,i}} = 0, \quad \forall w \in W_{d,i}^{RT}, \tag{2.3.22}$$

$$\nabla\cdot R_d^{RT}\boldsymbol{v} = \nabla\cdot\boldsymbol{v}, \quad \forall \boldsymbol{v} \in \boldsymbol{X}_{d,i}^h, \tag{2.3.23}$$

and for all element $E \in \mathcal{T}_{d,i}^h$,

$$\|R_d^{RT}\boldsymbol{v}\|_E \lesssim \|\boldsymbol{v}\|_E, \qquad \forall \boldsymbol{v} \in \boldsymbol{X}_{d,i}^h. \tag{2.3.24}$$

Furthermore, due to (2.3.15) and (2.3.20),

$$R_d^{RT}R_d^h\mathbf{q} = R_d^{RT}\mathbf{q}. \tag{2.3.25}$$

2.3.3 A quadrature rule for MFMFE in Darcy flow

In Darcy flow, its mixed finite element discretization needs to compute the integral $(K^{-1}\mathbf{q}, \boldsymbol{v})_{\Omega_{d,i}}$ for $\mathbf{q}, \boldsymbol{v} \in \boldsymbol{X}^h_{d,i}$. The MFMFE method employs a quadrature rule for the velocity mass matrix, in order to reduce the discrete problem on each subdomain to a cell-centered finite difference system for the pressure. We follow the development in [55, 29]. The integration on each element E is performed by mapping to the reference element $\hat{E}$, where the quadrature rule is defined. Using the definition (2.3.14) of the finite element spaces, for $\mathbf{q}, \boldsymbol{v} \in \boldsymbol{X}^h_{d,i}$,

$$(K^{-1}\mathbf{q}, \boldsymbol{v})_E = \left(\frac{1}{J_E} DF_E^T K^{-1}(F_E(\hat{x})) DF_E \hat{\mathbf{q}}, \hat{\boldsymbol{v}}\right)_{\hat{E}} \equiv (\mathcal{M}_E \hat{\mathbf{q}}, \hat{\boldsymbol{v}})_{\hat{E}},$$

where

$$\mathcal{M}_E = \frac{1}{J_E} DF_E^T K^{-1}(F_E(\hat{x})) DF_E. \tag{2.3.26}$$

Define a perburbed $\widetilde{\mathcal{M}_E}$ as

$$\widetilde{\mathcal{M}_E} = \frac{1}{J_E} DF_E^T(\hat{\boldsymbol{r}}_{c,\hat{E}}) \overline{K}_E^{-1}(F_E(\hat{x})) DF_E. \tag{2.3.27}$$

where $\hat{\boldsymbol{r}}_{c,\hat{E}}$ is the centroid of $\hat{E}$ and $\overline{K}_E$ denotes the mean of K on E. In addition, denote the trapezoidal rule on $\hat{E}$ by $\mathrm{Trap}(\cdot,\cdot)_{\hat{E}}$:

$$\mathrm{Trap}(\hat{\mathbf{q}}, \hat{\boldsymbol{v}})_{\hat{E}} \equiv \frac{|\hat{E}|}{n_v} \sum_{i=1}^{n_v} \hat{\mathbf{q}}(\hat{\mathbf{r}}_i) \cdot \hat{\boldsymbol{v}}(\hat{\mathbf{r}}_i) \tag{2.3.28}$$

where $\{\hat{\mathbf{r}}_i\}_{i=1}^{n_v}$ are vertices of $\hat{E}$.

The symmetric quadrature rule is based on the original $\mathcal{M}_E$ while the non-sysmetric one is based on the perturbed $\widetilde{\mathcal{M}_E}$. The quadrature rule on an element E is defined as

$$(K^{-1}\mathbf{q}, \boldsymbol{v})_{Q,E} \equiv \begin{cases} \mathrm{Trap}(\mathcal{M}_E \hat{\mathbf{q}}, \hat{\boldsymbol{v}})_{\hat{E}} = \dfrac{|\hat{E}|}{n_v} \displaystyle\sum_{i=1}^{n_v} \mathcal{M}_E(\hat{\mathbf{r}}_i) \hat{\mathbf{q}}(\hat{\mathbf{r}}_i) \cdot \hat{\boldsymbol{v}}(\hat{\mathbf{r}}_i), & \text{symmetric,} \\ \mathrm{Trap}(\widetilde{\mathcal{M}_E} \hat{\mathbf{q}}, \hat{\boldsymbol{v}})_{\hat{E}} = \dfrac{|\hat{E}|}{n_v} \displaystyle\sum_{i=1}^{n_v} \widetilde{\mathcal{M}_E}(\hat{\mathbf{r}}_i) \hat{\mathbf{q}}(\hat{\mathbf{r}}_i) \cdot \hat{\boldsymbol{v}}(\hat{\mathbf{r}}_i), & \text{non-symmetric.} \end{cases} \tag{2.3.29}$$

Mapping back to the physical element E, we have the quadrature rule on E as

$$(K^{-1}\mathbf{q},\boldsymbol{v})_{Q,E}=\begin{cases}\dfrac{1}{n_v}\displaystyle\sum_{i=1}^{n_v}J_E(\hat{\mathbf{r}}_i)K_E^{-1}\mathbf{q}(\mathbf{r}_i)\cdot\boldsymbol{v}(\mathbf{r}_i), & \text{symmetric,}\\ \dfrac{1}{n_v}\displaystyle\sum_{i=1}^{n_v}J_E(\hat{\mathbf{r}}_i)(DF_E^{-1})^T(\mathbf{r}_i)DF_E^T(\hat{\boldsymbol{r}}_{c,\hat{E}})\overline{K}_E^{-1}\mathbf{q}(\mathbf{r}_i)\cdot\boldsymbol{v}(\mathbf{r}_i), & \text{non-symmetric.}\end{cases} \tag{2.3.30}$$

The non-symmetric quadrature rule has certain critical properties on the physical elements that lead to a convergent method on rough quadrilaterals and hexahedra.

Then the global quadrature on Ω_d is then given as

$$(K^{-1}\mathbf{q},\boldsymbol{v})_{Q,\Omega_d}=\sum_{E\in\mathcal{T}_d^h}(K^{-1}\mathbf{q},\boldsymbol{v})_{Q,E}.$$

Note that

$$(K^{-1}\mathbf{q},\boldsymbol{v})_{Q,\Omega_d}=\sum_{E\in\mathcal{T}_d^h}(K^{-1}\mathbf{q},\boldsymbol{v})_{Q,E}=\sum_{c\in\mathcal{C}_d^h}\boldsymbol{v}_c^TM_c\mathbf{q}_c, \tag{2.3.31}$$

where $\mathcal{C}_d^h$ denotes the set of corner or vertex points in $\mathcal{T}_d^h$, $\mathbf{q}_c:=\{(\mathbf{q}\cdot\boldsymbol{n}_e)(x_c)\}_{e=1}^{n_c}$, x_c is the coordinate vector of point c, and n_c is the number of faces (or edges in 2D) that share the vertex point c.

The numerical quadrature error on each element is defined as

$$\sigma_E(\mathbf{q},\boldsymbol{v})\equiv(K^{-1}\mathbf{q},\boldsymbol{v})_E-(K^{-1}\mathbf{q},\boldsymbol{v})_{Q,E}, \tag{2.3.32}$$

and the global numerical quadrature error is given by $\sigma(\mathbf{q},\boldsymbol{v})_{\Omega_d}\equiv(K^{-1}\mathbf{q},\boldsymbol{v})_{\Omega_d}-(K^{-1}\mathbf{q},\boldsymbol{v})_{Q,\Omega_d}$.

Lemma 2.3.1 ([55, 29]). *The symmetric bilinear form $(K^{-1}\cdot,\cdot)_Q$ is coercive in $\boldsymbol{X}_d^h$ and induces a norm in $\boldsymbol{X}_d^h$ equivalent to the L^2 -norm:*

$$(K^{-1}\mathbf{q},\mathbf{q})_{Q,\Omega_d}\eqsim\|\mathbf{q}\|_{\Omega_d}^2\quad\forall\mathbf{q}\in\boldsymbol{X}_d^h. \tag{2.3.33}$$

The analysis of the non-symmetric MFMFE method requires some additional assumptions.

Lemma 2.3.2. *Assume that M_c is uniformly positive definite for all $c \in \mathcal{C}_d^h$:*

$$h^d \boldsymbol{\xi}^T \boldsymbol{\xi} \lesssim \boldsymbol{\xi}^T M_c \boldsymbol{\xi}, \quad \forall \boldsymbol{\xi} \in \mathbb{R}^{n_c}. \tag{2.3.34}$$

Then the non-symmetric bilinear form $(K^{-1}\cdot,\cdot)_{Q,\Omega_d}$ is coercive in $\boldsymbol{X}_d^h$ and satisfies (2.3.33). If in addition

$$\boldsymbol{\xi}^T M_c^T M_c \boldsymbol{\xi} \lesssim h^{2d} \boldsymbol{\xi}^T \boldsymbol{\xi}, \quad \forall \boldsymbol{\xi} \in \mathbb{R}^{n_c}. \tag{2.3.35}$$

then the following Cauchy-Schwarz type inequality holds:

$$(K^{-1}\mathbf{q}, \boldsymbol{v})_{Q,\Omega_d} \lesssim \|\mathbf{q}\|_{\Omega_d} \|\boldsymbol{v}\|_{\Omega_d}, \quad \forall \mathbf{q}, \boldsymbol{v} \in \boldsymbol{X}_d^h. \tag{2.3.36}$$

2.3.4 Meshes and discrete spaces

In view of discretization, we assume from now on that Ω and all its subdomains Ω_i, $1 \leq i \leq M$, have polygonal or polyhedral boundaries. Since none of the subdomains overlap, they form a mesh, $\mathcal{T}_d$ of Ω_d and $\mathcal{T}_s$ of Ω_s, and the union of these meshes constitutes a mesh $\mathcal{T}_\Omega$ of Ω. Furthermore, we suppose that this mesh satisfies the following assumptions:

Hypothesis 2.3.1. *1. $\mathcal{T}_\Omega$ is conforming, i.e. it has no hanging nodes.*

2. *The subdomains of $\mathcal{T}_\Omega$ can take at most L different configurations, where L is a fixed integer independent of M.*
3. *$\mathcal{T}_\Omega$ is shape-regular in the sense that there exists a real number σ, independent of M such that*

$$\forall i, 1 \leq i \leq M\,, \frac{\operatorname{diam}(\Omega_i)}{\operatorname{diam}(B_i)} \leq \sigma, \tag{2.3.37}$$

where $\operatorname{diam}(\Omega_i)$ is the diameter of Ω_i and $\operatorname{diam}(B_i)$ is the diameter of the largest ball contained in Ω_i. Without loss of generality, we can assume that $\operatorname{diam}(\Omega_i) \leq 1$.

As each subdomain Ω_i is polygonal or polyhedral, it can be entirely partitioned into affine finite elements. Let $h > 0$ denote a discretization parameter, and for each h, let $\mathcal{T}_i^h$ be a regular family of partitions of Ω_i made of triangles or tetrahedra T in the Stokes region and triangles, tetrahedra, parallelograms, or parallelepipeds in the Darcy region, with *no matching requirement* at the subdomains interfaces. Thus the meshes are independent and the parameter $h < 1$ is allowed to vary with i, but to reduce the notation, unless necessary,

we do not indicate its dependence on i. By regular, we mean that there exists a real number σ_0, independent of i and h such that

$$\forall i, 1 \leq i \leq M, \forall T \in \mathcal{T}_i^h \,, \; \frac{h_T}{\rho_T} \leq \sigma_0, \tag{2.3.38}$$

where h_T is the diameter of T and ρ_T is the diameter of the ball inscribed in T. In addition we assume that each element of $\mathcal{T}_i^h$ has at least one vertex in Ω_i. For the interfaces, let $H > 0$ be another discretization parameter and for each H and each $i < j$, let $\mathcal{T}_{ij}^H$ denote a regular family of partitions of Γ_{ij} into segments, triangles or parallelograms of diameter bounded by H, with no matching conditions between interfaces.

On these meshes, we define the following finite element spaces. In the Stokes region, for each $\Omega_{s,i}$, let $(X_{s,i}^h, W_{s,i}^h) \subset H^1(\Omega_{s,i})^n \times L^2(\Omega_{s,i})$ be a pair of finite element spaces satisfying a local uniform inf-sup condition for the divergence. More precisely, setting $X_{0,s,i}^h = X_{s,i}^h \cap H_0^1(\Omega_{s,i})^n$ and $W_{0,s,i}^h = W_{s,i}^h \cap L_0^2(\Omega_{s,i})$, we assume that there exists a constant $\beta_s^\star > 0$, independent of h and the diameter of $\Omega_{s,i}$, such that

$$\forall i, 1 \leq i \leq M_s \,, \; \inf_{w^h \in W_{0,s,i}^h} \sup_{\boldsymbol{v}^h \in X_{0,s,i}^h} \frac{\int_{\Omega_{s,i}} w^h \mathrm{div}\, \boldsymbol{v}^h}{|\boldsymbol{v}^h|_{H^1(\Omega_{s,i})} \|w^h\|_{L^2(\Omega_{s,i})}} \geq \beta_s^\star \,. \tag{2.3.39}$$

In addition, since $X_{0,s,i}^h \subset H_0^1(\Omega_{s,i})^n$, it satisfies a Korn inequality: There exists a constant $\alpha^\star > 0$, independent of h and the diameter of $\Omega_{s,i}$, such that

$$\forall i, 1 \leq i \leq M_s \,, \; \forall \boldsymbol{v}^h \in X_{0,s,i}^h \,, \; \|\boldsymbol{D}(\boldsymbol{v}^h)\|_{L^2(\Omega_{s,i})} \geq \alpha^\star |\boldsymbol{v}^h|_{H^1(\Omega_{s,i})}. \tag{2.3.40}$$

There are well-known examples of pairs satisfying (2.3.39) (cf. [25]), such as the mini-element, the Bernardi-Raugel element, or the Taylor-Hood element. Similarly, in the Darcy region, for each $\Omega_{d,i}$, let $(X_{d,i}^h, W_{d,i}^h) \subset H(\mathrm{div}; \Omega_{d,i}) \times L^2(\Omega_{d,i})$ be a pair of mixed finite element spaces satisfying a uniform inf-sup condition for the divergence. More precisely, setting $X_{0,d,i}^h = X_{d,i}^h \cap H_0(\mathrm{div}; \Omega_{d,i})$ and $W_{0,d,i}^h = W_{d,i}^h \cap L_0^2(\Omega_{d,i})$, we assume that there exists a constant $\beta_d^\star > 0$ independent of h and the diameter of $\Omega_{d,i}$, such that

$$\forall i, 1 \leq i \leq M_d \,, \; \inf_{w^h \in W_{0,d,i}^h} \sup_{\boldsymbol{v}^h \in X_{0,d,i}^h} \frac{\int_{\Omega_{d,i}} w^h \mathrm{div}\, \boldsymbol{v}^h}{\|\boldsymbol{v}^h\|_{H(\mathrm{div};\Omega_{d,i})} \|w^h\|_{L^2(\Omega_{d,i})}} \geq \beta_d^\star \,. \tag{2.3.41}$$

Furthermore, we assume that

$$\forall i, 1 \le i \le M_d\,,\ \forall \boldsymbol{v}^h \in X^h_{d,i}\,,\ \mathrm{div}\,\boldsymbol{v}^h \in W^h_{d,i}. \tag{2.3.42}$$

Again, there are well-known examples of pairs satisfying (2.3.41) and (2.3.42) (cf. [25] or [11]), such as the Raviart-Thomas elements, the Brezzi-Douglas-Marini elements, the Brezzi-Douglas-Fortin-Marini elements, the Brezzi-Douglas-Duràn-Fortin elements, or the Chen-Douglas elements. Since in this paper we only consider MFMFE method for efficient discretization of Darcy flow with irregular grids which is based on the lowest order BDM_1 space on simplices or quadrilaterals or an enhanced BDDF_1 space on hexahedra, then above conditions (2.3.41)–(2.3.42) still hold for MFMFE method and we take $X^h_{d,i}$ and $W^h_{d,i}$ to be spaces defined in (2.3.14).

Thus, the global finite element spaces are defined by:

$$X^h_d = \{\boldsymbol{v} \in L^2(\Omega_d)^n\,;\, \boldsymbol{v}|_{\Omega_{d,i}} \in X^h_{d,i}, 1 \le i \le M_d, \boldsymbol{v}\cdot\boldsymbol{n} = 0 \text{ on } \Gamma_d\},$$

$$X^h_s = \{\boldsymbol{v} \in L^2(\Omega_s)^n\,;\, \boldsymbol{v}|_{\Omega_{s,i}} \in X^h_{s,i}, 1 \le i \le M_s, \boldsymbol{v} = \boldsymbol{0} \text{ on } \Gamma_s\},$$

and we set

$$W^h_d = \{w \in L^2(\Omega_d)\,;\, w|_{\Omega_{d,i}} \in W^h_{d,i}\}\ ,\ W^h_s = \{w \in L^2(\Omega_s)\,;\, w|_{\Omega_{s,i}} \in W^h_{s,i}\},$$

$$X^h = \{\boldsymbol{v} \in L^2(\Omega)^n\,;\, \boldsymbol{v}|_{\Omega_d} \in X^h_d, \boldsymbol{v}|_{\Omega_s} \in X^h_s\}\ ,\ W^h = \{w \in L^2_0(\Omega)\,;\, w|_{\Omega_d} \in W^h_d, w|_{\Omega_s} \in W^h_s\}.$$

The finite elements regularity implies that $X^h_d \subset X_d$, $X^h_s \subset X_s$ and $X^h \subset X$. Of course, $W^h \subset W$.

In the mortar region, we take a finite element space Λ^H_s, a finite element space Λ^H_d, and a finite element space Λ^H_{sd}. These spaces consist of continuous or discontinuous piecewise polynomials. We will allow for varying polynomial degrees on different types of interfaces. Although the mortar meshes and the subdomain meshes so far are unrelated, we need compatibility conditions between Λ^H_s, Λ^H_{sd} and Λ^H_d on one hand, and X^h_d and X^h_s on the other hand.

1. For all $\Gamma_{ij} \in \Gamma_{ss} \cup \Gamma_{sd}$, $i < j$, and for all $\boldsymbol{v} \in \tilde{X}$, there exists $\boldsymbol{v}^h \in X^h_{s,i}$, $\boldsymbol{v}^h = \boldsymbol{0}$ on $\partial\Omega_{s,i} \setminus \Gamma_{ij}$ satisfying
$$\int_{\Gamma_{ij}} \boldsymbol{v}^h \cdot \boldsymbol{n}_{ij} = \int_{\Gamma_{ij}} \boldsymbol{v} \cdot \boldsymbol{n}_{ij}. \tag{2.3.43}$$
2. For all $\Gamma_{ij} \in \Gamma_{ss}$, $i < j$, and for all $\boldsymbol{v} \in \tilde{X}$, there exists $\boldsymbol{v}^h \in X^h_{s,j}$, $\boldsymbol{v}^h = \boldsymbol{0}$ on $\partial\Omega_{s,j} \setminus \Gamma_{ij}$ satisfying
$$\forall \boldsymbol{\mu}^H \in \Lambda^H_s\,, \int_{\Gamma_{ij}} \boldsymbol{\mu}^H \cdot \boldsymbol{v}^h = \int_{\Gamma_{ij}} \boldsymbol{\mu}^H \cdot \boldsymbol{v}. \tag{2.3.44}$$
3. For all $\Gamma_{ij} \in \Gamma_{dd} \cup \Gamma_{sd}$, $i < j$, and for all $\boldsymbol{v} \in \tilde{X}$, there exists $\boldsymbol{v}^h \in X^h_{d,j}$, $\boldsymbol{v}^h \cdot \boldsymbol{n}_j = \boldsymbol{0}$ on $\partial\Omega_{d,j} \setminus \Gamma_{ij}$ satisfying
$$\forall \mu^H \in \Lambda^H_d, \forall \mu^H \in \Lambda^H_{sd}\,, \int_{\Gamma_{ij}} \mu^H R_d^{RT} \boldsymbol{v}^h \cdot \boldsymbol{n}_{ij} = \int_{\Gamma_{ij}} \mu^H \boldsymbol{v} \cdot \boldsymbol{n}_{ij}. \tag{2.3.45}$$

Condition (2.3.43) is very easy to satisfy in practice and it trivially holds true for all examples of Stokes spaces considered in this paper. Conditions (2.3.44) and (2.3.45) state that the mortar space is controlled by the traces of the subdomain velocity spaces. Both conditions are easier to satisfy for coarser mortar grids. Condition (2.3.44) is more general than previously considered in the literature for mortar discretizations of the Stokes equations [6, 7]. The condition (2.3.45) is closely related to the mortar condition for Darcy flow in [58, 1, 42, 2] on Γ_{dd} and more general than existing mortar discretizations for Stokes-Darcy flows on Γ_{sd} [36, 44, 21, 8].

In the case of curved interfaces, we need following compatibility conditions on the reference grids:

1. For all $\hat{\Gamma}_{ij} \in \hat{\Gamma}_{ss} \cup \hat{\Gamma}_{sd}$, $i < j$, and for all $\hat{\boldsymbol{v}} \in \hat{X}$, there exists $\hat{\boldsymbol{v}}^h \in \hat{X}^h_{s,i}$, $\hat{\boldsymbol{v}}^h = \boldsymbol{0}$ on $\partial\hat{\Omega}_{s,i} \setminus \hat{\Gamma}_{ij}$ satisfying
$$\int_{\hat{\Gamma}_{ij}} \hat{\boldsymbol{v}}^h \cdot \hat{\boldsymbol{n}}_{ij} = \int_{\hat{\Gamma}_{ij}} \hat{\boldsymbol{v}} \cdot \hat{\boldsymbol{n}}_{ij}. \tag{2.3.46}$$
2. For all $\hat{\Gamma}_{ij} \in \hat{\Gamma}_{ss}$, $i < j$, and for all $\hat{\boldsymbol{v}} \in \hat{X}$, there exists $\hat{\boldsymbol{v}}^h \in \hat{X}^h_{s,j}$, $\hat{\boldsymbol{v}}^h = \boldsymbol{0}$ on $\partial\hat{\Omega}_{s,j} \setminus \hat{\Gamma}_{ij}$ satisfying
$$\forall \hat{\boldsymbol{\mu}}^H \in \hat{\Lambda}^H_s\,, \int_{\hat{\Gamma}_{ij}} \hat{\boldsymbol{\mu}}^H \cdot \hat{\boldsymbol{v}}^h = \int_{\hat{\Gamma}_{ij}} \hat{\boldsymbol{\mu}}^H \cdot \hat{\boldsymbol{v}}. \tag{2.3.47}$$

3. For all $\hat{\Gamma}_{ij} \in \hat{\Gamma}_{dd} \cup \hat{\Gamma}_{sd}$, $i < j$, and for all $\hat{\boldsymbol{v}} \in \hat{X}$, there exists $\hat{\boldsymbol{v}}^h \in \hat{X}^h_{d,j}$, $\hat{\boldsymbol{v}}^h \cdot \hat{\boldsymbol{n}}_j = \boldsymbol{0}$ on $\partial\hat{\Omega}_{d,j} \setminus \hat{\Gamma}_{ij}$ satisfying

$$\forall \hat{\mu}^H \in \hat{\Lambda}^H_d, \forall \hat{\mu}^H \in \hat{\Lambda}^H_{sd}, \int_{\hat{\Gamma}_{ij}} \hat{\mu}^H R_d^{RT} \hat{\boldsymbol{v}}^h \cdot \hat{\boldsymbol{n}}_{ij} = \int_{\hat{\Gamma}_{ij}} \hat{\mu}^H \hat{\boldsymbol{v}} \cdot \hat{\boldsymbol{n}}_{ij}. \tag{2.3.48}$$

2.3.5 Non-overlapping domain decomposition variational formulations and uniform stability of the discrete problem with straight interfaces

With above finite element spaces, the multiscale mortar multipoint flux mixed finite element discretiztion for this coupled model is given by: find$(\boldsymbol{u}^h, p^h, \lambda^H_{sd}, \lambda^H_{dd}, \boldsymbol{\lambda}^H_{ss}) \in X^h \times W^h \times \Lambda^H_{sd} \times \Lambda^H_d \times \Lambda^H_s$ such that

$$\begin{aligned}
\forall \boldsymbol{v}^h \in X^h,\ a^h(\boldsymbol{u}^h, \boldsymbol{v}^h) + b(\boldsymbol{v}^h, p^h) + b^h_{sd}(\boldsymbol{v}^h, \lambda^H_{sd}) + b^h_d(\boldsymbol{v}^h, \lambda^H_{dd}) + b_s(\boldsymbol{v}^h, \boldsymbol{\lambda}^H_{ss}) &= \int_\Omega \boldsymbol{f} \cdot \boldsymbol{v}^h, \\
\forall w^h \in W^h,\ b(\boldsymbol{u}^h, w^h) &= -\int_{\Omega_d} w^h\, q_d, \\
\forall \mu^H \in \Lambda^H_{sd},\ b^h_{sd}(\boldsymbol{u}^h, \mu^H) &= 0, \\
\forall \mu^H \in \Lambda^H_d,\ b^h_d \boldsymbol{u}^h, \mu^H) &= 0, \\
\forall \boldsymbol{\mu}^H \in \Lambda^H_s,\ b_s(\boldsymbol{u}^h, \boldsymbol{\mu}^H) &= 0.
\end{aligned} \tag{2.3.49}$$

where $a^h(\boldsymbol{u}^h, \boldsymbol{v}^h) = a^h_s(\boldsymbol{u}^h, \boldsymbol{v}^h) + a^h_d(\boldsymbol{u}^h, \boldsymbol{v}^h)$, $a^h_s(\boldsymbol{u}^h, \boldsymbol{v}^h) = a_s(\boldsymbol{u}^h, \boldsymbol{v}^h)$ in Ω_s and $a^h_d(\boldsymbol{u}^h, \boldsymbol{v}^h) = \sum_{i=1}^{M_d} \nu_d(K^{-1}\boldsymbol{u}^h, \boldsymbol{v}^h)_{Q,\Omega_{d,i}}$ in Ω_d based on the quadrature rule defined in subsection (2.3.3). The discrete interface bilinear form $b^h_d(\cdot,\cdot)$ and $b^h_{sd}(\cdot,\cdot)$ on quadrilaterals and hexahedra are given by:

$$\begin{aligned}
\forall \boldsymbol{v} \in X^h_d, \forall \mu \in \Lambda^H_d,\ b^h_d(\boldsymbol{v}, \mu) &= \sum_{\Gamma_{ij} \in \Gamma_{dd}} \langle [R_d^{RT} \boldsymbol{v} \cdot \boldsymbol{n}], \mu \rangle_{\Gamma_{ij}}, \\
\forall \boldsymbol{v} \in X^h, \forall \mu \in \Lambda^H_{sd},\ b^h_{sd}(\boldsymbol{v}, \mu) &= \sum_{\Gamma_{ij} \in \Gamma_{sd}} \langle [R_d^{RT} \boldsymbol{v} \cdot \boldsymbol{n}], \mu \rangle_{\Gamma_{ij}},
\end{aligned} \tag{2.3.50}$$

where $[R_d^{RT}\boldsymbol{v}\cdot\boldsymbol{n}] = R_d^{RT}\boldsymbol{v}_i^d\cdot\boldsymbol{n}_i + R_d^{RT}\boldsymbol{v}_j^d\cdot\boldsymbol{n}_j$ for Darcy-Darcy interfaces and $[R_d^{RT}\boldsymbol{v}\cdot\boldsymbol{n}] = R_d^{RT}\boldsymbol{v}_d\cdot\boldsymbol{n}_d + \boldsymbol{v}_s\cdot\boldsymbol{n}_s$ for Stokes-Darcy interfaces. Then we can define following spaces:

$$\begin{aligned}
V_d^h &= \{\boldsymbol{v}\in X_d^h\,;\,\forall\mu\in\Lambda_d^H, b_d^h(\boldsymbol{v},\mu)=0\},\\
V_s^h &= \{\boldsymbol{v}\in X_s^h\,;\,\forall\boldsymbol{\mu}\in\Lambda_s^H, b_s(\boldsymbol{v},\boldsymbol{\mu})=0\},\\
V^h &= \{\boldsymbol{v}\in X^h\,;\,\boldsymbol{v}|_{\Omega_d}\in V_d^h, \boldsymbol{v}|_{\Omega_s}\in V_s^h, \forall\mu\in\Lambda_{sd}^H, b_{sd}^h(\boldsymbol{v},\mu)=0\},\\
Z^h &= \{\boldsymbol{v}\in V^h\,;\,\forall w\in W^h, b(\boldsymbol{v},w)=0\}.
\end{aligned} \tag{2.3.51}$$

With above spaces definition, we can have a equivalent form of (2.3.74) : Find $\boldsymbol{u}^h\in V^h$, $p^h\in W^h$ such that

$$\begin{aligned}
\forall\boldsymbol{v}^h\in V^h,\ a^h(\boldsymbol{u}^h,\boldsymbol{v}^h)+b(\boldsymbol{v}^h,p^h) &= \int_\Omega \boldsymbol{f}\cdot\boldsymbol{v}^h,\\
\forall w^h\in W^h,\ b(\boldsymbol{u}^h,w^h) &= -\int_{\Omega_d} w^h\, q_d.
\end{aligned} \tag{2.3.52}$$

Remark 2.3.1. *The appearance of R_d^{RT} in the case of quadrilaterals and hexahedra is not standard. It is necessary to have R_d^{RT} in MFMFE weak formulation for accuracy. More precisely, the numerical quadrature error can only be controlled when one of arguments belongs to $X_{d,h}^{RT}$. On the other hand, in case of simplicial elements such as triangles and tedrahera, the numerical quadrature error bound still hold when the arguments are in X_d^h. Thus, for simplicial elements, we just need to replace R_d^{RT} by R_d^h,which means removing R_d^{RT}. As a result, terms of the type $\boldsymbol{v}_d - R_d^{RT}\boldsymbol{v}_d$ drop out.*

Lemma 2.3.3. *Under assumptions (2.3.44) and (2.3.45), the only solution $\left(\lambda_{sd}^H,\lambda_d^H,\boldsymbol{\lambda}_s^H\right)$ in $\Lambda_{sd}^H\times\Lambda_d^H\times\Lambda_s^H$ to the system*

$$\forall\boldsymbol{v}^h\in X^h\,,\ b_s(\boldsymbol{v}^h,\boldsymbol{\lambda}_s^H)+b_d^h(\boldsymbol{v}^h,\lambda_d^H)+b_{sd}^h(\boldsymbol{v}^h,\lambda_{sd}^H)=0 \tag{2.3.53}$$

is the zero solution.

Proof. Consider any $\Gamma_{ij} \in \Gamma_{dd}$ with $i < j$; the proof for the other interfaces being the same. Take an arbitrary $\boldsymbol{v}$ in $H_0(\mathrm{div};\Omega)$ and $\boldsymbol{v}^h$ associated with $\boldsymbol{v}$ by (2.3.45), extended by zero outside $\Omega_{d,j}$. Then on one hand,

$$\int_{\Gamma_{ij}} \lambda_d^H \boldsymbol{v}\cdot\boldsymbol{n}_{ij} = \int_{\Gamma_{ij}} \lambda_d^H R_d^{RT}\boldsymbol{v}^h\cdot\boldsymbol{n}_{ij} = b_d(\boldsymbol{v}^h,\lambda_d^H),$$

and on the other hand,

$$b_s(\boldsymbol{v}^h,\boldsymbol{\lambda}_s^H) = b_{sd}^h(\boldsymbol{v}^h,\lambda_{sd}^H) = 0.$$

Therefore

$$\forall \boldsymbol{v}\in H_0(\mathrm{div};\Omega)\,,\ \int_{\Gamma_{ij}} \lambda_d^H \boldsymbol{v}\cdot\boldsymbol{n}_{ij} = 0,$$

thus implying that $\lambda_d^H = 0$. □

Lemma 2.3.4. *Problems* (2.3.74) *and* (2.3.77) *are equivalent.*

Proof. Clearly, (2.3.74) implies (2.3.77). Conversely, if the pair $(\boldsymbol{u}^h, p^h)$ solves (2.3.77), existence of $\lambda_{sd}^H, \lambda_d^H, \boldsymbol{\lambda}_s^H$ such that all these variables satisfy (2.3.74) is an easy consequence of Lemma 2.3.9 and an algebraic argument. □

In view of this equivalence, it suffices to analyze problem (2.3.77). From the Babuška–Brezzi's theory, uniform stability of the solution of (2.3.77) stems from an ellipticity property of the bilinear form a in Z^h and an inf-sup condition of the bilinear form b. Let us prove an ellipticity property of the bilinear form a, valid when $n = 2, 3$. For this, we make the following assumptions on the mortar spaces:

Hypothesis 2.3.2. *1. On each $\Gamma_{ij} \in \Gamma_{dd}\cup\Gamma_{sd}$, $\Lambda_d^H|_{\Gamma_{ij}}$ and $\Lambda_{sd}^H|_{\Gamma_{ij}}$ contain at least $\mathbb{P}_0$.*

2. On each $\Gamma_{ij} \in \Gamma_{ss}$, on each hyperplane $F \subset \Gamma_{ij}$, $\Lambda_s^H|_F$ contains at least $\mathbb{P}_0^n$.

3. On each $\Gamma_{ij} \in \Gamma_{ss}$, $\Lambda_s^H|_{\Gamma_{ij}}$ contains at least $\mathbb{P}_1^n$.

The second assumption guarantees that $\boldsymbol{n}_{ij} \in \Lambda_s^H|_{\Gamma_{ij}}$; it follows from the third assumption when Γ_{ij} has no corner. The third assumption is solely used for deriving a discrete Korn inequality; it can be relaxed, as we shall see in the $3-D$ example. The first two assumptions imply that all functions $\boldsymbol{v}^h$ in V^h satisfy

$$\sum_{i=1}^M \int_{\Omega_i} \mathrm{div}\,\boldsymbol{v}^h = \sum_{i=1}^M \int_{\partial\Omega_i} \boldsymbol{v}^h\cdot\boldsymbol{n}_i = \sum_{i<j}\int_{\Gamma_{ij}} [\boldsymbol{v}^h\cdot\boldsymbol{n}] = 0.$$

Therefore, the zero mean-value restriction on the functions of W^h can be relaxed. Thus the condition $\boldsymbol{v}^h \in Z^h$ implies in particular that

$$\forall w^h \in W^h_{d,i}\,, \int_{\Omega_{d,i}} w^h \mathrm{div}\, \boldsymbol{v}^h_d = 0.$$

With (2.3.42), this means that $\mathrm{div}\, \boldsymbol{v}^h_d = 0$ in $\Omega_{d,i}$, $1 \leq i \leq M_d$. Hence

$$\forall \boldsymbol{v}^h \in Z^h\,, \; |\!|\!| \boldsymbol{v}^h_d |\!|\!|_{X_d} = \|\boldsymbol{v}^h_d\|_{L^2(\Omega_d)}. \tag{2.3.54}$$

First, we treat the simpler case when $|\Gamma_s| > 0$ and Ω_s is connected.

Lemma 2.3.5. *Let $|\Gamma_s| > 0$ and Ω_s be connected. Then under Hypothesis 2.3.3, we have*

$$\forall \boldsymbol{v}^h \in Z^h\,, \; a^h(\boldsymbol{v}^h, \boldsymbol{v}^h) \geq \nu_d C_1 |\!|\!| \boldsymbol{v}^h_d |\!|\!|^2_{X_d} + 2\frac{\nu_s}{C_2^2} |\!|\!| \boldsymbol{v}^h_s |\!|\!|^2_{X_s}, \tag{2.3.55}$$

where the constant C_1 is independent of mesh sizes h and H and C_2 only depends on the shape regularity of $\mathcal{T}_s$.

Proof. As $|\Gamma_s| > 0$ and Ω_s is connected, we have $\boldsymbol{v}^h_s|_{\Gamma_s} = \boldsymbol{0}$. In addition, since $\boldsymbol{v}^h_s \in V^h_s$ and $I\!P^n_1 \in \Lambda^H_{ss}|_{\Gamma_{ij}}$ for each $\Gamma_{ij} \in \Gamma_{ss}$, then $P_1[\boldsymbol{v}^h_s] = \boldsymbol{0}$, where P_1 is the orthogonal projection on $I\!P^n_1$ for the L^2 norm on each Γ_{ij}. Therefore, inequality (1.12) in [10] gives

$$\forall \boldsymbol{v}^h_s \in V^h_s\,, \; \sum_{i=1}^{M_s} |\boldsymbol{v}^h_s|^2_{H^1(\Omega_{s,i})} \leq C_2^2 \sum_{i=1}^{M_s} \|\boldsymbol{D}(\boldsymbol{v}^h_s)\|^2_{L^2(\Omega_{s,i})}, \tag{2.3.56}$$

where the constant C_2 only depends on the shape regularity of $\mathcal{T}_s$. Hence we have the analogue proof of proposition 2.1 in [27] and use (3.31)in [54]:

$$\forall \boldsymbol{v}^h \in Z^h\,, \; a^h(\boldsymbol{v}^h, \boldsymbol{v}^h) \geq \nu_d C_1 |\!|\!| \boldsymbol{v}^h_d |\!|\!|^2_{X_d} + 2\frac{\nu_s}{C^2} \sum_{i=1}^{M_s} |\boldsymbol{v}^h_s|^2_{H^1(\Omega_{s,i})}. \tag{2.3.57}$$

Finally the above argument permits to apply formula (1.3) in [9] in order to recover the full norm of X_s in the right-hand side of (2.3.82). In fact, it is enough that $I\!P^n_0 \in \Lambda^H_{ss}|_{\Gamma_{ij}}$ for each $\Gamma_{ij} \in \Gamma_{ss}$. □

Now we turn to the case when Ω_s is connected and $|\Gamma_s| = 0$, consequently $\Gamma_{sd} = \partial\Omega_s$, up to a set of zero measure.

Lemma 2.3.6. *Let $|\Gamma_s| = 0$ and Ω_s be connected, i.e. $\Gamma_{sd} = \partial\Omega_s$. Then under Hypothesis 2.3.3, we have*

$$\forall \boldsymbol{v}^h \in Z^h\,,\ a^h(\boldsymbol{v}^h,\boldsymbol{v}^h) \geq \nu_d C_1 |\!|\!| \boldsymbol{v}_d^h |\!|\!|_{X_d}^2 + \frac{\nu_s}{C_2^2}\min\big(2, \frac{\alpha}{\sqrt{\lambda_{\max}}|\Gamma_{sd}|}\big) |\!|\!| \boldsymbol{v}_s^h |\!|\!|_{X_s}^2, \tag{2.3.58}$$

where constant C_1 is independent of mesh sizes h and H and C_2 only depends on the shape regularity of $\mathcal{T}_s$.

Proof. The proof is almost same as the proof of Lemma 3.4 in [27] and the only difference is using (3.31)in [54] to hand coercivity of discrete bilinear form in Darcy part. □

The case when Ω_s is not connected follows from Lemmas 2.3.11 or 2.3.12 applied to each connected component of Ω_s according to if it is adjacent to Γ_s or not.

Note that $a^h(\cdot,\cdot)$ is continuous on $\boldsymbol{X}^h \times \boldsymbol{X}^h$:

$$\begin{aligned}\forall (\boldsymbol{u}^h,\boldsymbol{v}^h) \in \boldsymbol{X}^h \times \boldsymbol{X}^h\,,\ |a^h(\boldsymbol{u}^h,\boldsymbol{v}^h)| \leq & \frac{\nu_d}{\lambda_{\min}} \|\boldsymbol{u}_d^h\|_{L^2(\Omega_d)} \|\boldsymbol{v}_d^h\|_{L^2(\Omega_d)} + 2\,\nu_s \|\nabla\, \boldsymbol{u}_s^h\|_{L^2(\Omega_s)} \|\nabla\, \boldsymbol{v}_s^h\|_{L^2(\Omega_s)} \\ & + \sum_{l=1}^{n-1} \frac{\nu_s \alpha}{\sqrt{\lambda_{\min}}} \|\boldsymbol{u}_s^h \cdot \boldsymbol{\tau}_l\|_{L^2(\Gamma_{sd})} \|\boldsymbol{v}_s^h \cdot \boldsymbol{\tau}_l\|_{L^2(\Gamma_{sd})},\end{aligned} \tag{2.3.59}$$

and $b(\cdot,\cdot)$ is continuous on $\boldsymbol{X}^h \times W^h$:

$$\forall (\boldsymbol{v}^h, w^h) \in \boldsymbol{X}^h \times W^h\,,\ |b(\boldsymbol{v}^h, w^h)| \leq \|\boldsymbol{v}^h\|_{\boldsymbol{X}} \|w^h\|_{L^2(\Omega)}. \tag{2.3.60}$$

To control the bilinear form b in Ω_s, we make the following assumption: There exists a linear approximation operator $\Theta_s^h : H_0^1(\Omega)^n \mapsto V_s^h$ satisfying for all $\boldsymbol{v} \in H_0^1(\Omega)^n$:

- $$\forall i, 1 \leq i \leq M_s\,,\ \int_{\Omega_{s,i}} \operatorname{div}\big(\Theta_s^h(\boldsymbol{v}) - \boldsymbol{v}\big) = 0. \tag{2.3.61}$$
- For any Γ_{ij} in Γ_{sd},
$$\int_{\Gamma_{ij}} \big(\Theta_s^h(\boldsymbol{v}) - \boldsymbol{v}\big) \cdot \boldsymbol{n}_{ij} = 0. \tag{2.3.62}$$

- There exists a constant C independent of $\boldsymbol{v}$, h, H, and the diameter of $\Omega_{s,i}$, $1 \leq i \leq M_s$, such that

$$\|\Theta_s^h(\boldsymbol{v})\|_{X_s} \leq C|\boldsymbol{v}|_{H^1(\Omega)}. \tag{2.3.63}$$

The construction of the operator Θ_s^h is presented in Section 4 in [27]. In particular, a general construction strategy discussed in Section 4.1 in [27] gives an operator that satisfies (2.3.86) and (2.3.62). The stability bound (2.3.88) is shown to hold for the specific examples presented in Sections 4.2-4.4, see Corollary 4.2 in [27].

Lemma 2.3.7 ([27], Lemma 3.5)**.** *Assuming that an operator Θ_s^h satisfying (2.3.86)–(2.3.88) exists, then there exists a linear operator $\Pi_s^h : H_0^1(\Omega)^n \mapsto V_s^h$ such that for all $\boldsymbol{v} \in H_0^1(\Omega)^n$,*

$$\forall w^h \in W_s^h\,, \sum_{i=1}^{M_s} \int_{\Omega_{s,i}} w^h \mathrm{div}(\Pi_s^h(\boldsymbol{v}) - \boldsymbol{v}) = 0, \tag{2.3.64}$$

$$\forall \Gamma_{ij} \in \Gamma_{sd}\,, \int_{\Gamma_{ij}} \left(\Pi_s^h(\boldsymbol{v}) - \boldsymbol{v}\right) \cdot \boldsymbol{n}_{ij} = 0, \tag{2.3.65}$$

and there exists a constant C independent of $\boldsymbol{v}$, h, H, and the diameter of $\Omega_{s,i}$, $1 \leq i \leq M_s$, such that

$$\|\Pi_s^h(\boldsymbol{v})\|_{X_s} \leq C|\boldsymbol{v}|_{H^1(\Omega)}. \tag{2.3.66}$$

The idea of constructing the operator Π_s^h via the interior inf-sup condition (2.3.39) and the simplified operator Θ_s^h satisfying (2.3.86) and (2.3.88) is not new. It can be found for instance in [26] and [7].

To control the bilinear form b in Ω_d, we make the following assumption: There exists a linear operator $\Pi_d^h : H_0^1(\Omega)^n \mapsto V_d^h$ satisfying for all $\boldsymbol{v} \in H_0^1(\Omega)^n$:

- $$\forall w^h \in W_d^h\,, \sum_{i=1}^{M_d} \int_{\Omega_{d,i}} w^h \mathrm{div}\left(\Pi_d^h(\boldsymbol{v}) - \boldsymbol{v}\right) = 0. \tag{2.3.67}$$

- For any Γ_{ij} in Γ_{sd},

$$\forall \mu^H \in \Lambda_{sd}^H\,, \int_{\Gamma_{ij}} \mu^H \left(R_d^{RT} \Pi_d^h(\boldsymbol{v}) - \Pi_s^h(\boldsymbol{v})\right) \cdot \boldsymbol{n}_{ij} = 0. \tag{2.3.68}$$

- There exists a constant C independent of $\boldsymbol{v}$, h, H, and the diameter of $\Omega_{d,i}$, $1 \le i \le M_d$, such that

$$\|\Pi_d^h(\boldsymbol{v})\|_{X_d} \le C|\boldsymbol{v}|_{H^1(\Omega)}. \tag{2.3.69}$$

The construction of the operator Π_d^h is presented in Section 2.4. In particular, the general construction strategy discussed in Section 2.4.1 gives an operator that satisfies (2.3.92) and (2.3.68). The stability bound (2.3.94) is shown to hold for various cases in Section 2.4.2.

The next lemma follows readily from the properties of Π_s^h and Π_d^h.

Lemma 2.3.8. *Under the above assumptions, there exists a linear operator* $\Pi^h \in \mathcal{L}(H_0^1(\Omega)^n; V^h)$ *such that for all* $\boldsymbol{v} \in H_0^1(\Omega)^n$

$$\forall w^h \in W^h, \sum_{i=1}^{M} \int_{\Omega_i} w^h \mathrm{div}\big(\Pi^h(\boldsymbol{v}) - \boldsymbol{v}\big) = 0, \tag{2.3.70}$$

$$\|\Pi^h(\boldsymbol{v})\|_X \le C|\boldsymbol{v}|_{H^1(\Omega)}, \tag{2.3.71}$$

with a constant C *independent of* $\boldsymbol{v}$, h, H, *and the diameter of* Ω_i, $1 \le i \le M$.

Proof. Take $\Pi^h(\boldsymbol{v})|_{\Omega_s} = \Pi_s^h(\boldsymbol{v})$ and $\Pi^h(\boldsymbol{v})|_{\Omega_d} = \Pi_d^h(\boldsymbol{v})$. Then (2.3.95) follows from (2.3.89) and (2.3.92). The matching condition of the functions of V^h at the interfaces of Γ_{sd} holds by virtue of (2.3.68). Finally, the stability bound (2.3.96) stems from (2.3.91) and (2.3.94). □

The following inf-sup condition between W^h and V^h is an immediate consequence of a simple variant of Fortin's Lemma [25, 11] and Lemma 2.3.14.

Theorem 2.3.1. *Under the above assumptions, there exists a constant* $\beta^\star > 0$, *independent of* h, H, *and the diameter of* Γ_{ij} *for all* $i < j$ *such that*

$$\forall w^h \in W^h, \sup_{\boldsymbol{v}^h \in V^h} \frac{b(\boldsymbol{v}^h, w^h)}{\|\boldsymbol{v}^h\|_X} \ge \beta^\star \|w^h\|_{L^2(\Omega)}. \tag{2.3.72}$$

Finally, well-posedness of the discrete scheme (2.3.77) follows from Lemma 2.3.11 or 2.3.12 and Theorem 2.3.2.

Corollary 2.3.1 ([27],corollary 4.1)**.** *Under the above assumptions, problem* (2.3.77) *has a unique solution* $(\boldsymbol{u}^h, p^h) \in V^h \times W^h$ *and*

$$|||\boldsymbol{u}^h|||_X + \|p^h\|_{L^2(\Omega)} \leq C\big(\|\boldsymbol{f}\|_{L^2(\Omega)} + \|q_d\|_{L^2(\Omega_d)}\big), \tag{2.3.73}$$

with a constant C *independent of* h, H, *and the diameter of* Γ_{ij} *for all* $i < j$.

2.3.6 Non-overlapping domain decomposition variational formulations and uniform stability of the discrete problem with curved interfaces

In this subsection, we will propose a numerical scheme with curved interfaces: find $(\boldsymbol{u}^h, p^h, \lambda_{sd}^H, \lambda_{dd}^H, \boldsymbol{\lambda}_{ss}^H) \in X^h \times W^h \times \Lambda_{sd}^H \times \Lambda_d^H \times \Lambda_s^H$ such that

$$\begin{aligned}
\forall \boldsymbol{v}^h \in X^h\,,\ a^h(\boldsymbol{u}^h, \boldsymbol{v}^h) + b(\boldsymbol{v}^h, p^h) + \hat{b}_{sd}^h(\boldsymbol{v}^h, \lambda_{sd}^H) + \hat{b}_d^h(\boldsymbol{v}^h, \lambda_{dd}^H) + \hat{b}_s(\boldsymbol{v}^h, \boldsymbol{\lambda}_{ss}^H) &= \int_\Omega \boldsymbol{f}\cdot\boldsymbol{v}^h,\\
\forall w^h \in W^h\,,\ b(\boldsymbol{u}^h, w^h) &= -\int_{\Omega_d} w^h\, q_d,\\
\forall \mu^H \in \Lambda_{sd}^H\,,\ \hat{b}_{sd}^h(\boldsymbol{u}^h, \mu^H) &= 0,\\
\forall \mu^H \in \Lambda_d^H\,,\ \hat{b}_d^h\boldsymbol{u}^h, \mu^H) &= 0,\\
\forall \boldsymbol{\mu}^H \in \Lambda_s^H\,,\ \hat{b}_s(\boldsymbol{u}^h, \boldsymbol{\mu}^H) &= 0.
\end{aligned} \tag{2.3.74}$$

where $a^h(\boldsymbol{u}^h, \boldsymbol{v}^h) = a_s^h(\boldsymbol{u}^h, \boldsymbol{v}^h) + a_d^h(\boldsymbol{u}^h, \boldsymbol{v}^h)$, $a_s^h(\boldsymbol{u}^h, \boldsymbol{v}^h) = a_s(\boldsymbol{u}^h, \boldsymbol{v}^h)$ in Ω_s and $a_d^h(\boldsymbol{u}^h, \boldsymbol{v}^h) = \sum_{i=1}^{M_d} \nu_d(K^{-1}\boldsymbol{u}^h, \boldsymbol{v}^h)_{Q,\Omega_i}$ in Ω_d based on the quadrature rule defined in subsection (2.3.3). The discrete interface bilinear form $\hat{b}_s(\cdot,\cdot)$,$\hat{b}_d^h(\cdot,\cdot)$ and $\hat{b}_{sd}^h(\cdot,\cdot)$ on quadrilaterals and hexahedra are

given by:

$$
\begin{aligned}
\forall \boldsymbol{v} \in X_s^h, \forall \boldsymbol{\mu} \in \Lambda_s^H \,,\, \hat{b}_s(\boldsymbol{v}, \boldsymbol{\mu}) &= \sum_{\Gamma_{ij} \in \Gamma_{ss}} \langle [\boldsymbol{v}], \boldsymbol{\mu} \rangle_{\Gamma_{ij}} = \sum_{\hat{\Gamma}_{ij} \in \hat{\Gamma}_{ss}} \langle [\hat{\boldsymbol{v}}], \hat{\boldsymbol{\mu}} \rangle_{\hat{\Gamma}_{ij}}, \, \forall \hat{\boldsymbol{v}} \in \hat{X}_s, \forall \hat{\boldsymbol{\mu}} \in \hat{\Lambda}_s^H \\
\forall \boldsymbol{v} \in X_d^h, \forall \mu \in \Lambda_d^H \,,\, \hat{b}_d^h(\boldsymbol{v}, \mu) &= \sum_{\Gamma_{ij} \in \Gamma_{dd}} \langle [R_d^{RT} \boldsymbol{v} \cdot \boldsymbol{n}], \mu \rangle_{\Gamma_{ij}} \\
&= \sum_{\hat{\Gamma}_{ij} \in \hat{\Gamma}_{dd}} \langle [R_d^{RT} \hat{\boldsymbol{v}} \cdot \hat{\boldsymbol{n}}], \hat{\mu} \rangle_{\hat{\Gamma}_{ij}} \, \forall \hat{\boldsymbol{v}} \in \hat{X}_d, \forall \mu \in \hat{\Lambda}_d^H, \\
\forall \boldsymbol{v} \in X^h, \forall \mu \in \Lambda_{sd}^H \,,\, \hat{b}_{sd}^h(\boldsymbol{v}, \mu) &= \sum_{\Gamma_{ij} \in \Gamma_{sd}} \langle [R_d^{RT} \boldsymbol{v} \cdot \boldsymbol{n}], \mu \rangle_{\Gamma_{ij}} \\
&= \sum_{\hat{\Gamma}_{ij} \in \hat{\Gamma}_{sd}} \langle [R_d^{RT} \hat{\boldsymbol{v}} \cdot \hat{\boldsymbol{n}}], \hat{\mu} \rangle_{\hat{\Gamma}_{ij}}, \, \forall \hat{\boldsymbol{v}} \in \hat{X}, \forall \mu \in \hat{\Lambda}_{sd}^H
\end{aligned}
\tag{2.3.75}
$$

where$[\hat{\boldsymbol{v}} \cdot \hat{\boldsymbol{n}}] = \hat{\boldsymbol{v}}_i^s \cdot \hat{\boldsymbol{n}}_i + \hat{\boldsymbol{v}}_j^s \cdot \hat{\boldsymbol{n}}_j$ denotes the jump for Stokes-Stokes interfaces, $[R_d^{RT} \hat{\boldsymbol{v}} \cdot \hat{\boldsymbol{n}}] = R_d^{RT} \hat{\boldsymbol{v}}_i^d \cdot \hat{\boldsymbol{n}}_i + R_d^{RT} \hat{\boldsymbol{v}}_j^d \cdot \hat{\boldsymbol{n}}_j$ is the jump for Darcy-Darcy interfaces and $[R_d^{RT} \hat{\boldsymbol{v}} \cdot \hat{\boldsymbol{n}}] = R_d^{RT} \hat{\boldsymbol{v}}_d \cdot \hat{\boldsymbol{n}}_d + \hat{\boldsymbol{v}}_s \cdot \hat{\boldsymbol{n}}_s$ defines the jump for Stokes-Darcy interfaces. Then we can define following spaces:

$$
\begin{aligned}
V_d^h &= \{\boldsymbol{v} \in X_d^h \,;\, \forall \mu \in \Lambda_d^H, \hat{b}_d^h(\boldsymbol{v}, \mu) = 0\}, \\
V_s^h &= \{\boldsymbol{v} \in X_s^h \,;\, \forall \boldsymbol{\mu} \in \Lambda_s^H, \hat{b}_s(\boldsymbol{v}, \boldsymbol{\mu}) = 0\}, \\
V^h &= \{\boldsymbol{v} \in X^h \,;\, \boldsymbol{v}|_{\Omega_d} \in V_d^h, \boldsymbol{v}|_{\Omega_s} \in V_s^h, \forall \mu \in \Lambda_{sd}^H, \hat{b}_{sd}^h(\boldsymbol{v}, \mu) = 0\}, \\
Z^h &= \{\boldsymbol{v} \in V^h \,;\, \forall w \in W^h, b(\boldsymbol{v}, w) = 0\}.
\end{aligned}
\tag{2.3.76}
$$

With above spaces definition, we can have a equivalent form of (2.3.74) : Find $\boldsymbol{u}^h \in V^h$, $p^h \in W^h$ such that

$$
\begin{aligned}
\forall \boldsymbol{v}^h \in V^h, \;\; a^h(\boldsymbol{u}^h, \boldsymbol{v}^h) + b(\boldsymbol{v}^h, p^h) &= \int_\Omega \boldsymbol{f} \cdot \boldsymbol{v}^h, \\
\forall w^h \in W^h, \;\; b(\boldsymbol{u}^h, w^h) &= -\int_{\Omega_d} w^h \, q_d.
\end{aligned}
\tag{2.3.77}
$$

Remark 2.3.2. *The appearance of R_d^{RT} in the case of quadrilaterals and hexahedra is not standard. It is necessary to have R_d^{RT} in MFMFE weak formulation for accuracy. More precisely, the numerical quadrature error can only be controlled when one of arguments belongs to $X_{d,h}^{RT}$. On the other hand, in case of simplicial elements such as triangles and tedrahera, the numerical quadrature error bound still hold when the arguments are in X_d^h. Thus, for simplicial elements, we just need to replace R_d^{RT} by R_d^h,which means removing R_d^{RT}. As a result, terms of the type $\boldsymbol{v}_d - R_d^{RT}\boldsymbol{v}_d$ drop out.*

Lemma 2.3.9. *Under assumptions (2.3.47) and (2.3.48), the only solution $\left(\lambda_{sd}^H, \lambda_d^H, \boldsymbol{\lambda}_s^H\right)$ in $\Lambda_{sd}^H \times \Lambda_d^H \times \Lambda_s^H$ to the system*

$$\forall \boldsymbol{v}^h \in X^h\,,\ \hat{b}_s(\boldsymbol{v}^h, \boldsymbol{\lambda}_s^H) + \hat{b}_d^h(\boldsymbol{v}^h, \lambda_d^H) + \hat{b}_{sd}^h(\boldsymbol{v}^h, \lambda_{sd}^H) = 0 \tag{2.3.78}$$

is the zero solution.

Proof. Consider any $\hat{\Gamma}_{ij} \in \hat{\Gamma}_{dd}$ with $i < j$; the proof for the other interfaces being the same. Take an arbitrary $\hat{\boldsymbol{v}}$ in $\hat{H}_0(\mathrm{div};\Omega)$ and $\hat{\boldsymbol{v}}^h$ associated with $\hat{\boldsymbol{v}}$ by (2.3.45), extended by zero outside $\hat{\Omega}_{d,j}$. Then on one hand by Piola transformation,

$$\int_{\Gamma_{ij}} \lambda_d^H \boldsymbol{v}\cdot\boldsymbol{n}_{ij} = \int_{\hat{\Gamma}_{ij}} \hat{\lambda}_d^H \hat{\boldsymbol{v}}\cdot\hat{\boldsymbol{n}}_{ij} = \int_{\hat{\Gamma}_{ij}} \hat{\lambda}_d^H R_d^{RT}\hat{\boldsymbol{v}}^h\cdot\hat{\boldsymbol{n}}_{ij} = \int_{\Gamma_{ij}} \lambda_d^H R_d^{RT}\boldsymbol{v}^h\cdot\boldsymbol{n}_{ij} = \hat{b}_d(\boldsymbol{v}^h, \lambda_d^H),$$

and on the other hand,

$$\hat{b}_s(\boldsymbol{v}^h, \boldsymbol{\lambda}_s^H) = \hat{b}_{sd}^h(\boldsymbol{v}^h, \lambda_{sd}^H) = 0.$$

Therefore

$$\forall \boldsymbol{v} \in H_0(\mathrm{div};\Omega)\,,\ \int_{\Gamma_{ij}} \lambda_d^H \boldsymbol{v}\cdot\boldsymbol{n}_{ij} = 0,$$

thus implying that $\lambda_d^H = 0$. □

Lemma 2.3.10. *Problems (2.3.74) and (2.3.77) are equivalent.*

Proof. Clearly, (2.3.74) implies (2.3.77). Conversely, if the pair $(\boldsymbol{u}^h, p^h)$ solves (2.3.77), existence of $\lambda_{sd}^H, \lambda_d^H, \boldsymbol{\lambda}_s^H$ such that all these variables satisfy (2.3.74) is an easy consequence of Lemma 2.3.9 and an algebraic argument. □

In view of this equivalence, it suffices to analyze problem (2.3.77). From the Babuška–Brezzi's theory, uniform stability of the solution of (2.3.77) stems from an ellipticity property of the bilinear form a in Z^h and an inf-sup condition of the bilinear form b. Let us prove an ellipticity property of the bilinear form a, valid when $n = 2, 3$. For this, we make the following assumptions on the mortar spaces:

Hypothesis 2.3.3. *1. On each $\Gamma_{ij} \in \Gamma_{dd} \cup \Gamma_{sd}$, $\Lambda_d^H|_{\Gamma_{ij}}$ and $\Lambda_{sd}^H|_{\Gamma_{ij}}$ contain at least $\mathbb{P}_0$.*

2. On each $\Gamma_{ij} \in \Gamma_{ss}$, on each hyperplane $F \subset \Gamma_{ij}$, $\Lambda_s^H|_F$ contains at least $\mathbb{P}_0^n$.

3. On each $\Gamma_{ij} \in \Gamma_{ss}$, $\Lambda_s^H|_{\Gamma_{ij}}$ contains at least $\mathbb{P}_1^n$.

The second assumption guarantees that $\boldsymbol{n}_{ij} \in \Lambda_s^H|_{\Gamma_{ij}}$; it follows from the third assumption when Γ_{ij} has no corner. The third assumption is solely used for deriving a discrete Korn inequality; it can be relaxed, as we shall see in the $3-D$ example. The first two assumptions imply that all functions $\boldsymbol{v}^h$ in V^h satisfy

$$\sum_{i=1}^{M} \int_{\Omega_i} \operatorname{div} \boldsymbol{v}^h = \sum_{i=1}^{M} \int_{\partial\Omega_i} \boldsymbol{v}^h \cdot \boldsymbol{n}_i = \sum_{i<j} \int_{\Gamma_{ij}} [\boldsymbol{v}^h \cdot \boldsymbol{n}] = 0.$$

Therefore, the zero mean-value restriction on the functions of W^h can be relaxed. Thus the condition $\boldsymbol{v}^h \in Z^h$ implies in particular that

$$\forall w^h \in W_{d,i}^h\,, \int_{\Omega_{d,i}} w^h \operatorname{div} \boldsymbol{v}_d^h = 0.$$

With (2.3.42), this means that $\operatorname{div} \boldsymbol{v}_d^h = 0$ in $\Omega_{d,i}$, $1 \le i \le M_d$. Hence

$$\forall \boldsymbol{v}^h \in Z^h\,,\ |\!|\!| \boldsymbol{v}_d^h |\!|\!|_{X_d} = \|\boldsymbol{v}_d^h\|_{L^2(\Omega_d)}. \tag{2.3.79}$$

First, we treat the simpler case when $|\Gamma_s| > 0$ and Ω_s is connected.

Lemma 2.3.11. *Let $|\Gamma_s| > 0$ and Ω_s be connected. Then under Hypothesis 2.3.3, we have*

$$\forall \boldsymbol{v}^h \in Z^h\,,\ a^h(\boldsymbol{v}^h, \boldsymbol{v}^h) \ge \nu_d C_1 |\!|\!| \boldsymbol{v}_d^h |\!|\!|_{X_d}^2 + 2\frac{\nu_s}{C_2^2} |\!|\!| \boldsymbol{v}_s^h |\!|\!|_{X_s}^2, \tag{2.3.80}$$

where the constant C_1 is independent of mesh sizes h and H and C_2 only depends on the shape regularity of $\mathcal{T}_s$.

Proof. As $|\Gamma_s| > 0$ and Ω_s is connected, we have $\boldsymbol{v}_s^h|_{\Gamma_s} = \mathbf{0}$. In addition, since $\boldsymbol{v}_s^h \in V_s^h$ and $I\!P_1^n \in \Lambda_{ss}^H|_{\Gamma_{ij}}$ for each $\Gamma_{ij} \in \Gamma_{ss}$, then $P_1[\boldsymbol{v}_s^h] = \mathbf{0}$, where P_1 is the orthogonal projection on $I\!P_1^n$ for the L^2 norm on each Γ_{ij}. Therefore, inequality (1.12) in [10] gives

$$\forall \boldsymbol{v}_s^h \in V_s^h \,,\ \sum_{i=1}^{M_s} |\boldsymbol{v}_s^h|^2_{H^1(\Omega_{s,i})} \leq C_2^2 \sum_{i=1}^{M_s} \|\boldsymbol{D}(\boldsymbol{v}_s^h)\|^2_{L^2(\Omega_{s,i})}, \tag{2.3.81}$$

where the constant C_2 only depends on the shape regularity of $\mathcal{T}_s$. Hence we have the analogue proof of proposition 2.1 in [27] and use (3.31)in [54]:

$$\forall \boldsymbol{v}^h \in Z^h \,,\ a^h(\boldsymbol{v}^h, \boldsymbol{v}^h) \geq \nu_d C_1 |\!|\!| \boldsymbol{v}_d^h |\!|\!|^2_{X_d} + 2\frac{\nu_s}{C^2} \sum_{i=1}^{M_s} |\boldsymbol{v}_s^h|^2_{H^1(\Omega_{s,i})}. \tag{2.3.82}$$

Finally the above argument permits to apply formula (1.3) in [9] in order to recover the full norm of X_s in the right-hand side of (2.3.82). In fact, it is enough that $I\!P_0^n \in \Lambda_{ss}^H|_{\Gamma_{ij}}$ for each $\Gamma_{ij} \in \Gamma_{ss}$. □

Now we turn to the case when Ω_s is connected and $|\Gamma_s| = 0$, consequently $\Gamma_{sd} = \partial\Omega_s$, up to a set of zero measure.

Lemma 2.3.12. *Let $|\Gamma_s| = 0$ and Ω_s be connected, i.e. $\Gamma_{sd} = \partial\Omega_s$. Then under Hypothesis 2.3.3, we have*

$$\forall \boldsymbol{v}^h \in Z^h \,,\ a^h(\boldsymbol{v}^h, \boldsymbol{v}^h) \geq \nu_d C_1 |\!|\!| \boldsymbol{v}_d^h |\!|\!|^2_{X_d} + \frac{\nu_s}{C_2^2} \min\big(2, \frac{\alpha}{\sqrt{\lambda_{\max}}|\Gamma_{sd}|}\big) |\!|\!| \boldsymbol{v}_s^h |\!|\!|^2_{X_s}, \tag{2.3.83}$$

where constant C_1 is independent of mesh sizes h and H and C_2 only depends on the shape regularity of $\mathcal{T}_s$.

Proof. The proof is almost same as the proof of Lemma 3.4 in [27] and the only difference is using (3.31)in [54] to hand coercivity of discrete bilinear form in Darcy part. □

The case when Ω_s is not connected follows from Lemmas 2.3.11 or 2.3.12 applied to each connected component of Ω_s according to if it is adjacent to Γ_s or not.

Note that $a^h(\cdot,\cdot)$ is continuous on $\boldsymbol{X}^h \times \boldsymbol{X}^h$:

$$\begin{aligned}\forall(\boldsymbol{u}^h,\boldsymbol{v}^h)\in \boldsymbol{X}^h\times\boldsymbol{X}^h\,,\ |a^h(\boldsymbol{u}^h,\boldsymbol{v}^h)| \leq & \frac{\nu_d}{\lambda_{\min}}\|\boldsymbol{u}_d^h\|_{L^2(\Omega_d)}\|\boldsymbol{v}_d^h\|_{L^2(\Omega_d)} + 2\,\nu_s\|\nabla\,\boldsymbol{u}_s^h\|_{L^2(\Omega_s)}\|\nabla\,\boldsymbol{v}_s^h\|_{L^2(\Omega_s)} \\ & + \sum_{l=1}^{n-1}\frac{\nu_s\alpha}{\sqrt{\lambda_{\min}}}\|\boldsymbol{u}_s^h\cdot\boldsymbol{\tau}_l\|_{L^2(\Gamma_{sd})}\|\boldsymbol{v}_s^h\cdot\boldsymbol{\tau}_l\|_{L^2(\Gamma_{sd})},\end{aligned} \tag{2.3.84}$$

and $b(\cdot,\cdot)$ is continuous on $\boldsymbol{X}^h \times W^h$:

$$\forall(\boldsymbol{v}^h,w^h)\in\boldsymbol{X}^h\times W^h\,,\ |b(\boldsymbol{v}^h,w^h)|\leq\|\boldsymbol{v}^h\|_{\boldsymbol{X}}\|w^h\|_{L^2(\Omega)}. \tag{2.3.85}$$

To control the bilinear form b in Ω_s, we make the following assumption: There exists a linear approximation operator $\Theta_s^h : H_0^1(\Omega)^n \mapsto V_s^h$ satisfying for all $\boldsymbol{v}\in H_0^1(\Omega)^n$:

- $$\forall i, 1\leq i\leq M_s\,,\ \int_{\Omega_{s,i}}\operatorname{div}\big(\Theta_s^h(\boldsymbol{v})-\boldsymbol{v}\big)=0. \tag{2.3.86}$$
- For any $\hat{\Gamma}_{ij}$ in $\hat{\Gamma}_{sd}$,
$$\int_{\hat{\Gamma}_{ij}}\big(\Theta_s^h(\hat{\boldsymbol{v}})-\hat{\boldsymbol{v}}\big)\cdot\hat{\boldsymbol{n}}_{ij}=0. \tag{2.3.87}$$
- There exists a constant C independent of $\boldsymbol{v}$, h, H, and the diameter of $\Omega_{s,i}$, $1\leq i\leq M_s$, such that
$$\|\Theta_s^h(\boldsymbol{v})\|_{X_s}\leq C|\boldsymbol{v}|_{H^1(\Omega)}. \tag{2.3.88}$$

The construction of the operator Θ_s^h is presented in Section 4 in [27]. In particular, a general construction strategy discussed in Section 4.1 in [27] gives an operator that satisfies (2.3.86) and (2.3.62). The stability bound (2.3.88) is shown to hold for the specific examples presented in Sections 4.2-4.4, see Corollary 4.2 in [27].

Lemma 2.3.13 ([27], Lemma 3.5). *Assuming that an operator Θ_s^h satisfying (2.3.86)–(2.3.88) exists, then there exists a linear operator $\Pi_s^h : H_0^1(\Omega)^n \mapsto V_s^h$ such that for all $\boldsymbol{v} \in H_0^1(\Omega)^n$,*

$$\forall w^h \in W_s^h \,, \sum_{i=1}^{M_s} \int_{\Omega_{s,i}} w^h \mathrm{div}(\Pi_s^h(\boldsymbol{v}) - \boldsymbol{v}) = 0, \tag{2.3.89}$$

$$\forall \hat{\Gamma}_{ij} \in \hat{\Gamma}_{sd} \,, \int_{\hat{\Gamma}_{ij}} \big(\Pi_s^h(\hat{\boldsymbol{v}}) - \hat{\boldsymbol{v}}\big) \cdot \hat{\boldsymbol{n}}_{ij} = 0, \tag{2.3.90}$$

and there exists a constant C independent of $\boldsymbol{v}$, h, H, and the diameter of $\Omega_{s,i}$, $1 \leq i \leq M_s$, such that

$$\|\!|\Pi_s^h(\boldsymbol{v})|\!\|_{X_s} \leq C|\boldsymbol{v}|_{H^1(\Omega)}. \tag{2.3.91}$$

The idea of constructing the operator Π_s^h via the interior inf-sup condition (2.3.39) and the simplified operator Θ_s^h satisfying (2.3.86) and (2.3.88) is not new. It can be found for instance in [26] and [7].

To control the bilinear form b in Ω_d, we make the following assumption: There exists a linear operator $\Pi_d^h : H_0^1(\Omega)^n \mapsto V_d^h$ satisfying for all $\boldsymbol{v} \in H_0^1(\Omega)^n$:

- $$\forall w^h \in W_d^h \,, \sum_{i=1}^{M_d} \int_{\Omega_{d,i}} w^h \mathrm{div}\big(\Pi_d^h(\boldsymbol{v}) - \boldsymbol{v}\big) = 0. \tag{2.3.92}$$

- For any $\hat{\Gamma}_{ij}$ in $\hat{\Gamma}_{sd}$,

$$\forall \hat{\mu}^H \in \hat{\Lambda}_{sd}^H \,, \int_{\hat{\Gamma}_{ij}} \hat{\mu}^H \big(R_d^{RT} \Pi_d^h(\hat{\boldsymbol{v}}) - \Pi_s^h(\hat{\boldsymbol{v}})\big) \cdot \hat{\boldsymbol{n}}_{ij} = 0. \tag{2.3.93}$$

- There exists a constant C independent of $\boldsymbol{v}$, h, H, and the diameter of $\Omega_{d,i}$, $1 \leq i \leq M_d$, such that

$$\|\!|\Pi_d^h(\boldsymbol{v})|\!\|_{X_d} \leq C|\boldsymbol{v}|_{H^1(\Omega)}. \tag{2.3.94}$$

The construction of the operator Π_d^h is presented in Section 2.4. In particular, the general construction strategy discussed in Section 2.4.1 gives an operator that satisfies (2.3.92) and (2.3.68). The stability bound (2.3.94) is shown to hold for various cases in Section 2.4.2.

The next lemma follows readily from the properties of Π_s^h and Π_d^h.

Lemma 2.3.14. *Under the above assumptions, there exists a linear operator* $\Pi^h \in \mathcal{L}(H_0^1(\Omega)^n; V^h)$ *such that for all* $\boldsymbol{v} \in H_0^1(\Omega)^n$

$$\forall w^h \in W^h\,,\ \sum_{i=1}^{M} \int_{\Omega_i} w^h \mathrm{div}\big(\Pi^h(\boldsymbol{v}) - \boldsymbol{v}\big) = 0, \tag{2.3.95}$$

$$\|\!|\Pi^h(\boldsymbol{v})|\!\|_X \leq C|\boldsymbol{v}|_{H^1(\Omega)}, \tag{2.3.96}$$

with a constant C *independent of* $\boldsymbol{v}$, h, H, *and the diameter of* Ω_i, $1 \leq i \leq M$.

Proof. Take $\Pi^h(\boldsymbol{v})|_{\Omega_s} = \Pi_s^h(\boldsymbol{v})$ and $\Pi^h(\boldsymbol{v})|_{\Omega_d} = \Pi_d^h(\boldsymbol{v})$. Then (2.3.95) follows from (2.3.89) and (2.3.92). The matching condition of the functions of V^h at the interfaces of Γ_{sd} holds by virtue of (2.3.68). Finally, the stability bound (2.3.96) stems from (2.3.91) and (2.3.94). □

The following inf-sup condition between W^h and V^h is an immediate consequence of a simple variant of Fortin's Lemma [25, 11] and Lemma 2.3.14.

Theorem 2.3.2. *Under the above assumptions, there exists a constant* $\beta^\star > 0$, *independent of* h, H, *and the diameter of* Γ_{ij} *for all* $i < j$ *such that*

$$\forall w^h \in W^h,\ \sup_{\boldsymbol{v}^h \in V^h} \frac{b(\boldsymbol{v}^h, w^h)}{|\!\|\boldsymbol{v}^h|\!\|_X} \geq \beta^\star \|w^h\|_{L^2(\Omega)}. \tag{2.3.97}$$

Finally, well-posedness of the discrete scheme (2.3.77) follows from Lemma 2.3.11 or 2.3.12 and Theorem 2.3.2.

Corollary 2.3.2 ([27],corollary 4.1)**.** *Under the above assumptions, problem* (2.3.77) *has a unique solution* $(\boldsymbol{u}^h, p^h) \in V^h \times W^h$ *and*

$$|\!\|\boldsymbol{u}^h|\!\|_X + \|p^h\|_{L^2(\Omega)} \leq C\big(\|\boldsymbol{f}\|_{L^2(\Omega)} + \|q_d\|_{L^2(\Omega_d)}\big), \tag{2.3.98}$$

with a constant C *independent of* h, H, *and the diameter of* Γ_{ij} *for all* $i < j$.

2.4 CONSTRUCTION OF THE APPROXIMATION OPERATORS Θ_S^H AND Π_D^H

The Stokes interpolation operator Θ_s^h with values in V_s^h, satisfying (2.3.86)–(2.3.88), uniformly stable with respect to the diameter of the subdomains and interfaces has been constrcuted in [27] . Thus, in this section we only propose a construction of Darcy approximation operator Π_d^h .A general construction of Π_d^h in Ω_d can be found in [1], and we shall adapt it so that it matches suitably Θ_s^h on Γ_{sd}.

2.4.1 General construction strategy

We propose the following two-step construction algorithm in Ω_d.

1. Starting step. Set $P_d^h(\boldsymbol{v}) = R_d^h(\boldsymbol{v}) \in X_d^h$, where $R_d^h(\boldsymbol{v})$ is a standard mixed approximation operator associated with W_d^h. It preserves the normal component on the boundary:

$$\forall \Gamma_{ij} \subset \partial\Omega_{d,k}, 1 \leq k \leq M_d\,,\ \forall \boldsymbol{v}^h \in X_d^h,\ \int_{\Gamma_{ij}} \boldsymbol{v}^h \cdot \boldsymbol{n}_{ij} \left(R_d^h(\boldsymbol{v})|_{\Omega_{d,k}} - \boldsymbol{v}\right) \cdot \boldsymbol{n}_{ij} = 0, \quad (2.4.1)$$

and satisfies

$$\forall 1 \leq i \leq M_d\,,\ \forall w^h \in W_d^h\,,\ \int_{\Omega_{d,i}} w^h \mathrm{div}\big(R_d^h(\boldsymbol{v}) - \boldsymbol{v}\big) = 0. \quad (2.4.2)$$

2. Correction step. It remains to prescribe the jump condition. For each $\Gamma_{ij} \in \Gamma_{dd} \cup \Gamma_{sd}$ with $i < j$, correct $P_d^h(\boldsymbol{v})$ in $\Omega_{d,j}$ by setting:

$$P_d^h(\boldsymbol{v})|_{\Omega_{d,j}} := P_d^h(\boldsymbol{v})|_{\Omega_{d,j}} + \boldsymbol{c}_{j,\Gamma_{ij}}^h(\boldsymbol{v}),$$

where $\boldsymbol{c}_{j,\Gamma_{ij}}^h(\boldsymbol{v}) \in X_{d,j}^h$, $\boldsymbol{c}_{j,\Gamma_{ij}}^h(\boldsymbol{v}) \cdot \boldsymbol{n}_j = 0$ on $\partial\Omega_{d,j} \setminus \Gamma_{ij}$, $\mathrm{div}\, \boldsymbol{c}_{j,\Gamma_{ij}}^h(\boldsymbol{v}) = 0$ in $\Omega_{d,j}$,

$$\begin{aligned}
&\forall \mu^H \in \Lambda_d^H\,,\ \int_{\Gamma_{ij}} \mu^H R_d^{RT} \boldsymbol{c}_{j,\Gamma_{ij}}^h(\boldsymbol{v}) \cdot \boldsymbol{n}_{ij} = \int_{\Gamma_{ij}} \mu^H \big(R_d^{RT} R_d^h(\boldsymbol{v})|_{\Omega_{d,i}} - R_d^{RT} R_d^h(\boldsymbol{v})|_{\Omega_{d,j}}\big) \cdot \boldsymbol{n}_{ij}, \\
&\forall \mu^H \in \Lambda_{sd}^H\,,\ \int_{\Gamma_{ij}} \mu^H R_d^{RT} \boldsymbol{c}_{j,\Gamma_{ij}}^h(\boldsymbol{v}) \cdot \boldsymbol{n}_{ij} = \int_{\Gamma_{ij}} \mu^H \big(\Pi_s^h(\boldsymbol{v})|_{\Omega_{s,i}} - R_d^{RT} R_d^h(\boldsymbol{v})|_{\Omega_{d,j}}\big) \cdot \boldsymbol{n}_{ij},
\end{aligned} \quad (2.4.3)$$

and $\boldsymbol{c}^h_{j,\Gamma_{ij}}(\boldsymbol{v})$ satisfies adequate bounds. Existence of a non necessarily divergence-free $\boldsymbol{c}^h_{j,\Gamma_{ij}}(\boldsymbol{v})$ (without bounds) follows from (2.3.45); it suffices to extend suitably $R^h_d(\boldsymbol{v})|_{\Omega_{d,j}}$ and $R^h_d(\boldsymbol{v})|_{\Omega_{d,i}}$ or $\Pi^h_s(\boldsymbol{v})|_{\Omega_{s,i}}$. The zero divergence will be prescribed in the examples. Note that $\boldsymbol{c}^h_{j,\Gamma_{ij}}(\boldsymbol{v})$ has no effect on interfaces other than Γ_{ij} and no effect on the restriction of $P^h_d(\boldsymbol{v})$ in $\Omega_{d,i}$ or on that of $\Pi^h_s(\boldsymbol{v})$ in $\Omega_{s,i}$. Therefore these corrections can be superimposed.

When step 2 is done on all $\Gamma_{ij} \in \Gamma_{dd} \cup \Gamma_{sd}$ with $i < j$, the resulting function $P^h_d(\boldsymbol{v})$ has zero normal trace on Γ_d, it belongs to V^h_d since, due to the first equation in (2.4.3), it satisfies for all $\Gamma_{ij} \in \Gamma_{dd}$ with $i < j$

$$\forall \mu^H \in \Lambda^H_d \, , \int_{\Gamma_{ij}} \mu^H [R^{RT}_d P^h_d(\boldsymbol{v}) \cdot \boldsymbol{n}] = 0, \tag{2.4.4}$$

and, as the corrections are assumed to be divergence-free in each subdomain,

$$\forall w^h \in W^h_d \, , \, \forall 1 \leq i \leq M_d \, , \int_{\Omega_{d,i}} w^h \mathrm{div}\big(P^h_d(\boldsymbol{v}) - \boldsymbol{v}\big) = 0. \tag{2.4.5}$$

Furthermore, due to the second equation in (2.4.3), it satisfies for all $\Gamma_{ij} \in \Gamma_{sd}$,

$$\forall \mu^H \in \Lambda^H_{sd} \, , \int_{\Gamma_{ij}} \mu^H \big(\Pi^h_s(\boldsymbol{v})|_{\Omega_{s,i}} - R^{RT}_d P^h_d(\boldsymbol{v})|_{\Omega_{d,j}}\big) \cdot \boldsymbol{n}_{ij} = 0. \tag{2.4.6}$$

Therefore, taking $\Pi^h_d(\boldsymbol{v}) = P^h_d(\boldsymbol{v})$ in Ω_d, it satisfies (2.3.92) and (2.3.68).

We need to refine the assumptions on the meshes at the interfaces and refine Hypothesis 2.3.1 on the mesh of subdomains.

Hypothesis 2.4.1. *For $i < j$, let T be any element of $\mathcal{T}^h_i$ that is adjacent to Γ_{ij}, and let $\{T_\ell\}$ denote the set of elements of $\mathcal{T}^h_j$ that intersect T. The number of elements in this set is bounded by a fixed integer and there exists a constant C such that*

$$\frac{|T_\ell|}{|T|} \leq C.$$

The same is true if the indices i and j of the triangulations are interchanged. These constants are independent of i, j, h, and the diameters of the interfaces and subdomains.

Hypothesis 2.4.2. *1. Each Ω_i, $1 \leq i \leq M$, is the image of a "reference" polygonal or polyhedral domain by an homothety and a rigid body motion:*

$$\Omega_i = F_i(\hat{\Omega}_i) \ , \ \boldsymbol{x} = F_i(\hat{\boldsymbol{x}}) = A_i R_i \hat{\boldsymbol{x}} + \boldsymbol{b}_i, \tag{2.4.7}$$

where $A_i = \mathrm{diam}(\Omega_i)$, R_i is an orthogonal matrix with constant coefficients and $\boldsymbol{b}_i$ a constant vector.

2. There exists a constant σ_1 independent of M such that for any pair of adjacent subdomains Ω_i and Ω_j, $1 \leq i, j \leq M$, we have

$$\frac{A_i}{A_j} \leq \sigma_1. \tag{2.4.8}$$

By (2.4.7) $\mathrm{diam}(\hat{\Omega}_i) = 1$. In addition, it follows from Hypothesis 2.3.1 that on one hand the reference domains $\hat{\Omega}_i$ can take at most L configurations and on the other hand,

$$\forall i, 1 \leq i \leq M \ , \ \mathrm{diam}(\hat{B}_i) \geq \frac{1}{\sigma}, \tag{2.4.9}$$

where $\hat{B}_i$ is the largest ball contained in $\hat{\Omega}_i$ and σ is the constant of (2.3.37).

2.4.2 A construction of $\boldsymbol{c}^h_{j,\Gamma_{ij}}(\boldsymbol{v})$ in Ω_d.

Here we construct a correction $\boldsymbol{c}^h_{j,\Gamma_{ij}}(\boldsymbol{v})$ in Ω_d satisfying (2.4.3) and suitable continuity bounds that are needed to establish the stability estimate (2.3.94). Recall that the existence of $\boldsymbol{c}^h_{j,\Gamma_{ij}}(\boldsymbol{v})$ relies on (2.3.45). In the construction below we directly show that (2.3.45) holds for a wide range of mesh configurations.

Let $\boldsymbol{v}$ be given in $H^1_0(\Omega)^n$. Recall that the mixed approximation operator R^h_d defined in each $\Omega_{d,i}$ takes its values in X^h_d and satisfies (2.4.1) on each $\Gamma_{ij} \subset \partial\Omega_{d,k}$, $1 \leq k \leq M_d$, and (2.4.2) in each $\Omega_{d,i}$, $1 \leq i \leq M_d$. Furthermore there exists a constant C independent of h and the geometry of $\Omega_{d,i}$, such that

$$\forall \boldsymbol{v} \in H^1_0(\Omega)^n \ , \ \|R^h_d(\boldsymbol{v})\|_{H(\mathrm{div};\Omega_{d,i})} \leq C\|\boldsymbol{v}\|_{H^1(\Omega_{d,i})}, 1 \leq i \leq M_d. \tag{2.4.10}$$

This is easily established by observing that the moments defining the degrees of freedom of $R_d^h(\boldsymbol{v})$ are invariant by homothety and rigid-body motion; in particular the normal vector is preserved. In addition, it satisfies (2.3.42):

$$\forall i, 1 \leq i \leq M_d\,,\ \forall \boldsymbol{v}^h \in X_{d,i}^h\,,\ \mathrm{div}\,\boldsymbol{v}^h \in W_{d,i}^h.$$

The above properties also imply (2.3.41): for all i, $1 \leq i \leq M_d$,

$$\inf_{w^h \in W_{0,d,i}^h} \sup_{\boldsymbol{v}^h \in X_{0,d,i}^h} \frac{\int_{\Omega_{d,i}} w^h \mathrm{div}\,\boldsymbol{v}^h}{\|\boldsymbol{v}^h\|_{H(\mathrm{div};\Omega_{d,i})}\|w^h\|_{L^2(\Omega_{d,i})}} \geq \beta_d^\star,$$

with a constant $\beta_d^\star > 0$ independent of h and A_i.

Now, let $\Gamma_{ij} \in \Gamma_{dd} \cup \Gamma_{sd}$; by analogy with the situation in the Stokes region, we denote by $X_{d,j,\Gamma_{ij}}^h$ the trace space of $X_{d,j}^h$ on Γ_{ij}. Following [1], we define the space of normal traces

$$X_{j,\Gamma_{ij}}^{\boldsymbol{n}} = \{\boldsymbol{w} \cdot \boldsymbol{n}_{ij}\,;\ \boldsymbol{w} \in X_{d,j,\Gamma_{ij}}^h\},$$

and the orthogonal projection $Q_{j,\Gamma_{ij}}^h$ from $L^2(\Gamma_{ij})$ into $X_{j,\Gamma_{ij}}^{\boldsymbol{n}}$. Then we make the following assumption: There exists a constant C, independent of H, h, i, j, and the diameters of Γ_{ij} and $\Omega_{d,j}$, such that

$$\forall \mu^H \in \Lambda_d^H\,, \forall \mu^H \in \Lambda_{sd}^H\,,\ \|\mu^H\|_{L^2(\Gamma_{ij})} \leq C\|Q_{j,\Gamma_{ij}}^h(\mu^H)\|_{L^2(\Gamma_{ij})}. \tag{2.4.11}$$

It is shown in [58] that (2.4.11) holds for both continuous and discontinuous mortar spaces, if the mortar grid $\mathcal{T}_{ij}^H$ is a coarsening by two of $\mathcal{T}_{j,\Gamma_{ij}}^h$. A similar inequality for more general grid configurations is shown in [42]. Formula (2.4.11) implies that the projection $Q_{j,\Gamma_{ij}}^h$ is an isomorphism from the restriction of Λ_{sd}^H, respectively Λ_d^H, to Γ_{ij}, say $\Lambda_{sd,ij}^H$ respectively $\Lambda_{d,ij}^H$, onto its image in $X_{j,\Gamma_{ij}}^{\boldsymbol{n}}$, and the norm of its inverse is bounded by C. Then a standard algebraic argument shows that its dual operator, namely the orthogonal projection from $X_{j,\Gamma_{ij}}^{\boldsymbol{n}}$ into $\Lambda_{sd,ij}^H$, respectively $\Lambda_{d,ij}^H$, is also an isomorphism from the orthogonal complement in $X_{j,\Gamma_{ij}}^{\boldsymbol{n}}$ of the projection's kernel onto $\Lambda_{sd,ij}^H$, respectively $\Lambda_{d,ij}^H$, and the norm of its inverse is also bounded by C. As a consequence, for each $f \in L^2(\Gamma_{ij})$, there exists $\boldsymbol{v}^h \cdot \boldsymbol{n}_{ij} \in X_{j,\Gamma_{ij}}^{\boldsymbol{n}}$ such that

$$\forall \mu_H \in \Lambda_d^H\,, \forall \mu_H \in \Lambda_{sd}^H\,,\ \int_{\Gamma_{ij}} \mu^H R_d^{RT} \boldsymbol{v}^h \cdot \boldsymbol{n}_{ij} = \int_{\Gamma_{ij}} f\mu^H,$$

and there exists a constant C independent of h, and the diameter of Γ_{ij}, such that

$$\|\boldsymbol{v}^h \cdot \boldsymbol{n}_{ij}\|_{L^2(\Gamma_{ij})} \leq C\|f\|_{L^2(\Gamma_{ij})}.$$

This implies that (2.3.45) holds. Furthermore, the solution $\boldsymbol{v}^h \cdot \boldsymbol{n}_{ij}$ is unique in the orthogonal complement of the projection's kernel and by virtue of this uniqueness, $\boldsymbol{v}^h \cdot \boldsymbol{n}_{ij}$ depends linearly on f. This result permits to partially solve (2.4.3).

Lemma 2.4.1. *Let $\boldsymbol{v} \in H_0^1(\Omega)^n$. Under assumption (2.4.11), for each $\Gamma_{ij} \in \Gamma_{dd} \cup \Gamma_{sd}$, there exists $\boldsymbol{w}^h \cdot \boldsymbol{n}_{ij} \in X^{\boldsymbol{n}}_{j,\Gamma_{ij}}$ such that*

$$\begin{aligned} \forall \mu^H \in \Lambda_d^H\,,\ \int_{\Gamma_{ij}} \mu^H R_d^{RT} \boldsymbol{w}^h \cdot \boldsymbol{n}_{ij} &= \int_{\Gamma_{ij}} \mu^H \big[R_d^{RT} R_d^h(\boldsymbol{v}) \cdot \boldsymbol{n}\big], \\ \|\boldsymbol{w}^h \cdot \boldsymbol{n}_{ij}\|_{L^2(\Gamma_{ij})} &\leq C\|\big[R_d^h(\boldsymbol{v}) \cdot \boldsymbol{n}\big]\|_{L^2(\Gamma_{ij})}, \end{aligned} \tag{2.4.12}$$

$$\begin{aligned} \forall \mu^H \in \Lambda_{sd}^H\,,\ \int_{\Gamma_{ij}} \mu^H R_d^{RT} \boldsymbol{w}^h \cdot \boldsymbol{n}_{ij} &= \int_{\Gamma_{ij}} \mu^H \big(\Theta_s^h(\boldsymbol{v})|_{\Omega_{s,i}} - R_d^{RT} R_d^h(\boldsymbol{v})|_{\Omega_{d,j}}\big) \cdot \boldsymbol{n}_{ij}, \\ \|\boldsymbol{w}^h \cdot \boldsymbol{n}_{ij}\|_{L^2(\Gamma_{ij})} &\leq C\|\big(\Theta_s^h(\boldsymbol{v})|_{\Omega_{s,i}} - R_d^h(\boldsymbol{v})|_{\Omega_{d,j}}\big) \cdot \boldsymbol{n}_{ij}\|_{L^2(\Gamma_{ij})}, \end{aligned} \tag{2.4.13}$$

with the constant C of (2.4.11). The mapping $\boldsymbol{v} \mapsto \boldsymbol{w}^h \cdot \boldsymbol{n}_{ij}$ is linear.

Lemma 2.4.1 constructs a normal trace $\boldsymbol{w}^h \cdot \boldsymbol{n}_{ij}$ on Γ_{ij} and we must extend it inside $\Omega_{d,j}$. To this end, let $\ell^h \in L^2(\partial\Omega_{d,j})$ be the extension of $\boldsymbol{w}^h \cdot \boldsymbol{n}_{ij}$ by zero on $\partial\Omega_{d,j}$. Next, we solve the problem: Find $q \in H^1(\Omega_{d,j}) \cap L_0^2(\Omega_{d,j})$ such that

$$\Delta\, q = 0 \text{ in } \Omega_{d,j}\ ,\ \frac{\partial q}{\partial \boldsymbol{n}_j} = \ell^h \text{ on } \partial\Omega_{d,j}. \tag{2.4.14}$$

Lemma 2.4.2 (Lemma 4.8, [27])**.** *Problem (2.4.14) has one and only one solution $q \in H^{3/2}(\Omega_{d,j}) \cap L_0^2(\Omega_{d,j})$ and*

$$\begin{aligned} &|q|_{H^1(\Omega_{d,j})} \leq C\sqrt{A_j}\|[R_d^h(\boldsymbol{v}) \cdot \boldsymbol{n}]\|_{L^2(\Gamma_{ij})}, \\ &|q|_{H^{3/2}(\Omega_{d,j})} \leq C\|[R_d^h(\boldsymbol{v}) \cdot \boldsymbol{n}]\|_{L^2(\Gamma_{ij})},\ \Gamma_{ij} \in \Gamma_{dd}, \end{aligned} \tag{2.4.15}$$

$$\begin{aligned} &|q|_{H^1(\Omega_{d,j})} \leq C\sqrt{A_j}\|\big(\Theta_s^h(\boldsymbol{v})|_{\Omega_{s,i}} - R_d^h(\boldsymbol{v})|_{\Omega_{d,j}}\big) \cdot \boldsymbol{n}_{ij}\|_{L^2(\Gamma_{ij})}, \\ &|q|_{H^{3/2}(\Omega_{d,j})} \leq C\|\big(\Theta_s^h(\boldsymbol{v})|_{\Omega_{s,i}} - R_d^h(\boldsymbol{v})|_{\Omega_{d,j}}\big) \cdot \boldsymbol{n}_{ij}\|_{L^2(\Gamma_{ij})},\ \Gamma_{ij} \in \Gamma_{sd}, \end{aligned} \tag{2.4.16}$$

with constants C independent of h, H, q, i, j, and the diameters of Γ_{ij} and $\Omega_{d,j}$.

Now define $\boldsymbol{c} = \nabla q$ in $\Omega_{d,j}$. Then $\boldsymbol{c}$ belongs to $H(\mathrm{div};\Omega_{d,j}) \cap H^{1/2}(\Omega_{d,j})^n$ and $\mathrm{div}\,\boldsymbol{c} = 0$. Therefore $R_d^h(\boldsymbol{c})$ is well defined [11] and satisfies the approximation property for divergence-free functions [38]

$$\|\boldsymbol{c} - R_d^h(\boldsymbol{c})\|_{L^2(\Omega_{d,j})} \leq Ch^r |\boldsymbol{c}|_{H^r(\Omega_{d,j})}, \quad 0 < r \leq 1/2, \tag{2.4.17}$$

with a constant C independent of h, j, and the diameter of $\Omega_{d,j}$. We are now ready to define the correction $\boldsymbol{c}_{j,\Gamma_{ij}}^h(\boldsymbol{v})$. In particular, take $\boldsymbol{c}_{j,\Gamma_{ij}}^h(\boldsymbol{v}) = R_d^h(\boldsymbol{c})$ applied in $\Omega_{d,j}$. Note that $\boldsymbol{c}_{j,\Gamma_{ij}}^h(\boldsymbol{v})$ belongs to $X_{d,j}^h$, and (2.4.2) and (2.4.1) imply that $\mathrm{div}\,\boldsymbol{c}_{j,\Gamma_{ij}}^h(\boldsymbol{v}) = 0$ in $\Omega_{d,j}$ and $\boldsymbol{c}_{j,\Gamma_{ij}}^h(\boldsymbol{v}) \cdot \boldsymbol{n}_j = \ell^h = \boldsymbol{w}^h \cdot \boldsymbol{n}_{ij}$ on Γ_{ij}. Therefore (2.4.12) and (2.4.13) imply that $\boldsymbol{c}_{j,\Gamma_{ij}}^h(\boldsymbol{v})$ satisfies (2.4.3). Furthermore, (2.4.17) yields

$$\|\boldsymbol{c}_{j,\Gamma_{ij}}^h(\boldsymbol{v})\|_{L^2(\Omega_{d,j})} \leq \|R_d^h(\boldsymbol{c}) - \boldsymbol{c}\|_{L^2(\Omega_{d,j})} + \|\boldsymbol{c}\|_{L^2(\Omega_{d,j})} \leq Ch_j^{1/2} |\boldsymbol{c}|_{H^{1/2}(\Omega_{d,j})} + \|\boldsymbol{c}\|_{L^2(\Omega_{d,j})},$$

with a constant C independent of the geometry of $\Omega_{d,j}$. Considering that $h_j \leq A_j$, Lemma 2.4.2 gives

$$\|\boldsymbol{c}_{j,\Gamma_{ij}}^h(\boldsymbol{v})\|_{L^2(\Omega_{d,j})} \leq C\sqrt{A_j}\|[R_d^h(\boldsymbol{v}) \cdot \boldsymbol{n}]\|_{L^2(\Gamma_{ij})}, \quad \Gamma_{ij} \in \Gamma_{dd}, \tag{2.4.18}$$

$$\|\boldsymbol{c}_{j,\Gamma_{ij}}^h(\boldsymbol{v})\|_{L^2(\Omega_{d,j})} \leq C\sqrt{A_j}\|(\Theta_s^h(\boldsymbol{v})|_{\Omega_{s,i}} - R_d^h(\boldsymbol{v})|_{\Omega_{d,j}}) \cdot \boldsymbol{n}_{ij}\|_{L^2(\Gamma_{ij})}, \quad \Gamma_{ij} \in \Gamma_{sd}, \tag{2.4.19}$$

with a constant C independent of h, H, $\boldsymbol{v}$, i, j, and the diameters of Γ_{ij} and $\Omega_{d,j}$.

Corollary 2.4.1 (Corollary 4.3, [27]). *The approximation operator Π_d^h constructed in Section 2.4.1 with corrections $\boldsymbol{c}_{j,\Gamma_{ij}}^h(\boldsymbol{v})$ described above satisfies assumption (2.3.94).*

2.5 ERROR ANALYSIS

In this section we establish *a priori* error estimates for our method. Let us assume that the finite element spaces X_s^h and W_s^h in Ω_s contain at least polynomials of degree r_s and $r_s - 1$, respectively. Let X_d^h and W_d^h in Ω_d contain at least polynomials of degree r_d and l_d, respectively. Since here we employ MFMFE in Darcy flow, then $r_d = l_d = 0$. Let Λ_{sd}^H, Λ_d^H, and Λ_s^H contain at least polynomials of degree r_{sd}, r_{dd}, and r_{ss}, respectively. In the analysis we will make use of the following well known approximation properties of the mixed interpolants on simplicial, h^2-parallelogram, and h^2-parallelepiped grids, the following bounds hold on any element E:

$$\|\mathbf{q} - R_d^{RT}\mathbf{q}\|_E + \|\mathbf{q} - R_d^h\mathbf{q}\|_E \lesssim h\|\mathbf{q}\|_{1,E}, \tag{2.5.1}$$

$$\|\nabla\cdot(\mathbf{q} - R_d^{RT}\mathbf{q})\|_E + \|\nabla\cdot(\mathbf{q} - R_d^h\mathbf{q})\|_E \lesssim h\|\nabla\cdot\mathbf{q}\|_{1,E}. \tag{2.5.2}$$

The above bounds can be found in [11, 32] for simplicial elements, [33, 15] for h^2-parallelograms, and [29] for h^2-parallelepipeds. A higher order approximation property also holds for simplicial, h^2-parallelogram, and regular h^2-parallelepiped grids:

$$\|\mathbf{q} - R_d^h\mathbf{q}\|_E \lesssim h^2\|\mathbf{q}\|_{2,E}. \tag{2.5.3}$$

On general quadrilaterals, bound (2.5.1) is also valid [15]. However, in this case for the divergence bound it only holds for

$$\|\nabla\cdot(\mathbf{q} - R_d^h\mathbf{q})\|_E \lesssim \|\nabla\cdot\mathbf{q}\|_E.$$

We will need following well-know estimates for the non-symmetric MFMFE error analysis. There exits $s^1 \in P_1(E)$ such that

$$\|p - s^1\|_{j,E} \lesssim h^{2-j}\|p\|_{2,E}, \quad j = 0, 1, \tag{2.5.4}$$

and

$$\|p - s^1\|_E \lesssim h\|p\|_{1,E}. \tag{2.5.5}$$

We also have

$$\|\boldsymbol{K} - \overline{\boldsymbol{K}}_E\|_E \lesssim h\|\boldsymbol{K}\|_{1,E}. \tag{2.5.6}$$

Lemma 2.5.1. *The following estimates hold for all* $\mathbf{q} \in (H^1(E))^d$*:*

$$\|R_d^h \mathbf{q}\|_E \lesssim \|\mathbf{q}\|_E + h|\mathbf{q}|_{1,E}, \tag{2.5.7}$$

The following lemma for symmetric MFMFE has been shown in [55, 29].

Lemma 2.5.2. *For all elements* E*,*

$$\|R_d^h \mathbf{q}\|_{j,E} \lesssim \|\mathbf{q}\|_{j,E}, \quad \forall \mathbf{q} \in H^j(E)^d, \tag{2.5.8}$$

holds for $j = 1, 2$ *on simplicial elements,* h^2*-parallelograms, and regular* h^2*-parallelepipeds, as well as* $j = 1$ *on* h^2*-parallelepipeds. Furthermore, on simplicial elements,* h^2*-parallelograms, and* h^2*-parallelepipeds,*

$$\|R_d^{RT} \mathbf{q}\|_{1,E} \lesssim \|\mathbf{q}\|_{1,E}, \quad \forall \mathbf{q} \in H^1(E)^d. \tag{2.5.9}$$

Lemma 2.5.3. *Under assumption (5.24) in [54], there exists a projection operator* $\Pi_d^h : \left(H^{1/2+\epsilon}(\Omega)\right)^d \cap \boldsymbol{X}_d \to \boldsymbol{V}_d^h$ *such that*

$$(\nabla \cdot (\Pi_d^h \mathbf{q} - \mathbf{q}), w)_{\Omega_{d,i}} = 0, \quad w \in W_h, \quad 1 \le i \le n, \tag{2.5.10}$$

$$\|\Pi_d^h \mathbf{q} - R_d^h \mathbf{q}\|_{\Omega_d} \lesssim \|\mathbf{q}\|_{r+1/2} h^r H^{1/2}, \quad 0 < r \le 1, \tag{2.5.11}$$

$$\|\Pi_d^h \mathbf{q} - \mathbf{q}\|_{\Omega_d} \lesssim \sum_{i=1}^{n} \|\mathbf{q}\|_{1,\Omega_{d,i}} h + \|\mathbf{q}\|_{r+1/2} h^r H^{1/2}, \quad 0 < r \le 1, \tag{2.5.12}$$

Lemma 2.5.4 ([55, 29])**.** *On* h^2*-parallelograms and* h^2*-parallelepipeds, if* $K^{-1} \in W^{1,\infty}_{\mathcal{T}_d^h}$*, then for all* $\mathbf{v} \in \mathbf{X}_d^h$*,*

$$|(K^{-1} R_d^h \mathbf{u}, \mathbf{v} - R_d^{RT} \mathbf{v})_{Q,\Omega_d}| \lesssim \sum_{i=M_s+1}^{M} h \|\!| K^{-1} |\!\|_{1,\infty} \|\mathbf{u}\|_{1,\Omega_i} \|\mathbf{v}\|_{\Omega_i}. \tag{2.5.13}$$

Lemma 2.5.5 ([55, 29])**.** *On simplicial elements,* h^2*-parallelograms, and* h^2*-parallelepipeds, if* $K^{-1} \in W^{1,\infty}_{\mathcal{T}_h}$*, then for all* $\mathbf{q} \in \mathbf{X}_d^h$ *and for all* $\mathbf{v} \in \mathbf{X}_{d,h}^{RT}$*, the numerical quadrature error satisfies*

$$|\sigma(K^{-1}\mathbf{q}, \mathbf{v})_{\Omega_d}| \lesssim \sum_{E \in \mathcal{T}_d^h} h \|K^{-1}\|_{1,\infty,E} \|\mathbf{q}\|_{1,E} \|\mathbf{v}\|_{0,E}. \tag{2.5.14}$$

We begin with the following approximation result for the operator Π^h defined in Lemma 2.3.14.

Lemma 2.5.6 ([27], Lemma 5.1)**.** *Under the assumptions of Lemma 2.3.14, the operator* $\Pi^h \in \mathcal{L}(H_0^1(\Omega)^n; V^h)$ *satisfies for all* $\boldsymbol{v} \in \left(H^t(\Omega) \cap H_0^1(\Omega)\right)^n$, $t \geq 1$,

$$\|\!|\boldsymbol{v} - \Pi^h(\boldsymbol{v})|\!\|_{X_s} \leq C h^r |\boldsymbol{v}|_{H^{r+1}(\Omega)}, \quad 0 \leq r \leq \min(r_s, t-1), \tag{2.5.15}$$

$$\begin{aligned} \|\!|\boldsymbol{v} - \Pi^h(\boldsymbol{v})|\!\|_{X_d} \leq C \left(h^r \|\boldsymbol{v}\|_{H^{r+1/2}(\Omega)} + h^q \|\operatorname{div} \boldsymbol{v}\|_{H^q(\Omega)} + h^s \|\boldsymbol{v}\|_{H^{s+1}(\Omega)} \right), \\ 1/2 \leq r \leq \min(1, t-1/2),\ 0 \leq q \leq \min(1, t-1),\ 0 \leq s \leq \min(r_s, t-1). \end{aligned} \tag{2.5.16}$$

Proof. The proof is almost same as Lemma 5.3 in [27] by using the continuity of Raviart-Thomas interpolant (2.3.24). □

Next, we need to approximate the functions for the pressure. For any $q \in L^2(\Omega_i)$, let $\mathcal{P}^h q$ be its $L^2(\Omega_i)$-projection onto $W_i^h = W^h|_{\Omega_i}$,

$$(q - \mathcal{P}^h q, w^h) = 0, \ \forall w^h \in W_i^h \ ,$$

satisfying the approximation property

$$\|q - \mathcal{P}^h q\|_{0,\Omega_i} \leq C\, h^r |q|_r \ , \ 0 \leq r \leq r_i + 1, \tag{2.5.17}$$

where r_i is the polynomial degree in the space W_i^h: $r_i = r_s - 1$ in Ω_s and $r_i = l_d$ in Ω_d.

Lemma 2.5.7. *There exists a constant* C *independent of* h, H, *and the diameters of the subdomains such that, for all* $\boldsymbol{v}^h \in X^h$*:*

$$|b_s(\boldsymbol{v}^h, \boldsymbol{\lambda}_s - \mathcal{I}^H(\boldsymbol{\lambda}_s))| \leq C\, H^s \sum_{i=1}^{M_s} A_i^{-1/2} \|\boldsymbol{v}^h\|_{H^1(\Omega_{s,i})} |\boldsymbol{\lambda}_s|_{H^s(\partial\Omega_{s,i} \cap \Gamma_{ss} \cup \mathcal{O})}, \quad 0 \leq s \leq r_{ss} + 1, \tag{2.5.18}$$

provided $\boldsymbol{\lambda}_s$ *is sufficiently smooth.*

Proof. The proof is same as Lemma 5.2 in [27]. □

Lemma 2.5.8. *Under Hypothesis 5.1 in [27], there exists a constant C independent of h, H, and the diameters of the subdomains such that, for all $\boldsymbol{v}^h \in X^h$:*

$$
\begin{aligned}
&|b^h_{sd}(\boldsymbol{v}^h, \lambda_{sd} - \mathcal{I}^H(\lambda_{sd})) + b^h_d(\boldsymbol{v}^h, \lambda_d - \mathcal{I}^H(\lambda_d))| \\
&\qquad \leq C \Big(\sum_{i=1}^{M_d} \|\boldsymbol{v}^h\|_{H(\mathrm{div};\Omega_{d,i})} \big(H^{q-1/2} |\lambda|_{H^q(\partial\Omega_{d,i}\cap\Gamma_{dd}\cup\mathcal{O})} + H^{r-1/2} |\lambda|_{H^r(\partial\Omega_{d,i}\cap\Gamma_{sd}\cup\mathcal{O})} \big) \\
&\qquad\qquad + \sum_{i=1}^{M_d} \sum_j A_j^{-1/2} \|\boldsymbol{v}^h\|_{H^1(\Omega_{s,j})} H^r |\lambda|_{H^r(\partial\Omega_{d,i}\cap\Gamma_{sd}\cup\mathcal{O})} \Big), \\
&\qquad\qquad\qquad 1/2 \leq q \leq r_{dd} + 1, \;\; 1/2 \leq r \leq r_{sd} + 1,
\end{aligned}
\tag{2.5.19}
$$

provided λ_{sd} and λ_d are sufficiently smooth, and where the last sum runs over all $\Omega_{s,j}$ adjacent to $\Omega_{d,i}$.

Proof. The proof is almost same as Lemma 5.3 in [27] by using the continuity of R_d^{RT} (2.3.24) . □

Lemma 2.5.9. *There exists a constant C independent of h, H, and the diameters of the subdomains such that, for all $\boldsymbol{v}^h \in X^h$:*

$$
|\hat{b}_s(\boldsymbol{v}^h, \boldsymbol{\lambda}_s - \mathcal{I}^H(\boldsymbol{\lambda}_s))| \leq C\, H^s \sum_{i=1}^{M_s} A_i^{-1/2} \|\boldsymbol{v}^h\|_{H^1(\Omega_{s,i})} |\boldsymbol{\lambda}_s|_{H^s(\partial\Omega_{s,i}\cap\Gamma_{ss}\cup\mathcal{O})}, \quad 0 \leq s \leq r_{ss} + 1,
\tag{2.5.20}
$$

provided $\boldsymbol{\lambda}_s$ is sufficiently smooth.

Proof. The proof is almost same as Lemma 5.2 in [27] by assuming that there exist a the global smooth map to guarantee $\|\hat{\lambda}\| \lesssim \|\lambda\|$ and $\|\hat{\boldsymbol{v}}\| \lesssim \|\boldsymbol{v}\|$. □

Lemma 2.5.10. *Under Hypothesis 5.1 in [27], there exists a constant C independent of h, H, and the diameters of the subdomains such that, for all $\boldsymbol{v}^h \in X^h$:*

$$
\begin{aligned}
&|\hat{b}^h_{sd}(\boldsymbol{v}^h, \lambda_{sd} - \mathcal{I}^H(\lambda_{sd})) + \hat{b}^h_d(\boldsymbol{v}^h, \lambda_d - \mathcal{I}^H(\lambda_d))| \\
&\qquad \leq C \Big(\sum_{i=1}^{M_d} \|\boldsymbol{v}^h\|_{H(\mathrm{div};\Omega_{d,i})} \big(H^{q-1/2} |\lambda|_{H^q(\partial\Omega_{d,i}\cap\Gamma_{dd}\cup\mathcal{O})} + H^{r-1/2} |\lambda|_{H^r(\partial\Omega_{d,i}\cap\Gamma_{sd}\cup\mathcal{O})} \big) \\
&\qquad\qquad + \sum_{i=1}^{M_d} \sum_{j} A_j^{-1/2} \|\boldsymbol{v}^h\|_{H^1(\Omega_{s,j})} H^r |\lambda|_{H^r(\partial\Omega_{d,i}\cap\Gamma_{sd}\cup\mathcal{O})} \Big), \\
&\qquad\qquad\qquad 1/2 \leq q \leq r_{dd} + 1, \;\; 1/2 \leq r \leq r_{sd} + 1,
\end{aligned}
\tag{2.5.21}
$$

provided λ_{sd} and λ_d are sufficiently smooth, and where the last sum runs over all $\Omega_{s,j}$ adjacent to $\Omega_{d,i}$.

Proof. The proof is almost same as Lemma 5.3 in [27] by using the continuity of R_d^{RT} (2.3.24) and assuming that there exist a the global smooth map to guarantee $\|\hat{\lambda}\| \lesssim \|\lambda\|$ and $\|\hat{\boldsymbol{v}}\| \lesssim \|\boldsymbol{v}\|$. □

2.5.1 Error estimates with straight interfaces

In order to get error estimates for the global veolicty and pressure, we first need to get the error equations for Darcy part and then combine Stokes part error equation to get the global error estimates. Since we have symmetric and non-symmetric MFMFE for Darcy flow, we first present an analysis based on the symmetric scheme, then we propose a non-symmetric analysis for the non-symmetric scheme.

Theorem 2.5.1. *The symmetric MFMFE of coupled Stokes-Darcy problem has following optimal convergence results:*

$$
\begin{aligned}
&\|\!|\boldsymbol{u}-\boldsymbol{u}^h|\!\|_X + \|p-p^h\|_W \\
&\quad \le C\big(h^{r_1}(\|\boldsymbol{u}\|_{H^{r_1+1}(\Omega)} + \|p\|_{H^{r_1}(\Omega)}) + h^{r_2}\|\boldsymbol{u}\|_{H^{r_2+1/2}(\Omega)} + h^{r_3}(\|\operatorname{div}\boldsymbol{u}\|_{H^{r_3}(\Omega)} + \|p\|_{H^{r_3}(\Omega)}) \\
&\qquad + A^{-1}H^{r_4}(\|\boldsymbol{u}_s\|_{H^{r_4+3/2}(\Omega_s)} + \|p_s\|_{H^{r_4+1/2}(\Omega_s)}) \\
&\qquad + A^{-1/2}H^{r_5-1/2}\|p_d\|_{H^{r_5+1/2}(\Omega_d)} + A^{-1/2}H^{r_6-1/2}\|p_d\|_{H^{r_6+1/2}(\Omega_d)}\big), \\
&\qquad\qquad 0 \le r_1 \le r_s,\ 1/2 \le r_2 \le 1,\ 0 \le r_3 \le 1, \\
&\qquad\qquad 0 < r_4 \le r_{ss}+1,\ 1/2 \le r_5 \le r_{dd}+1,\ 1/2 \le r_6 \le r_{sd}+1.
\end{aligned}
$$

Proof. From Darcy weak formulation, we have

$$
\begin{aligned}
\forall \boldsymbol{v}_d \in \boldsymbol{X}_d \quad \nu_d(\boldsymbol{K}^{-1}\boldsymbol{u}_d, \boldsymbol{v}_d)_{\Omega_d} - \sum_{i=1}^{M_d}(p_d, \nabla\cdot\boldsymbol{v}_d)_{\Omega_{d,i}} &= -\sum_{\Gamma_{ij}\in\Gamma_{dd}}\langle\lambda_{dd}, \boldsymbol{v}_d\cdot\boldsymbol{n}_{ij}\rangle_{\Gamma_{ij}} \\
&\quad - \sum_{\Gamma_{ij}\in\Gamma_{sd}}\langle\lambda_{sd}, \boldsymbol{v}_d\cdot\boldsymbol{n}_{ij}\rangle_{\Gamma_{ij}} + (\boldsymbol{f}_d, \boldsymbol{v}_d)_{\Omega_d}.
\end{aligned} \tag{2.5.22}
$$

By symmetric MFMFE, we have

$$
\begin{aligned}
\forall \boldsymbol{v}_d \in \boldsymbol{X}_d^h \quad \nu_d(\boldsymbol{K}^{-1}\boldsymbol{u}_d^h, \boldsymbol{v}_d)_{Q,\Omega_d} - \sum_{i=1}^{M_d}(p_d^h, \nabla\cdot\boldsymbol{v}_d)_{\Omega_{d,i}} &= -\sum_{\Gamma_{ij}\in\Gamma_{dd}}\langle\lambda_{dd}^H, R_d^{RT}\boldsymbol{v}_d\cdot\boldsymbol{n}_{ij}\rangle_{\Gamma_{ij}} \\
&\quad - \sum_{\Gamma_{ij}\in\Gamma_{sd}}\langle\lambda_{sd}^H, R_d^{RT}\boldsymbol{v}_d\cdot\boldsymbol{n}_{ij}\rangle_{\Gamma_{ij}} + (\boldsymbol{f}_d, R_d^{RT}\boldsymbol{v}_d)_{\Omega_d}.
\end{aligned} \tag{2.5.23}
$$

Then, from above two equations, we can have the error equation for Darcy flow: for all $\boldsymbol{v}_d \in V_d^h$ such that $\nabla\cdot\boldsymbol{v}_d = 0$ in each subdomain,

$$
\begin{aligned}
\nu_d(\boldsymbol{K}^{-1}\boldsymbol{u}_d, \boldsymbol{v}_d)_{\Omega_d} - \nu_d(\boldsymbol{K}^{-1}\boldsymbol{u}_d^h, \boldsymbol{v}_d)_{Q,\Omega_d} &= -\sum_{\Gamma_{ij}\in\Gamma_{dd}}\langle\lambda_{dd}, (\boldsymbol{v}_d - R_d^{RT}\boldsymbol{v}_d)\cdot\boldsymbol{n}_{ij}\rangle_{\Gamma_{ij}} \\
- \sum_{\Gamma_{ij}\in\Gamma_{dd}}\langle\lambda_{dd}-\lambda_{dd}^H, R_d^{RT}\boldsymbol{v}_d\cdot\boldsymbol{n}_{ij}\rangle_{\Gamma_{ij}} - \sum_{\Gamma_{ij}\in\Gamma_{sd}}\langle\lambda_{sd}, \boldsymbol{v}_d\cdot\boldsymbol{n}_{ij}\rangle_{\Gamma_{ij}} &+ \sum_{\Gamma_{ij}\in\Gamma_{sd}}\langle\lambda_{sd}^H, R_d^{RT}\boldsymbol{v}_d\cdot\boldsymbol{n}_{ij}\rangle_{\Gamma_{ij}} \\
&+ (\boldsymbol{f}_d, \boldsymbol{v}_d - R_d^{RT}\boldsymbol{v}_d)_{\Omega_d}.
\end{aligned} \tag{2.5.24}
$$

Taking $\boldsymbol{v}_d - R_d^{RT}\boldsymbol{v}_d$ as a test function in (2.5.22) :

$$\begin{aligned}\nu_d(\boldsymbol{K}^{-1}\boldsymbol{u}_d, \boldsymbol{v}_d - R_d^{RT}\boldsymbol{v}_d)_{\Omega_d} = &-\sum_{\Gamma_{ij}\in\Gamma_{dd}} \langle \lambda_{dd}, (\boldsymbol{v}_d - R_d^{RT}\boldsymbol{v}_d)\cdot\boldsymbol{n}_{ij}\rangle_{\Gamma_{ij}} \\ &- \sum_{\Gamma_{ij}\in\Gamma_{sd}} \langle \lambda_{sd}, (\boldsymbol{v}_d - R_d^{RT}\boldsymbol{v}_d)\cdot\boldsymbol{n}_{ij}\rangle_{\Gamma_{ij}} + (\boldsymbol{f}_d, \boldsymbol{v}_d - R_d^{RT}\boldsymbol{v}_d)_{\Omega_d}.\end{aligned} \tag{2.5.25}$$

Here we use the identity (3.23) in [54]. Then from (2.5.24) and (2.5.25), we have:

$$\begin{aligned}\nu_d(\boldsymbol{K}^{-1}\boldsymbol{u}_d^h, \boldsymbol{v}_d)_{Q,\Omega_d} = \nu_d(\boldsymbol{K}^{-1}\boldsymbol{u}_d, R_d^{RT}\boldsymbol{v}_d)_{\Omega_d} &+ \sum_{\Gamma_{ij}\in\Gamma_{dd}} \langle \lambda_{dd} - \lambda_{dd}^H, R_d^{RT}\boldsymbol{v}_d\cdot\boldsymbol{n}_{ij}\rangle_{\Gamma_{ij}} \\ &+ \sum_{\Gamma_{ij}\in\Gamma_{sd}} \langle \lambda_{sd} - \lambda_{sd}^H, R_d^{RT}\boldsymbol{v}_d\cdot\boldsymbol{n}_{ij}\rangle_{\Gamma_{ij}}.\end{aligned} \tag{2.5.26}$$

By using (2.5.26), we rewrite $\nu_d(\boldsymbol{K}^{-1}(\Pi_d^h\boldsymbol{u}_d - \boldsymbol{u}_d^h), \boldsymbol{v}_d)_{Q,\Omega_d}$ as

$$\begin{aligned}\forall \boldsymbol{v}_d \in \boldsymbol{V}_d^h \quad \nu_d(\boldsymbol{K}^{-1}(\Pi_d^h\boldsymbol{u}_d - \boldsymbol{u}_d^h), \boldsymbol{v}_d)_{Q,\Omega_d} &= \nu_d(\boldsymbol{K}^{-1}\Pi_d^h\boldsymbol{u}_d, \boldsymbol{v}_d)_{Q,\Omega_d} - \nu_d(\boldsymbol{K}^{-1}\boldsymbol{u}_d, R_d^{RT}\boldsymbol{v}_d)_{\Omega_d} \\ &- \sum_{\Gamma_{ij}\in\Gamma_{dd}} \langle \lambda_{dd} - \lambda_{dd}^H, R_d^{RT}\boldsymbol{v}_d\cdot\boldsymbol{n}_{ij}\rangle_{\Gamma_{ij}} - \sum_{\Gamma_{ij}\in\Gamma_{sd}} \langle \lambda_{sd} - \lambda_{sd}^H, R_d^{RT}\boldsymbol{v}_d\cdot\boldsymbol{n}_{ij}\rangle_{\Gamma_{ij}} \\ &= \nu_d(\boldsymbol{K}^{-1}(\Pi_d^h\boldsymbol{u}_d - R_d^h\boldsymbol{u}_d), \boldsymbol{v}_d)_{Q,\Omega_d} + \nu_d(\boldsymbol{K}^{-1}R_d^h\boldsymbol{u}_d, \boldsymbol{v}_d - R_d^{RT}\boldsymbol{v}_d)_{Q,\Omega_d} \\ &\quad -\nu_d\sigma(\boldsymbol{K}^{-1}R_d^h\boldsymbol{u}_d, R_d^{RT}\boldsymbol{v}_d) + \nu_d(\boldsymbol{K}^{-1}(R_d^h\boldsymbol{u}_d - \boldsymbol{u}_d), R_d^{RT}\boldsymbol{v}_d) \\ &- \sum_{\Gamma_{ij}\in\Gamma_{dd}} \langle \lambda_{dd} - \lambda_{dd}^H, R_d^{RT}\boldsymbol{v}_d\cdot\boldsymbol{n}_{ij}\rangle_{\Gamma_{ij}} - \sum_{\Gamma_{ij}\in\Gamma_{sd}} \langle \lambda_{sd} - \lambda_{sd}^H, R_d^{RT}\boldsymbol{v}_d\cdot\boldsymbol{n}_{ij}\rangle_{\Gamma_{ij}}.\end{aligned} \tag{2.5.27}$$

From Stokes error equation we have:

$$\begin{aligned}\forall \boldsymbol{v}_s \in \boldsymbol{V}_s^h \quad a_s^h(\boldsymbol{u}_s - \boldsymbol{u}_s^h, \boldsymbol{v}_s) + b^s(\boldsymbol{v}_s, p_s - p_s^h) + b_s(\boldsymbol{v}_s, \boldsymbol{\lambda}_s - \boldsymbol{\lambda}_s^H) + \sum_{\Gamma_{ij}\in\Gamma_{sd}} \langle \boldsymbol{v}_s\cdot\boldsymbol{n}_{ij}, \lambda_{sd} - \lambda_{sd}^H\rangle_{\Gamma_{ij}} \\ = 0,\end{aligned} \tag{2.5.28}$$

where $b^s(\cdot,\cdot) = \sum_{i=1}^{M_s} b_i(\cdot,\cdot)$. We can rewrite above equation as

$$\begin{aligned}\forall \boldsymbol{v}_s \in \boldsymbol{V}_s^h \quad a_s^h(\Pi_s^h\boldsymbol{u}_s - \boldsymbol{u}_s^h, \boldsymbol{v}_s) = -a_s^h(\boldsymbol{u}_s - \Pi_s^h\boldsymbol{u}_s, \boldsymbol{v}_s) - b^s(\boldsymbol{v}_s, p_s - p_s^h) - b_s(\boldsymbol{v}_s, \boldsymbol{\lambda}_{ss} - \boldsymbol{\lambda}_{ss}^H) \\ - \sum_{\Gamma_{ij}\in\Gamma_{sd}} \langle \boldsymbol{v}_s\cdot\boldsymbol{n}_{ij}, \lambda_{sd} - \lambda_{sd}^H\rangle_{\Gamma_{ij}}.\end{aligned} \tag{2.5.29}$$

Then by (2.5.27) and (2.5.29), $\forall \boldsymbol{v} \in \boldsymbol{Z}^h, \forall p^h \in W_h$ we have

$$\begin{aligned}
a^h(\Pi^h \boldsymbol{u} - \boldsymbol{u}^h, \boldsymbol{v}) &= -a_s^h(\boldsymbol{u}_s - \Pi_s^h \boldsymbol{u}_s, \boldsymbol{v}_s) - b(\boldsymbol{v}, p - p^h) \\
+\nu_d(\boldsymbol{K}^{-1}(\Pi_d^h \boldsymbol{u}_d - R_d^h \boldsymbol{u}_d), \boldsymbol{v}_d)_{Q,\Omega_d} &+ \nu_d(\boldsymbol{K}^{-1} R_d^h \boldsymbol{u}_d, \boldsymbol{v}_d - R_d^{RT} \boldsymbol{v}_d)_{Q,\Omega_d} \\
-\nu_d \sigma(\boldsymbol{K}^{-1} R_d^h \boldsymbol{u}_d, R_d^{RT} \boldsymbol{v}_d) &+ \nu_d(\boldsymbol{K}^{-1}(R_d^h \boldsymbol{u}_d - \boldsymbol{u}_d), R_d^{RT} \boldsymbol{v}_d) \\
-b_{sd}^h(\boldsymbol{v}, \lambda_{sd} - \lambda_{sd}^H) - b_d^h(\boldsymbol{v}, \lambda_{dd} - \lambda_{dd}^H) &- b_s(\boldsymbol{v}, \boldsymbol{\lambda}_{ss} - \boldsymbol{\lambda}_{ss}^H) \\
= -a_s^h(\boldsymbol{u}_s - \Pi_s^h \boldsymbol{u}_s, \boldsymbol{v}_s) &- b(\boldsymbol{v}, p - \mathcal{P}^h p) \\
+\nu_d(\boldsymbol{K}^{-1}(\Pi_d^h \boldsymbol{u}_d - R_d^h \boldsymbol{u}_d), \boldsymbol{v}_d)_{Q,\Omega_d} &+ \nu_d(\boldsymbol{K}^{-1} R_d^h \boldsymbol{u}_d, \boldsymbol{v}_d - R_d^{RT} \boldsymbol{v}_d)_{Q,\Omega_d} \\
-\nu_d \sigma(\boldsymbol{K}^{-1} R_d^h \boldsymbol{u}_d, R_d^{RT} \boldsymbol{v}_d) &+ \nu_d(\boldsymbol{K}^{-1}(R_d^h \boldsymbol{u}_d - \boldsymbol{u}_d), R_d^{RT} \boldsymbol{v}_d) \\
-b_{sd}^h(\boldsymbol{v}, \lambda_{sd} - \mathcal{I}^H(\lambda_{sd})) - b_d^h(\boldsymbol{v}, \lambda_{dd} - \mathcal{I}^H(\lambda_{dd})) &- b_s(\boldsymbol{v}, \boldsymbol{\lambda}_{ss} - \mathcal{I}^H(\boldsymbol{\lambda}_{ss}))
\end{aligned} \tag{2.5.30}$$

The first two terms on the right hand side of (2.5.30) can be bounded by using continuity property of bilinear form (2.3.84) and (2.3.85). The third and sixth terms on the right hand side of (2.5.30) can be estimated by using (2.5.11) and (2.5.1), respectively:

$$\nu_d \left(\boldsymbol{K}^{-1}(\Pi_d^h \mathbf{u}_d - R_d^h \mathbf{u}_d), \boldsymbol{v}_d\right)_{Q,\Omega_d} \lesssim h^{r_d} H^{1/2} \|\mathbf{u}_d\|_{r_d+1/2} \|\mathbf{v}_d\|, \quad 0 < r_d \leq 1, \tag{2.5.31}$$

$$\nu_d \left(\boldsymbol{K}^{-1}(R_d^h \mathbf{u}_d - \boldsymbol{u}_d), R_d^{RT} \boldsymbol{v}_d\right)_{\Omega_d} \lesssim \sum_{i=M_s+1}^{M} h \|\mathbf{u}_d\|_{1,\Omega_i} \|\mathbf{v}_d\|_{\Omega_i}, \tag{2.5.32}$$

where we have also used (2.3.24). Using (2.5.14), (2.3.24), and (2.5.8), we bound the fifth term on the right in (2.5.30) as

$$|\nu_d \sigma(\boldsymbol{K}^{-1} R_d^h \mathbf{u}_d, R_d^{RT} \boldsymbol{v}_d)_{\Omega_d}| \lesssim \sum_{E \in \mathcal{T}_d^h} h \|R_d^h \mathbf{u}_d\|_{1,E} \|R_d^{RT} \mathbf{v}_d\|_E \lesssim \sum_{i=M_s+1}^{M} h \|\mathbf{u}_d\|_{1,\Omega_i} \|\mathbf{v}_d\|_{\Omega_i}. \tag{2.5.33}$$

The fourth term can be bounded by Lemma 2.5.4.

$$|\nu_d(\boldsymbol{K}^{-1} R_d^h \boldsymbol{u}_d, \boldsymbol{v}_d - R_d^{RT} \boldsymbol{v}_d)_{Q,\Omega_d}| \lesssim \sum_{i=M_s+1}^{M} h \|\!| K^{-1} |\!\|_{1,\infty} \|\mathbf{u}_d\|_{1,\Omega_i} \|\mathbf{v}_d\|_{\Omega_i}. \tag{2.5.34}$$

The last three terms on the right hand side of (2.5.30) can be estimated from Lemma 2.5.7 and Lemma 2.5.8 .

Now let $\boldsymbol{v} = \Pi^h \boldsymbol{u} - \boldsymbol{u}^h$,then the proof is done with coercivity of $a^h(\cdot,\cdot)$, triangle inequality and Lemma 2.5.6,. □

In the case of the non-symmetric scheme, we have the following convergent result:

Theorem 2.5.2. *The non-symmetric MFMFE of coupled Stokes-Darcy problem has following optimal convergence results:*

$$
\begin{aligned}
&\|\!|\boldsymbol{u}-\boldsymbol{u}^h|\!\|_X+\|p-p^h\|_W\\
&\quad\le C\big(h^{r_1}(\|\boldsymbol{u}\|_{H^{r_1+1}(\Omega)}+\|p\|_{H^{r_1}(\Omega)})+h^{r_2}\|\boldsymbol{u}\|_{H^{r_2+1/2}(\Omega)}\\
&\qquad+h^{r_3}(\|\operatorname{div}\boldsymbol{u}\|_{H^{r_3}(\Omega)}+\|p\|_{H^{r_3}(\Omega)}+\|p_d\|_{H^{r_3+1}(\Omega_d)})\\
&\qquad+A^{-1}H^{r_4}(\|\boldsymbol{u}_s\|_{H^{r_4+3/2}(\Omega_s)}+\|p_s\|_{H^{r_4+1/2}(\Omega_s)})\\
&\qquad+A^{-1/2}H^{r_5-1/2}\|p_d\|_{H^{r_5+1/2}(\Omega_d)}+A^{-1/2}H^{r_6-1/2}\|p_d\|_{H^{r_6+1/2}(\Omega_d)}\big),\\
&\qquad\qquad 0\le r_1\le r_s,\ 1/2\le r_2\le 1,\ 0\le r_3\le 1,\\
&\qquad\qquad 0<r_4\le r_{ss}+1,\ 1/2\le r_5\le r_{dd}+1,\ 1/2\le r_6\le r_{sd}+1.
\end{aligned}
$$

Proof.

$$
\begin{aligned}
\forall\boldsymbol{v}_d\in\boldsymbol{X}_d^h\quad \nu_d(\boldsymbol{K}^{-1}\boldsymbol{u}_d^h,\boldsymbol{v}_d)_{Q,\Omega_d}-\sum_{i=1}^{M_d}(p_d^h,\nabla\cdot\boldsymbol{v}_d)_{\Omega_{d,i}}&=-\sum_{\Gamma_{ij}\in\Gamma_{dd}}\langle\lambda_{dd}^H,R_d^{RT}\boldsymbol{v}_d\cdot\boldsymbol{n}_{ij}\rangle_{\Gamma_{ij}}\\
&\quad-\sum_{\Gamma_{ij}\in\Gamma_{sd}}\langle\lambda_{sd}^H,R_d^{RT}\boldsymbol{v}_d\cdot\boldsymbol{n}_{ij}\rangle_{\Gamma_{ij}}+(\boldsymbol{f}_d,R_d^{RT}\boldsymbol{v}_d)_{\Omega_d}.
\end{aligned}
\tag{2.5.35}
$$

then combine with (2.5.22) we have error equation for Darcy flow with non-symmetric scheme by using $\nabla\cdot\boldsymbol{v}_d=0$ on each subdomain:

$$
\begin{aligned}
\nu_d(\boldsymbol{K}^{-1}(R_d^h\boldsymbol{u}_d-\boldsymbol{u}_d^h),\boldsymbol{v}_d)_{Q,\Omega_d}&=-\nu_d(\boldsymbol{K}^{-1}\boldsymbol{u}_d,\boldsymbol{v}_d)_{\Omega_d}+\nu_d(\boldsymbol{K}^{-1}R_d^h\boldsymbol{u}_d,\boldsymbol{v}_d)_{Q,\Omega_d}\\
&\quad-\sum_{\Gamma_{ij}\in\Gamma_{dd}}\langle\lambda_{dd}-\lambda_{dd}^H,R_d^{RT}\boldsymbol{v}_d\cdot\boldsymbol{n}_{ij}\rangle_{\Gamma_{ij}}-\sum_{\Gamma_{ij}\in\Gamma_{sd}}\langle\lambda_{sd}-\lambda_{sd}^H,R_d^{RT}\boldsymbol{v}_d\cdot\boldsymbol{n}_{ij}\rangle_{\Gamma_{ij}}\\
&\quad-\sum_{\Gamma_{ij}\in\Gamma_{dd}}\langle\lambda_{dd},(\boldsymbol{v}_d-R_d^{RT}\boldsymbol{v}_d)\cdot\boldsymbol{n}_{ij}\rangle_{\Gamma_{ij}}-\sum_{\Gamma_{ij}\in\Gamma_{sd}}\langle\lambda_{sd},(\boldsymbol{v}_d-R_d^{RT}\boldsymbol{v}_d)\cdot\boldsymbol{n}_{ij}\rangle_{\Gamma_{ij}}\\
&\quad+(\boldsymbol{f}_d,\boldsymbol{v}_d-R_d^{RT}\boldsymbol{v}_d)_{\Omega_d}.
\end{aligned}
\tag{2.5.36}
$$

Choosing $\boldsymbol{v}_d - R_d^{RT}\boldsymbol{v}_d$ as a test function in (2.5.22), we have :

$$\nu_d(\boldsymbol{K}^{-1}\boldsymbol{u}_d, \boldsymbol{v}_d - R_d^{RT}\boldsymbol{v}_d)_{\Omega_d} - (\boldsymbol{f}_d, \boldsymbol{v}_d - R_d^{RT}\boldsymbol{v}_d)_{\Omega_d} = -\sum_{\Gamma_{ij}\in\Gamma_{dd}} \langle \lambda_{dd}, (\boldsymbol{v}_d - R_d^{RT}\boldsymbol{v}_d)\cdot\boldsymbol{n}_{ij}\rangle_{\Gamma_{ij}} - \sum_{\Gamma_{ij}\in\Gamma_{sd}} \langle \lambda_{sd}, (\boldsymbol{v}_d - R_d^{RT}\boldsymbol{v}_d)\cdot\boldsymbol{n}_{ij}\rangle_{\Gamma_{ij}}. \tag{2.5.37}$$

Here we use the identity (3.23) in [54]. Combining with (2.5.36), we can have the new error equation for the non-symmetric MFMFE:

$$\begin{aligned}\nu_d(\boldsymbol{K}^{-1}(R_d^h\boldsymbol{u}_d - \boldsymbol{u}_d^h), \boldsymbol{v}_d)_{Q,\Omega_d} &= -\nu_d(\boldsymbol{K}^{-1}\boldsymbol{u}_d, R_d^{RT}\boldsymbol{v}_d)_{\Omega_d} + \nu_d(\boldsymbol{K}^{-1}R_d^h\boldsymbol{u}_d, \boldsymbol{v}_d)_{Q,\Omega_d} \\ &- \sum_{\Gamma_{ij}\in\Gamma_{dd}} \langle \lambda_{dd} - \lambda_{dd}^H, R_d^{RT}\boldsymbol{v}_d\cdot\boldsymbol{n}_{ij}\rangle_{\Gamma_{ij}} - \sum_{\Gamma_{ij}\in\Gamma_{sd}} \langle \lambda_{sd} - \lambda_{sd}^H, R_d^{RT}\boldsymbol{v}_d\cdot\boldsymbol{n}_{ij}\rangle_{\Gamma_{ij}}.\end{aligned} \tag{2.5.38}$$

Together with stokes error equaion (2.5.28), we can have the global error equation for the non-symmetric scheme:

$$\begin{aligned} a^h(\Pi^h\boldsymbol{u} - \boldsymbol{u}^h, \boldsymbol{v}) &= -a_s^h(\boldsymbol{u}_s - \Pi_s^h\boldsymbol{u}_s, \boldsymbol{v}_s) - b(\boldsymbol{v}, p - p^h) \\ +\nu_d(\boldsymbol{K}^{-1}(\Pi_d^h\boldsymbol{u}_d - R_d^h\boldsymbol{u}_d), \boldsymbol{v}_d)_{Q,\Omega_d} - \nu_d(\boldsymbol{K}^{-1}\boldsymbol{u}_d, R_d^{RT}\boldsymbol{v}_d)_{\Omega_d} + \nu_d(\boldsymbol{K}^{-1}R_d^h\boldsymbol{u}_d, \boldsymbol{v}_d)_{Q,\Omega_d} \\ -b_{sd}^h(\boldsymbol{v}, \lambda_{sd} - \lambda_{sd}^H) - b_d^h(\boldsymbol{v}, \lambda_{dd} - \lambda_{dd}^H) - b_s(\boldsymbol{v}, \boldsymbol{\lambda}_{ss} - \boldsymbol{\lambda}_{ss}^H) \\ &= -a_s^h(\boldsymbol{u}_s - \Pi_s^h\boldsymbol{u}_s, \boldsymbol{v}_s) - b(\boldsymbol{v}, p - \mathcal{P}^h p) \\ +\nu_d(\boldsymbol{K}^{-1}(\Pi_d^h\boldsymbol{u}_d - R_d^h\boldsymbol{u}_d), \boldsymbol{v}_d)_{Q,\Omega_d} - \nu_d(\boldsymbol{K}^{-1}\boldsymbol{u}_d, R_d^{RT}\boldsymbol{v}_d)_{\Omega_d} + \nu_d(\boldsymbol{K}^{-1}R_d^h\boldsymbol{u}_d, \boldsymbol{v}_d)_{Q,\Omega_d} \\ -b_{sd}^h(\boldsymbol{v}, \lambda_{sd} - \mathcal{I}^H(\lambda_{sd})) - b_d^h(\boldsymbol{v}, \lambda_{dd} - \mathcal{I}^H(\lambda_{dd})) - b_s(\boldsymbol{v}, \boldsymbol{\lambda}_{ss} - \mathcal{I}^H(\boldsymbol{\lambda}_{ss})) \end{aligned} \tag{2.5.39}$$

The first three and last three terms on the right hand side of (2.5.39) can be estimated same as symmetric schemes. By using (2.5.22) and integration by parts we can rewrite fourth and fifth terms on right hand side of (2.5.39) as:

$$\begin{aligned} -\nu_d(\boldsymbol{K}^{-1}\boldsymbol{u}_d, R_d^{RT}\boldsymbol{v}_d)_{\Omega_d} + \nu_d(\boldsymbol{K}^{-1}R_d^h\boldsymbol{u}_d, \boldsymbol{v}_d)_{Q,\Omega_d} &= \sum_{i=1}^{M_d}(\nabla p_d, R_d^{RT}\boldsymbol{v}_d)_{\Omega_{d,i}} \\ + \sum_{E\in\mathcal{T}_d^h} \nu_d(\boldsymbol{K}^{-1}R_d^h(\boldsymbol{u}_d + \nu_d^{-1}\overline{\boldsymbol{K}}_E\nabla s^1), \boldsymbol{v}_d)_{Q,E} - \sum_{E\in\mathcal{T}_d^h}(\boldsymbol{K}^{-1}R_d^h\overline{\boldsymbol{K}}_E\nabla s^1, \boldsymbol{v}_d)_{Q,E} \\ -(\boldsymbol{f}_d, R_d^{RT}\boldsymbol{v}_d)_{\Omega_d} \end{aligned} \tag{2.5.40}$$

where s^1 is defined in (2.5.4).

The second term on the right hand side of (2.5.40) can be written as:

$$
\begin{aligned}
I_2 &= \sum_{E\in\mathcal{T}_d^h} \nu_d(\boldsymbol{K}^{-1}R_d^h(\boldsymbol{u}_d+\nu_d^{-1}\overline{\boldsymbol{K}}\nabla s^1),\boldsymbol{v}_d)_{Q,E} = \sum_{E\in\mathcal{T}_d^h} \nu_d(\boldsymbol{K}^{-1}R_d^h(\boldsymbol{u}_d-R_d^h\boldsymbol{u}_d),\boldsymbol{v}_d)_{Q,E}\\
&+ \sum_{E\in\mathcal{T}_d^h} \nu_d(\boldsymbol{K}^{-1}R_d^h(R_d^h\boldsymbol{u}_d+\nu_d^{-1}\overline{\boldsymbol{K}}\nabla s^1),\boldsymbol{v}_d)_{Q,E} = \sum_{E\in\mathcal{T}_d^h} \nu_d(\boldsymbol{K}^{-1}R_d^h(\boldsymbol{u}_d-R_d^h\boldsymbol{u}_d),\boldsymbol{v}_d)_{Q,E}\\
&+ \sum_{E\in\mathcal{T}_d^h} \nu_d(\boldsymbol{K}^{-1}(R_d^h\boldsymbol{u}_d+\nu_d^{-1}\overline{\boldsymbol{K}}\nabla s^1),R_d^{RT}\boldsymbol{v}_d)_{Q,E}\\
&= \sum_{E\in\mathcal{T}_d^h} \nu_d(\boldsymbol{K}^{-1}R_d^h(\boldsymbol{u}_d-R_d^h\boldsymbol{u}_d),\boldsymbol{v}_d)_{Q,E} + \sum_{E\in\mathcal{T}_d^h} \nu_d(\overline{\boldsymbol{K}}^{-1}(R_d^h\boldsymbol{u}_d\\
&+ \nu_d^{-1}\overline{\boldsymbol{K}}\nabla s^1),R_d^{RT}\boldsymbol{v}_d)_E = \sum_{E\in\mathcal{T}_d^h} \nu_d(\boldsymbol{K}^{-1}R_d^h(\boldsymbol{u}_d-R_d^h\boldsymbol{u}_d),\boldsymbol{v}_d)_{Q,E}\\
&+ \sum_{E\in\mathcal{T}_d^h} (\nu_d\overline{\boldsymbol{K}}^{-1}R_d^h\boldsymbol{u}_d\\
&+ \nabla p_d,R_d^{RT}\boldsymbol{v}_d)_E + \sum_{E\in\mathcal{T}_d^h} (\nabla(s^1-p_d),R_d^{RT}\boldsymbol{v}_d)_E\\
&= \sum_{E\in\mathcal{T}_d^h} \nu_d(\boldsymbol{K}^{-1}R_d^h(\boldsymbol{u}_d-R_d^h\boldsymbol{u}_d),\boldsymbol{v}_d)_{Q,E} + \sum_{E\in\mathcal{T}_d^h} (\nu_d\overline{\boldsymbol{K}}^{-1}\boldsymbol{u}_d\\
&+ \nabla p_d,R_d^{RT}\boldsymbol{v}_d)_E + \sum_{E\in\mathcal{T}_d^h} (\nabla(s^1-p_d),R_d^{RT}\boldsymbol{v}_d)_E\\
&+ \sum_{E\in\mathcal{T}_d^h} (\nu_d\overline{\boldsymbol{K}}^{-1}(R_d^h\boldsymbol{u}_d-\boldsymbol{u}_d),R_d^{RT}\boldsymbol{v}_d)_E\\
&= \sum_{E\in\mathcal{T}_d^h} \nu_d(\boldsymbol{K}^{-1}R_d^h(\boldsymbol{u}_d-R_d^h\boldsymbol{u}_d),\boldsymbol{v}_d)_{Q,E} + \sum_{E\in\mathcal{T}_d^h} (\nu_d\boldsymbol{K}^{-1}\boldsymbol{u}_d\\
&+ \nabla p_d,R_d^{RT}\boldsymbol{v}_d)_E + \sum_{E\in\mathcal{T}_d^h} (\nabla(s^1-p_d),R_d^{RT}\boldsymbol{v}_d)_E\\
&+ \sum_{E\in\mathcal{T}_d^h} (\nu_d\overline{\boldsymbol{K}}^{-1}(R_d^h\boldsymbol{u}_d-\boldsymbol{u}_d),R_d^{RT}\boldsymbol{v}_d)_E + \sum_{E\in\mathcal{T}_d^h} (\nu_d(\overline{\boldsymbol{K}}^{-1}-\boldsymbol{K}^{-1}),R_d^{RT}\boldsymbol{v}_d)_E\\
&= \sum_{E\in\mathcal{T}_d^h} \nu_d(\boldsymbol{K}^{-1}R_d^h(\boldsymbol{u}_d-R_d^h\boldsymbol{u}_d),\boldsymbol{v}_d)_{Q,E} + (\boldsymbol{f}_d,R_d^{RT}\boldsymbol{v}_d)_{\Omega_d}\\
&+ \sum_{E\in\mathcal{T}_d^h} (\nabla(s^1-p_d),R_d^{RT}\boldsymbol{v}_d)_E\\
&+ \sum_{E\in\mathcal{T}_d^h} (\nu_d\overline{\boldsymbol{K}}^{-1}(R_d^h\boldsymbol{u}_d-\boldsymbol{u}_d),R_d^{RT}\boldsymbol{v}_d)_E + \sum_{E\in\mathcal{T}_d^h} (\nu_d(\overline{\boldsymbol{K}}^{-1}-\boldsymbol{K}^{-1}),R_d^{RT}\boldsymbol{v}_d)_E\\
&\equiv (\boldsymbol{f}_d,R_d^{RT}\boldsymbol{v}_d) + T_1(\boldsymbol{v}_d)
\end{aligned}
\tag{2.5.41}
$$

Then (2.5.40) can be written as

$$\begin{aligned} &-\nu_d(\boldsymbol{K}^{-1}\boldsymbol{u}_d, R_d^{RT}\boldsymbol{v}_d)_{\Omega_d} + \nu_d(\boldsymbol{K}^{-1}R_d^h\boldsymbol{u}_d, \boldsymbol{v}_d)_{Q,\Omega_d} = \sum_{i=1}^{M_d}(\nabla p_d, R_d^{RT}\boldsymbol{v}_d)_{\Omega_{d,i}} \\ &-\sum_{E\in\mathcal{T}_d^h}(\boldsymbol{K}^{-1}R_d^h\overline{\boldsymbol{K}}_E\nabla s^1, \boldsymbol{v}_d)_{Q,E} + T_1(\boldsymbol{v}_d) \equiv I_1 + I_2 + T_1 \end{aligned} \tag{2.5.42}$$

By Lemma 3.11, Lemma 2.2, and Lemma 2.4 in [53], the term I_2 can be written as

$$\begin{aligned} -I_2 = (\boldsymbol{K}^{-1}R_d^h\overline{\boldsymbol{K}}_E\nabla s^1, \boldsymbol{v}_d)_{Q,E} = (\boldsymbol{K}^{-1}\overline{\boldsymbol{K}}_E\nabla s^1, \boldsymbol{v}_d)_{Q,E} = (\boldsymbol{K}^{-1}R_d^h\overline{\boldsymbol{K}}_E\nabla s^1, R_d^{RT}\boldsymbol{v}_d)_{Q,E} \\ = (\nabla s^1, R_d^{RT}\boldsymbol{v}_d)_E \end{aligned} \tag{2.5.43}$$

Then we have

$$|I_1 + I_2| = |\sum_{E\in\mathcal{T}_d^h}(\nabla(p_d - s^1), R_d^{RT}\boldsymbol{v}_d)_E| \lesssim \sum_{E\in\mathcal{T}_d^h}\|\nabla(p_d - s^1)\|_E\|R_d^{RT}\boldsymbol{v}_d\|_E \lesssim h\|p\|_2\|\boldsymbol{v}_d\|_{\Omega_d}, \tag{2.5.44}$$

where we have used (2.5.4) and (2.3.24). Substituting (2.5.42) into (2.5.39), we only left $T_1(\boldsymbol{v}_d)$ to be estimated. Actually by using Lemma 2.5.1,(2.5.1),(2.5.4) and (2.5.6) we can immediately get the bound for $T_1(\boldsymbol{v}_d)$:

$$T_1(\boldsymbol{v}_d) \lesssim h(\|p\|_2 + \|\boldsymbol{u}_d\|_1)\|\boldsymbol{v}_d\|. \tag{2.5.45}$$

Now let $\boldsymbol{v} = \Pi^h\boldsymbol{u} - \boldsymbol{u}^h$, with coercivity of $a^h(\cdot,\cdot)$, triangle inequality and Lemma 2.5.6,we can finish the proof. □

Remark 2.5.1. *In the above estimate, the fine scale subdomain approximation error terms are of optimal order with constants independent of the size of the subdomains A. The constants of the coarse scale mortar consistency error terms deteriorate with decrease in A, since in that case the number of interfaces grows. Nevertheless, higher order mortar polynomials can be employed to balance the error terms, giving optimal fine scale convergence.*

2.5.2 Error estimates with curved interfaces

In order to get error estimates for the global veolicty and pressure with curved interfaces, we still first need to get the error equations for Darcy part and then combine Stokes part error equation to get the global error estimates. Here we only present sysmetric scheme, the non-symmetric scheme is done by the similar way.

Theorem 2.5.3. *The symmetric MFMFE of coupled Stokes-Darcy problem with curved interfaces has following optimal convergence results:*

$$
\begin{aligned}
&|\!|\!|\boldsymbol{u}-\boldsymbol{u}^h|\!|\!|_X+\|p-p^h\|_W\\
&\quad\le C\big(h^{r_1}(\|\boldsymbol{u}\|_{H^{r_1+1}(\Omega)}+\|p\|_{H^{r_1}(\Omega)})+h^{r_2}\|\boldsymbol{u}\|_{H^{r_2+1/2}(\Omega)}+h^{r_3}(\|\operatorname{div}\boldsymbol{u}\|_{H^{r_3}(\Omega)}+\|p\|_{H^{r_3}(\Omega)})\\
&\qquad+A^{-1}H^{r_4}(\|\boldsymbol{u}_s\|_{H^{r_4+3/2}(\Omega_s)}+\|p_s\|_{H^{r_4+1/2}(\Omega_s)})\\
&\qquad+A^{-1/2}H^{r_5-1/2}\|p_d\|_{H^{r_5+1/2}(\Omega_d)}+A^{-1/2}H^{r_6-1/2}\|p_d\|_{H^{r_6+1/2}(\Omega_d)}\big),\\
&\qquad\qquad 0\le r_1\le r_s,\ 1/2\le r_2\le 1,\ 0\le r_3\le 1,\\
&\qquad\qquad 0<r_4\le r_{ss}+1,\ 1/2\le r_5\le r_{dd}+1,\ 1/2\le r_6\le r_{sd}+1.
\end{aligned}
$$

Proof. From Darcy weak formulation and Piola transformation, we have

$$
\begin{aligned}
\forall\boldsymbol{v}_d\in\boldsymbol{X}_d\quad \nu_d(\boldsymbol{K}^{-1}\boldsymbol{u}_d,\boldsymbol{v}_d)_{\Omega_d}-\sum_{i=1}^{M_d}(p_d,\nabla\cdot\boldsymbol{v}_d)_{\Omega_{d,i}}&=-\sum_{\hat\Gamma_{ij}\in\Gamma_{dd}}\langle\hat\lambda_{dd},\hat{\boldsymbol{v}}_d\cdot\hat{\boldsymbol{n}}_{ij}\rangle_{\hat\Gamma_{ij}}\\
&\quad-\sum_{\hat\Gamma_{ij}\in\hat\Gamma_{sd}}\langle\hat\lambda_{sd},\hat{\boldsymbol{v}}_d\cdot\hat{\boldsymbol{n}}_{ij}\rangle_{\hat\Gamma_{ij}}+(\boldsymbol{f}_d,\boldsymbol{v}_d)_{\Omega_d}.
\end{aligned}
\tag{2.5.46}
$$

By symmetric MFMFE and Piola transformation, we have

$$
\begin{aligned}
\forall\boldsymbol{v}_d\in\boldsymbol{X}_d^h\quad \nu_d(\boldsymbol{K}^{-1}\boldsymbol{u}_d^h,\boldsymbol{v}_d)_{Q,\Omega_d}-\sum_{i=1}^{M_d}(p_d^h,\nabla\cdot\boldsymbol{v}_d)_{\Omega_{d,i}}&=-\sum_{\hat\Gamma_{ij}\in\hat\Gamma_{dd}}\langle\hat\lambda_{dd}^H,R_d^{RT}\hat{\boldsymbol{v}}_d\cdot\hat{\boldsymbol{n}}_{ij}\rangle_{\hat\Gamma_{ij}}\\
&\quad-\sum_{\hat\Gamma_{ij}\in\hat\Gamma_{sd}}\langle\hat\lambda_{sd}^H,R_d^{RT}\hat{\boldsymbol{v}}_d\cdot\hat{\boldsymbol{n}}_{ij}\rangle_{\hat\Gamma_{ij}}+(\boldsymbol{f}_d,R_d^{RT}\boldsymbol{v}_d)_{\Omega_d}.
\end{aligned}
\tag{2.5.47}
$$

Then, from above two equations, we can have the error equation for Darcy flow: for all $\boldsymbol{v}_d \in V_d^h$ such that $\nabla \cdot \boldsymbol{v}_d = 0$ in each subdomain,

$$\begin{aligned}\nu_d(\boldsymbol{K}^{-1}\boldsymbol{u}_d, \boldsymbol{v}_d)_{\Omega_d} - \nu_d(\boldsymbol{K}^{-1}\boldsymbol{u}_d^h, \boldsymbol{v}_d)_{Q,\Omega_d} = &- \sum_{\hat{\Gamma}_{ij}\in\hat{\Gamma}_{dd}} \langle \hat{\lambda}_{dd}, (\hat{\boldsymbol{v}}_d - R_d^{RT}\hat{\boldsymbol{v}}_d)\cdot\hat{\boldsymbol{n}}_{ij}\rangle_{\hat{\Gamma}_{ij}} \\ - \sum_{\hat{\Gamma}_{ij}\in\hat{\Gamma}_{dd}} \langle \hat{\lambda}_{dd} - \hat{\lambda}_{dd}^H, R_d^{RT}\hat{\boldsymbol{v}}_d\cdot\hat{\boldsymbol{n}}_{ij}\rangle_{\hat{\Gamma}_{ij}} &- \sum_{\hat{\Gamma}_{ij}\in\hat{\Gamma}_{sd}} \langle \hat{\lambda}_{sd}, \hat{\boldsymbol{v}}_d\cdot\hat{\boldsymbol{n}}_{ij}\rangle_{\hat{\Gamma}_{ij}} + \sum_{\hat{\Gamma}_{ij}\in\hat{\Gamma}_{sd}} \langle \hat{\lambda}_{sd}^H, R_d^{RT}\hat{\boldsymbol{v}}_d\cdot\hat{\boldsymbol{n}}_{ij}\rangle_{\hat{\Gamma}_{ij}} \\ &+ (\boldsymbol{f}_d, \boldsymbol{v}_d - R_d^{RT}\boldsymbol{v}_d)_{\Omega_d}.\end{aligned} \tag{2.5.48}$$

Taking $\boldsymbol{v}_d - R_d^{RT}\boldsymbol{v}_d$ as a test function in (2.5.22) :

$$\begin{aligned}\nu_d(\boldsymbol{K}^{-1}\boldsymbol{u}_d, \boldsymbol{v}_d - R_d^{RT}\boldsymbol{v}_d)_{\Omega_d} = &- \sum_{\hat{\Gamma}_{ij}\in\hat{\Gamma}_{dd}} \langle \hat{\lambda}_{dd}, (\hat{\boldsymbol{v}}_d - R_d^{RT}\hat{\boldsymbol{v}}_d)\cdot\hat{\boldsymbol{n}}_{ij}\rangle_{\hat{\Gamma}_{ij}} \\ &- \sum_{\hat{\Gamma}_{ij}\in\hat{\Gamma}_{sd}} \langle \hat{\lambda}_{sd}, (\hat{\boldsymbol{v}}_d - R_d^{RT}\hat{\boldsymbol{v}}_d)\cdot\hat{\boldsymbol{n}}_{ij}\rangle_{\hat{\Gamma}_{ij}} + (\boldsymbol{f}_d, \boldsymbol{v}_d - R_d^{RT}\boldsymbol{v}_d)_{\Omega_d}.\end{aligned} \tag{2.5.49}$$

Here we use the identity (3.23) in [54]. Then from (2.5.48) and (2.5.49), we have:

$$\begin{aligned}\nu_d(\boldsymbol{K}^{-1}\boldsymbol{u}_d^h, \boldsymbol{v}_d)_{Q,\Omega_d} = \nu_d(\boldsymbol{K}^{-1}\boldsymbol{u}_d, R_d^{RT}\boldsymbol{v}_d)_{\Omega_d} &+ \sum_{\hat{\Gamma}_{ij}\in\hat{\Gamma}_{dd}} \langle \hat{\lambda}_{dd} - \hat{\lambda}_{dd}^H, R_d^{RT}\hat{\boldsymbol{v}}_d\cdot\hat{\boldsymbol{n}}_{ij}\rangle_{\hat{\Gamma}_{ij}} \\ &+ \sum_{\hat{\Gamma}_{ij}\in\hat{\Gamma}_{sd}} \langle \hat{\lambda}_{sd} - \hat{\lambda}_{sd}^H, R_d^{RT}\hat{\boldsymbol{v}}_d\cdot\hat{\boldsymbol{n}}_{ij}\rangle_{\hat{\Gamma}_{ij}}.\end{aligned} \tag{2.5.50}$$

By using (2.5.50), we rewrite $\nu_d(\boldsymbol{K}^{-1}(\Pi_d^h\boldsymbol{u}_d - \boldsymbol{u}_d^h), \boldsymbol{v}_d)_{Q,\Omega_d}$ as

$$\begin{aligned}\forall \boldsymbol{v}_d \in \boldsymbol{V}_d^h \quad \nu_d(\boldsymbol{K}^{-1}(\Pi_d^h\boldsymbol{u}_d - \boldsymbol{u}_d^h), \boldsymbol{v}_d)_{Q,\Omega_d} &= \nu_d(\boldsymbol{K}^{-1}\Pi_d^h\boldsymbol{u}_d, \boldsymbol{v}_d)_{Q,\Omega_d} - \nu_d(\boldsymbol{K}^{-1}\boldsymbol{u}_d, R_d^{RT}\boldsymbol{v}_d)_{\Omega_d} \\ &- \sum_{\hat{\Gamma}_{ij}\in\hat{\Gamma}_{dd}} \langle \hat{\lambda}_{dd} - \hat{\lambda}_{dd}^H, R_d^{RT}\hat{\boldsymbol{v}}_d\cdot\hat{\boldsymbol{n}}_{ij}\rangle_{\hat{\Gamma}_{ij}} - \sum_{\hat{\Gamma}_{ij}\in\hat{\Gamma}_{sd}} \langle \hat{\lambda}_{sd} - \hat{\lambda}_{sd}^H, R_d^{RT}\hat{\boldsymbol{v}}_d\cdot\hat{\boldsymbol{n}}_{ij}\rangle_{\hat{\Gamma}_{ij}} \\ &= \nu_d(\boldsymbol{K}^{-1}(\Pi_d^h\boldsymbol{u}_d - R_d^h\boldsymbol{u}_d), \boldsymbol{v}_d)_{Q,\Omega_d} + \nu_d(\boldsymbol{K}^{-1}R_d^h\boldsymbol{u}_d, \boldsymbol{v}_d - R_d^{RT}\boldsymbol{v}_d)_{Q,\Omega_d} \\ &\quad -\nu_d\sigma(\boldsymbol{K}^{-1}R_d^h\boldsymbol{u}_d, R_d^{RT}\boldsymbol{v}_d) + \nu_d(\boldsymbol{K}^{-1}(R_d^h\boldsymbol{u}_d - \boldsymbol{u}_d), R_d^{RT}\boldsymbol{v}_d) \\ &- \sum_{\hat{\Gamma}_{ij}\in\hat{\Gamma}_{dd}} \langle \hat{\lambda}_{dd} - \hat{\lambda}_{dd}^H, R_d^{RT}\hat{\boldsymbol{v}}_d\cdot\hat{\boldsymbol{n}}_{ij}\rangle_{\hat{\Gamma}_{ij}} - \sum_{\hat{\Gamma}_{ij}\in\hat{\Gamma}_{sd}} \langle \hat{\lambda}_{sd} - \hat{\lambda}_{sd}^H, R_d^{RT}\hat{\boldsymbol{v}}_d\cdot\hat{\boldsymbol{n}}_{ij}\rangle_{\hat{\Gamma}_{ij}}.\end{aligned} \tag{2.5.51}$$

From Stokes error equation we have:

$$\begin{aligned}\forall \boldsymbol{v}_s \in \boldsymbol{V}_s^h \quad a_s^h(\boldsymbol{u}_s - \boldsymbol{u}_s^h, \boldsymbol{v}_s) + b^s(\boldsymbol{v}_s, p_s - p_s^h) + \hat{b}_s(\boldsymbol{v}_s, \boldsymbol{\lambda}_s - \boldsymbol{\lambda}_s^H) \\ + \sum_{\hat{\Gamma}_{ij} \in \hat{\Gamma}_{sd}} \langle \hat{\boldsymbol{v}}_s \cdot \hat{\boldsymbol{n}}_{ij}, \hat{\lambda}_{sd} - \hat{\lambda}_{sd}^H \rangle_{\hat{\Gamma}_{ij}} = 0,\end{aligned} \tag{2.5.52}$$

where $b^s(\cdot,\cdot) = \sum_{i=1}^{M_s} b_i(\cdot,\cdot)$. We can rewrite above equation as

$$\begin{aligned}\forall \boldsymbol{v}_s \in \boldsymbol{V}_s^h \quad a_s^h(\Pi_s^h \boldsymbol{u}_s - \boldsymbol{u}_s^h, \boldsymbol{v}_s) = -a_s^h(\boldsymbol{u}_s - \Pi_s^h \boldsymbol{u}_s, \boldsymbol{v}_s) - b^s(\boldsymbol{v}_s, p_s - p_s^h) - \hat{b}_s(\boldsymbol{v}_s, \boldsymbol{\lambda}_{ss} - \boldsymbol{\lambda}_{ss}^H) \\ - \sum_{\hat{\Gamma}_{ij} \in \hat{\Gamma}_{sd}} \langle \hat{\boldsymbol{v}}_s \cdot \hat{\boldsymbol{n}}_{ij}, \hat{\lambda}_{sd} - \hat{\lambda}_{sd}^H \rangle_{\hat{\Gamma}_{ij}}.\end{aligned} \tag{2.5.53}$$

Then by (2.5.51) and (2.5.53), $\forall \boldsymbol{v} \in \boldsymbol{Z}^h, \forall p^h \in W_h$ we have

$$\begin{aligned} a^h(\Pi^h \boldsymbol{u} - \boldsymbol{u}^h, \boldsymbol{v}) &= -a_s^h(\boldsymbol{u}_s - \Pi_s^h \boldsymbol{u}_s, \boldsymbol{v}_s) - b(\boldsymbol{v}, p - p^h) \\ +\nu_d(\boldsymbol{K}^{-1}(\Pi_d^h \boldsymbol{u}_d - R_d^h \boldsymbol{u}_d), \boldsymbol{v}_d)_{Q,\Omega_d} &+ \nu_d(\boldsymbol{K}^{-1} R_d^h \boldsymbol{u}_d, \boldsymbol{v}_d - R_d^{RT} \boldsymbol{v}_d)_{Q,\Omega_d} \\ -\nu_d \sigma(\boldsymbol{K}^{-1} R_d^h \boldsymbol{u}_d, R_d^{RT} \boldsymbol{v}_d) &+ \nu_d(\boldsymbol{K}^{-1}(R_d^h \boldsymbol{u}_d - \boldsymbol{u}_d), R_d^{RT} \boldsymbol{v}_d) \\ -\hat{b}_{sd}^h(\boldsymbol{v}, \lambda_{sd} - \lambda_{sd}^H) - \hat{b}_d^h(\boldsymbol{v}, \lambda_{dd} - \lambda_{dd}^H) &- \hat{b}_s(\boldsymbol{v}, \boldsymbol{\lambda}_{ss} - \boldsymbol{\lambda}_{ss}^H) \\ = -a_s^h(\boldsymbol{u}_s - \Pi_s^h \boldsymbol{u}_s, \boldsymbol{v}_s) &- b(\boldsymbol{v}, p - \mathcal{P}^h p) \\ +\nu_d(\boldsymbol{K}^{-1}(\Pi_d^h \boldsymbol{u}_d - R_d^h \boldsymbol{u}_d), \boldsymbol{v}_d)_{Q,\Omega_d} &+ \nu_d(\boldsymbol{K}^{-1} R_d^h \boldsymbol{u}_d, \boldsymbol{v}_d - R_d^{RT} \boldsymbol{v}_d)_{Q,\Omega_d} \\ -\nu_d \sigma(\boldsymbol{K}^{-1} R_d^h \boldsymbol{u}_d, R_d^{RT} \boldsymbol{v}_d) &+ \nu_d(\boldsymbol{K}^{-1}(R_d^h \boldsymbol{u}_d - \boldsymbol{u}_d), R_d^{RT} \boldsymbol{v}_d) \\ -\hat{b}_{sd}^h(\boldsymbol{v}, \lambda_{sd} - \mathcal{I}^H(\lambda_{sd})) - \hat{b}_d^h(\boldsymbol{v}, \lambda_{dd} - \mathcal{I}^H(\lambda_{dd})) &- \hat{b}_s(\boldsymbol{v}, \boldsymbol{\lambda}_{ss} - \mathcal{I}^H(\boldsymbol{\lambda}_{ss})) \end{aligned} \tag{2.5.54}$$

The first two terms on the right hand side of (2.5.54) can be bounded by using continuity property of bilinear form (2.3.84) and (2.3.85). The third and sixth terms on the right hand side of (2.5.54) can be estimated by using (2.5.11) and (2.5.1), respectively:

$$\nu_d \left(\boldsymbol{K}^{-1}(\Pi_d^h \boldsymbol{u}_d - R_d^h \boldsymbol{u}_d), \boldsymbol{v}_d\right)_{Q,\Omega_d} \lesssim h^{r_d} H^{1/2} \|\mathbf{u}_d\|_{r_d+1/2} \|\mathbf{v}_d\|, \quad 0 < r_d \leq 1, \tag{2.5.55}$$

$$\nu_d \left(\boldsymbol{K}^{-1}(R_d^h \boldsymbol{u}_d - \boldsymbol{u}_d), R_d^{RT} \boldsymbol{v}_d\right)_{\Omega_d} \lesssim \sum_{i=M_s+1}^{M} h \|\mathbf{u}_d\|_{1,\Omega_i} \|\mathbf{v}_d\|_{\Omega_i}, \tag{2.5.56}$$

where we have also used (2.3.24). Using (2.5.14), (2.3.24), and (2.5.8), we bound the fifth term on the right in (2.5.54) as

$$|\nu_d\sigma(\boldsymbol{K}^{-1}R_d^h\boldsymbol{u}_d, R_d^{RT}\boldsymbol{v}_d)_{\Omega_d}| \lesssim \sum_{E\in\mathcal{T}_d^h} h\|R_d^h\mathbf{u}_d\|_{1,E}\|R_d^{RT}\mathbf{v}_d\|_E \lesssim \sum_{i=M_s+1}^{M} h\|\mathbf{u}_d\|_{1,\Omega_i}\|\mathbf{v}_d\|_{\Omega_i}. \tag{2.5.57}$$

The fourth term can be bounded by Lemma 2.5.4.

$$|\nu_d(\boldsymbol{K}^{-1}R_d^h\boldsymbol{u}_d, \boldsymbol{v}_d - R_d^{RT}\boldsymbol{v}_d)_{Q,\Omega_d}| \lesssim \sum_{i=M_s+1}^{M} h|||K^{-1}|||_{1,\infty}\|\mathbf{u}_d\|_{1,\Omega_i}\|\mathbf{v}_d\|_{\Omega_i}. \tag{2.5.58}$$

The last three terms on the right hand side of (2.5.54) can be estimated from Lemma 2.5.9 and Lemma 2.5.10 .

Now let $\boldsymbol{v} = \Pi^h\boldsymbol{u} - \boldsymbol{u}^h$,then the proof is done with coercivity of $a^h(\cdot,\cdot)$, triangle inequality and Lemma 2.5.6,. □

2.6 NUMERICAL TESTS

In this section we will present several numerical examples to verify our analysis. In all tests the computational domain is taken to be $\overline{\Omega} = \overline{\Omega}_s \cup \overline{\Omega}_d$, where $\Omega_s = (0,1)\times(\frac{1}{2},1)$ and $\Omega_d = (0,1)\times(0,\frac{1}{2})$. For simplicity we set

$$\boldsymbol{\sigma}(\boldsymbol{u}_s, p_s) = -p_s\boldsymbol{I} + \nu_s\nabla\boldsymbol{u}_s$$

in the Stokes equation in Ω_s, and

$$\boldsymbol{K} = K\boldsymbol{I}$$

in the Darcy equation in Ω_d, where K is a positive constant.

To test for convergence we construct two analytical solutions satisfying the flow equations in Ω_s and Ω_d along with the conditions on the interface Γ_{sd}. In example 1, we use:

$$\boldsymbol{u}_s = \begin{bmatrix} sec(x+0.45)+tan(x+0.45) \\ (1+sin(x+0.45))e^y \end{bmatrix},$$

$$\boldsymbol{u}_d = \begin{bmatrix} \frac{sin(x+1.45)}{cos(x+0.45)} + ((x+0.45)sin(x+0.45))e^y \\ (sin(x+0.45)+1-(x+0.45)cos(x+0.45))e^y \end{bmatrix},$$

$$p_s = ln(\frac{(cos^2(x+0.45)sin(x+0.45)}{1+sin(x+0.45)}) + ((x+0.45)cos(x+0.45)$$
$$+sin^2(x+0.45)-1)e^(0.5 - ln(sin(x+0.45))) + sin(x+0.45)+0.5+y,$$

$$p_d = ln(\frac{cos(x+0.45)}{sec(x+0.45)+tan(x+0.45)}) + ((x+0.45)cos(x+0.45)$$
$$-sin(x+0.45)-1)e^y,$$

while in example 2, we use:

$$\boldsymbol{u}_s = \begin{bmatrix} (2-x)(1.5-y)(y-\xi) \\ -\frac{y^3}{3} + \frac{y^2}{2}(\xi+1.5) - 1.5\xi y - 0.5 + \sin(\omega x) \end{bmatrix},$$

$$\boldsymbol{u}_d = \begin{bmatrix} \omega\cos(\omega x)y \\ \chi(y+0.5) + \sin(\omega x) \end{bmatrix},$$

$$p_s = -\frac{\sin(\omega x)+\chi}{2K} + \nu_s(0.5-\xi) + \cos(\pi y),$$

$$p_d = -\frac{\chi}{K}\frac{(y+0.5)^2}{2} - \frac{\sin(\omega x)y}{K},$$

where

$$\nu_s = 0.1,\ K=1,\ \alpha = 0.5,\ G = \frac{\sqrt{\nu_s K}}{\alpha}, \xi = \frac{1-G}{2(1+G)},\ \chi = \frac{-30\xi - 17}{48},\ \text{and } \omega = 6.0.$$

The right hand sides $\boldsymbol{f}_s$, $\boldsymbol{f}_d$, and q_d for the Stokes-Darcy flow system are obtained by plugging the analytical solution into flow equations. The boundary conditions are as follows: for the Stokes region, the velocity $\boldsymbol{u}_s$ is specified on the left and top boundaries, and the normal and tangential stresses $(\boldsymbol{\sigma n}_s)\cdot\boldsymbol{n}_s$ and $(\boldsymbol{\sigma n}_s)\cdot\boldsymbol{\tau}_s$ are specified on the right boundary; for the Darcy region, the pressure p_d is specified on the bottom, left and right boundaries. Each region Ω_s and Ω_d is divided into two subdomains, giving a total of four subdomains. The subdomain

grids do not match across the interfaces. The Stokes subdomains are discretized by the Taylor–Hood triangular finite elements with quadratic velocities and linear pressures ($r_s = 2$). The Darcy subdomains are discretized by the lowest order Raviart–Thomas rectangular finite elements ($r_d = l_d = 0$). We use discontinuous piecewise linear mortars on all interfaces ($r_{ss} = r_{dd} = r_{sd} = 1$). To test convergence, we solve the problem on a sequence of grid refinements. On the coarsest level, the subdomain grids are 3×4 in the lower left and upper right subdomains and 2×3 in the other two subdomains. We test two cases, $H = 2h$ and $H = \sqrt{h}$. In both cases the coarsest mortar grids have a single element per interface. In the first case the mortar grids are refined by two each time the subdomain grids are refined by two. In the second case the mortar grids are refined by two each time the subdomain grids are refined by four. Figures 1–2 show the vertical velocity and errors for each example. In Example 1, the vertical velocity is not continuous across the Stokes-Darcy interface, as the latter is not flat, but the normal velocity is continuous. In Example 2, the vertical velocity is normal to the Stokes-Darcy interface and it is continuous. In both cases the velocity is continuous across the Stokes-Stokes and Darcy-Darcy interfaces. The depicted errors show that the error is generally smaller in the Stokes region, while the larger error in the Darcy region is associated with the non-matching interface or the corners of the domain. Figure 3-5 show that multiscale solution has a good match with fine scale solution, but multicale solution only takes 80 total CG iterations instead of 256 iterations for matching grids solution, which means less expensive for a multiscale solution. The numerical errors and convergence rates on all refinement levels are reported in Tables. In the case $H = 2h$ we observe convergence for the Stokes velocity and pressure of order between $h^{3/2}$ and h^2, as well as first order convergence for the Darcy velocity and pressure. We note that the optimal convergence rates for stand alone discretizations are second order for Stokes and first order for Darcy. The reduction in the Stokes convergence in the coupled case is expected, due to the coupling with the lower order Darcy discretization and the effect of the non-matching mortar error. In the case $H = \sqrt{h}$, we observe approximately $O(h)$ convergence for all error norms. Note that in this case the interface consistency error terms are $O(h^{(r_{ss}+1)/2}) = O(h)$ and $O(h^{(r_{dd}+1/2)/2}) = O(h^{(r_{sd}+1/2)/2}) = O(h^{3/4})$, so their effect on the convergence in the Stokes and Darcy regions is more significant. In this multiscale case, one may utilize higher

order mortars to recover optimal fine scale subdomain convergence, see [2] for the Darcy case.

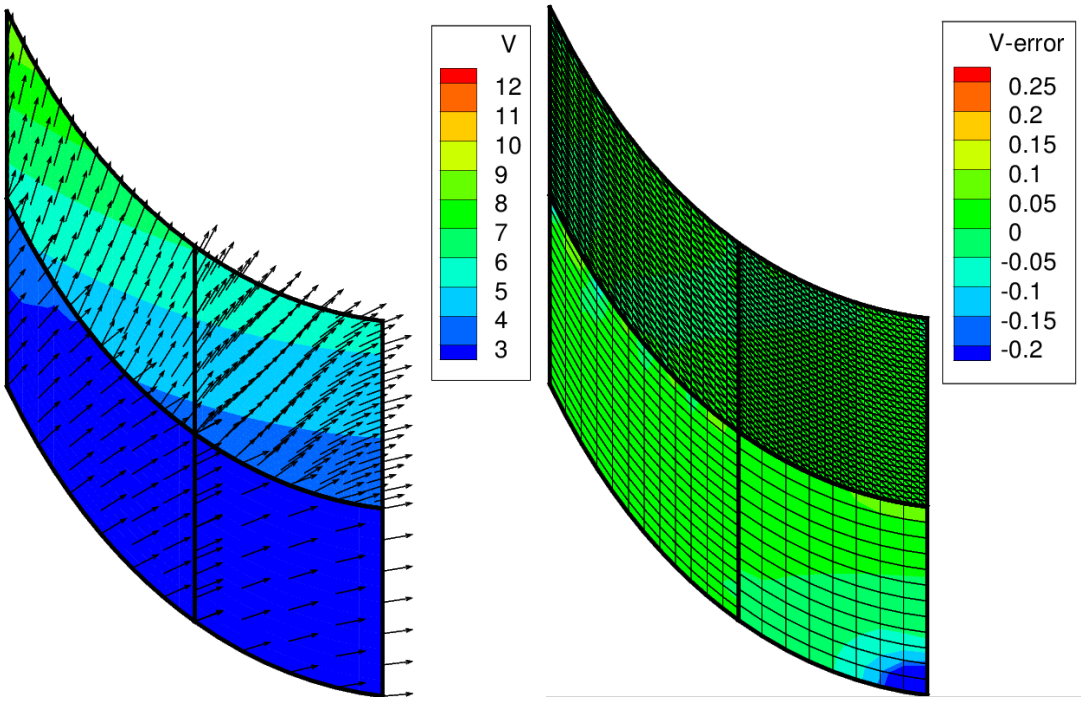

Figure 2.6.1: Computed vertical velocity (left) and error (right) on subdomain meshes 8×12 and 12×16 for Example 1.

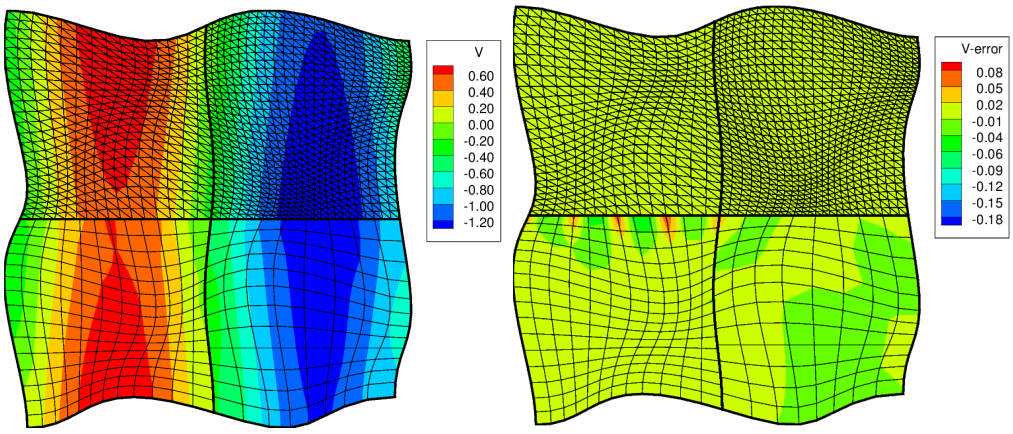

Figure 2.6.2: Computed vertical velocity (left) and error (right) on subdomain meshes 8×12 and 12×16 for Example 2.

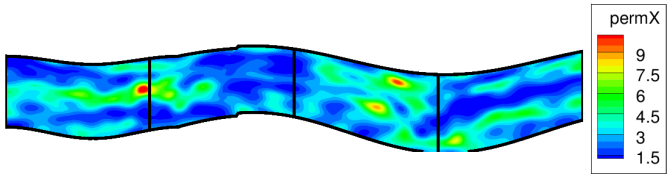

Figure 2.6.3: Permeability in Example 3.

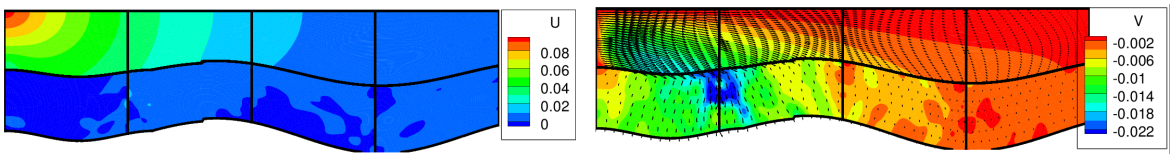

Figure 2.6.4: Computed multiscale solution with horizontal (left) and vertical velocity (right) in Example 3.

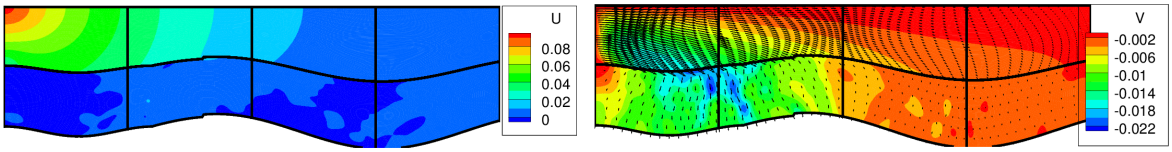

Figure 2.6.5: Computed fine scale solution with horizontal (left) and vertical velocity (right) in Example 3.

mesh	$\|\boldsymbol{u}_s - \boldsymbol{u}_s^h\|_{H^1(\Omega_s)}$	*rate*	$\|p_s - p_s^h\|_{L^2(\Omega_s)}$	*rate*
2x3 3x4	2.68e+00		7.27e-01	
4x6 6x8	1.02e+00	1.39	1.72e-01	2.08
8x12 12x16	3.09e-01	1.72	3.20e-02	2.43
16x24 24x32	8.28e-02	1.90	5.74e-03	2.48
32x48 48x64	2.12e-02	1.97	2.19e-03	1.39

Table 1: Test 1: $H = 2h$. Numerical errors and convergence rates in Ω_s

mesh	$\|\boldsymbol{u}_d - \boldsymbol{u}_d^h\|_{H(\mathrm{div},\Omega_d)}$	*rate*	$\|p_d - p_d^h\|_{L^2(\Omega_d)}$	*rate*
2x3 3x4	2.91e+00		5.23e-01	
4x6 6x8	3.92e-01	2.89	2.67e-01	0.97
8x12 12x16	1.15e-01	1.77	1.32e-01	1.02
16x24 24x32	3.62e-02	1.66	6.60e-02	1.00
32x48 48x64	1.31e-02	1.47	3.30e-02	1.00

Table 2: Test 1: $H = 2h$. Numerical errors and convergence rates in Ω_d

mesh	$\|\boldsymbol{u}_s - \boldsymbol{u}_s^h\|_{H^1(\Omega_s)}$	*rate*	$\|p_s - p_s^h\|_{L^2(\Omega_s)}$	*rate*
2x3 3x4	3.55e-01		3.06e-02	
4x6 6x8	9.27e-02	1.94	7.57e-03	2.01
8x12 12x16	2.17e-02	2.09	1.86e-03	2.02
16x24 24x32	5.42e-03	2.00	5.07e-04	1.88
32x48 48x64	1.51e-03	1.84	1.59e-04	1.67

Table 3: Test 2: $H = 2h$. Numerical errors and convergence rates in Ω_s

mesh	$\|\boldsymbol{u}_d - \boldsymbol{u}_d^h\|_{H(\mathrm{div},\Omega_d)}$	*rate*	$\|p_d - p_d^h\|_{L^2(\Omega_d)}$	*rate*
2x3 3x4	4.96e-01		1.09e-01	
4x6 6x8	2.44e-01	1.02	5.41e-02	1.01
8x12 12x16	1.22e-01	1.00	2.71e-02	1.00
16x24 24x32	6.07e-02	1.00	1.36e-02	0.99
32x48 48x64	3.03e-02	1.00	6.78e-03	1.00

Table 4: Test 2: $H = 2h$. Numerical errors and convergence rates in Ω_d

mesh	$\|\boldsymbol{u}_s - \boldsymbol{u}_s^h\|_{H^1(\Omega_s)}$	*rate*	$\|p_s - p_s^h\|_{L^2(\Omega_s)}$	*rate*
2x3 3x4	2.68e+00		7.27e-01	
8x12 12x16	3.09e-01	1.55	3.44e-02	2.20
32x48 48x64	2.13e-02	1.93	3.00e-03	1.75

Table 5: Test 1: $H = \sqrt{h}$. Numerical errors and convergence rates in Ω_s

mesh	$\|\boldsymbol{u}_d - \boldsymbol{u}_d^h\|_{H(\mathrm{div},\Omega_d)}$	*rate*	$\|p_d - p_d^h\|_{L^2(\Omega_d)}$	*rate*
2x3 3x4	2.91e+00		5.23e-01	
8x12 12x16	2.68e-01	1.72	1.33e-01	0.99
32x48 48x64	1.27e-01	0.54	3.30e-02	1.01

Table 6: Test 1: $H = \sqrt{h}$. Numerical errors and convergence rates in Ω_d

mesh	$\|\boldsymbol{u}_s - \boldsymbol{u}_s^h\|_{H^1(\Omega_s)}$	*rate*	$\|p_s - p_s^h\|_{L^2(\Omega_s)}$	*rate*
2x3 3x4	3.55e-01		3.06e-02	
8x12 12x16	5.79e-02	1.31	4.12e-03	1.45
32x48 48x64	1.05e-02	1.23	7.29e-04	1.24

Table 7: Test 2: $H = \sqrt{h}$. Numerical errors and convergence rates in Ω_s

mesh	$\|\boldsymbol{u}_d - \boldsymbol{u}_d^h\|_{H(\mathrm{div},\Omega_d)}$	*rate*	$\|p_d - p_d^h\|_{L^2(\Omega_d)}$	*rate*
2x3 3x4	4.96e-01		1.09e-01	
8x12 12x16	1.82e-01	0.72	2.72e-02	1.00
32x48 48x64	6.25e-02	0.77	6.82e-03	1.00

Table 8: Test 2: $H = \sqrt{h}$. Numerical errors and convergence rates in Ω_d

3.0 DOMAIN DECOMPOSITION FOR STOKES-DARCY FLOWS WITH CURVED INTERFACES

In this paper, we consider a multidomain formulation, where the simulation domain is decomposed into a union of non-overlapping subdomains of either Stokes or Darcy type. The subdomains are discretized by appropriate stable finite elements on a fine scale, allowing for the grids to be non-matching across interfaces. Coarse scale mortar finite elements are used to impose weakly continuity conditions [27]. Since we consider multiple subdomains, we must account for three types interfaces conditions: Stokes-Darcy, Darcy-Darcy and Stokes-Stokes. On Stokes-Darcy interfaces, normal velocity and normal stress are continuous. On Stokes-Stokes interfaces, both normal and tangential velocity and stress are continuous. On Darcy-Darcy interfaces, normal velocity and pressure are continuous. We employ a non-overlapping domain decomposition (DD) [28, 43, 48] method to reduce the global problem to an interface problem which is solved by the conjugate gradient method. Each iteration involves solving subdomain problems of either Stokes or Darcy type, which is done in parallel.

We consider efficient and accurate discretizations for subdomains with curved interfaces, allowing for the grids to be non-matching across interfaces. In the Darcy region we employ the multipoint flux mixed finite element (MFMFE) method [55, 29, 54]. The method can handle irregular grids and reduces to cell-centered finite differences for the pressure. Standard conforming Stokes elements are used in the Stokes region. Interface mortar conditions on curved interfaces with non-matching grids are imposed by mapping the physical grids to reference grids with flat interfaces.

3.1 DOMAIN DECOMPOSITION VARIATIONAL FORMULATION

Let Ω_s, respectively Ω_d, be decomposed into N_s, respectively N_d, non-overlapping polyhedral subdomains: $\overline{\Omega}_s = \cup_{i=1}^{N_s} \overline{\Omega}_{s,i}$, $\overline{\Omega}_d = \cup_{i=N_s+1}^{N} \overline{\Omega}_{d,i}$, where $N = N_s + N_d$. We can also number the subdomains with a single index $1 \leq i \leq N$, the Stokes subdomains running from 1 to N_s. We denote $\Gamma_{ij} = \partial\Omega_i \cap \partial\Omega_j, 1 \leq i < j \leq N$. Let Γ_{ss} and Γ_{dd} denote the set of Stokes-Stokes and Darcy-Darcy interfaces: $\Gamma_{ss} = \cup_{1\leq i<j\leq N_s} (\partial\Omega_i \cap \partial\Omega_j)$, $\Gamma_{dd} = \cup_{N_s+1\leq i<j\leq N} (\partial\Omega_i \cap \partial\Omega_j)$. The union of all the interfaces is denoted by $\Gamma = \Gamma_{sd} \cup \Gamma_{dd} \cup \Gamma_{ss}$. In addition to the interface conditions on Γ_{sd}, we have

$$[\mathbf{u}_d \cdot \mathbf{n}] = 0, \quad [p_d] = 0 \quad \text{on } \Gamma_{dd}, \quad [\mathbf{u}_s] = \mathbf{0}, \quad [\mathbf{T}(\mathbf{u}_s, p_s)\mathbf{n}] = \mathbf{0} \quad \text{on } \Gamma_{ss}, \tag{3.1.1}$$

where the jumps on an interface Γ_{ij}, for $1 \leq i < j \leq N$, are defined as: $[\mathbf{v}\cdot\mathbf{n}] = \mathbf{v}_i\cdot\mathbf{n}_i + \mathbf{v}_j\cdot\mathbf{n}_j$, $[\mathbf{Tn}] = \mathbf{T}_i\mathbf{n}_i + \mathbf{T}_j\mathbf{n}_j$, and $[\mathbf{v}] = (\mathbf{v}_i - \mathbf{v}_j)|_{\Gamma_{ij}}$, where $\mathbf{v}_i = \mathbf{v}|_{\Omega_i}$ and $\mathbf{n}_i$ denotes the outward unit normal vector on $\partial\Omega_i$.

In the fluid region Ω_s, the velocity and pressure spaces are given by

$$X_s = \left\{\mathbf{v}_s \in L^2(\Omega_s)^d : \mathbf{v}_{s,i} \in H^1(\Omega_{s,i})^d, \mathbf{v}_s = 0 \ \text{ on } \Gamma_s\right\} \ \text{ and } \ W_s = L^2(\Omega_s).$$

In the porous medium region Ω_d, we define the velocity and pressure spaces by

$$X_d = \left\{\mathbf{v}_d \in L^2(\Omega_d)^d : \mathbf{v}_{d,i} \in H(\mathrm{div}; \Omega_{d,i}), \mathbf{v}_d \cdot \mathbf{n}_d = 0 \ \text{ on } \Gamma_d\right\} \ \text{ and } \ W_d = L^2(\Omega_d),$$

where $H(\mathrm{div}; \Omega_{d,i}) = \{\mathbf{v}_d \in (L^2(\Omega_{d,i}))^d : \nabla \cdot \mathbf{v}_{d,i} \in L^2(\Omega_{d,i})\}$. The spaces on the whole domain are defined by

$$X = X_s \oplus X_d \ \text{ and } \ W = \left\{w = (w_s, w_d) \in W_s \oplus W_d : \int_\Omega w\, dx = 0\right\}.$$

The interface space Λ is the dual of the trace of $\mathbf{u}_s$ on Γ_{ss} or the normal trace $\mathbf{u}_d \cdot \mathbf{n}$ on Γ_{sd} and Γ_{dd}. The non-overlapping domain decomposition weak formulation for the coupled problem is given by: find $(\mathbf{u}, p, \boldsymbol{\lambda}) \in X \times W \times \Lambda$ such that

$$a(\mathbf{u}, \mathbf{v}) + b(\mathbf{v}, p) + b_\Gamma(\mathbf{v}, \boldsymbol{\lambda}) = \int_\Omega \mathbf{f} \cdot \mathbf{v}, \ \forall \mathbf{v} \in X, \tag{3.1.2}$$

$$b(\mathbf{u}, w) = -\int_{\Omega_d} q_d \, w, \ \forall w \in W \tag{3.1.3}$$

$$b_\Gamma(\mathbf{u}, \boldsymbol{\mu}) = 0, \ \forall \boldsymbol{\mu} \in \Lambda, \tag{3.1.4}$$

where the bilinear forms are defined as

$$\begin{aligned}
&\forall\, (\mathbf{u}_s, \mathbf{v}_s) \in X_s \times X_s\,,\ a_{s,i}(\mathbf{u}_s, \mathbf{v}_s) = 2\,\nu_s \int_{\Omega_{s,i}} \mathbf{D}(\mathbf{u}_{s,i}) : \mathbf{D}(\mathbf{v}_{s,i}) \\
&\qquad + \sum_{j=1}^{d-1} \int_{\partial\Omega_{s,i} \cap \Gamma_{sd}} \frac{\nu_s \alpha}{\sqrt{K_j}} (\mathbf{u}_{s,i} \cdot \boldsymbol{\tau}_j)(\mathbf{v}_s \cdot \boldsymbol{\tau}_j)\ ,\ 1 \le i \le N_s, \\
&\forall\, (\mathbf{u}_d, \mathbf{v}_d) \in X_d \times X_d\,,\ a_{d,i}(\mathbf{u}_d, \mathbf{v}_d) = \nu_d \int_{\Omega_{d,i}} \mathbf{K}^{-1} \mathbf{u}_{d,i} \cdot \mathbf{v}_{d,i}\ ,\ 1 \le i \le N_d, \\
&\forall\, (\mathbf{v}, w) \in X \times W\,,\ b_i(\mathbf{v}, w) = -\int_{\Omega_i} w_i \, \nabla \cdot \mathbf{v}_i\ ,\ 1 \le i \le N, \\
&a(\mathbf{u}, \mathbf{v}) = \sum_{i=1}^{N_s} a_{s,i}(\mathbf{u}, \mathbf{v}) + \sum_{i=1}^{N_d} a_{d,i}(\mathbf{u}, \mathbf{v}), \quad b(\mathbf{v}, w) = \sum_{i=1}^{N} b_i(\mathbf{v}, w),
\end{aligned}$$

and the global interface bilinear form is given by:

$$\forall\, (\mathbf{v}, \boldsymbol{\mu}) \in X \times \Lambda\,,\ b_\Gamma(\mathbf{v}, \boldsymbol{\mu}) = \int_{\Gamma_{ss}} [\mathbf{v}]\, \boldsymbol{\mu} + \int_{\Gamma_{dd}} [\mathbf{v} \cdot \mathbf{n}]\, \boldsymbol{\mu} + \int_{\Gamma_{sd}} [\mathbf{v} \cdot \mathbf{n}]\, \boldsymbol{\mu}.$$

Existence and uniqueness of a solution to (3.1.2)–(3.1.4) are shown in [27], see also [36].

3.2 FINITE ELEMENT DISCRETIZATION

Let $\mathcal{T}_i^h$ to be a family of shape regular partitions of Ω_i consisting of triangles or tetrahedra in the Stokes region and triangles, tetrahedra, quadrilaterals, or hexahedra in the Darcy region, where h is the maximum element diameter. Partitions $\mathcal{T}_i^h$ and $\mathcal{T}_j^h$ may not match on the interface Γ_{ij}. On the interface we define a coarse scale partition $\mathcal{T}_{ij}^H$ with a maximum element size H consisting of segments, triangles, or parallelograms.

In the Stokes region, for each $\Omega_{s,i}$, let $(X_{s,i}^h, W_{s,i}^h) \subset H^1(\Omega_{s,i})^n \times L^2(\Omega_{s,i})$ be a pair of finite element spaces which satisfy a uniform discrete inf-sup condition for the divergence and Korn inequality for the deformation tensor, such as the MINI elements, the Taylor-Hood elements or the Bernardi-Raugel elements [11]. We assume that each pair contains at least polynomials of degree r_s and $r_s - 1$ for velocity and pressure, respectively. In the Darcy region, let $(X_{d,i}^h, W_{d,i}^h) \subset H(\mathrm{div}; \Omega_{d,i}) \times L^2(\Omega_{d,i})$ be a pair of mixed finite element spaces which satisfy a uniform discrete inf-sup condition for the divergence, such as the Raviart-Thomas (RT) elements, the Brezzi-Douglas-Marini (BDM) elements, the Brezzi-Douglas-Fortin-Marini (BDFM) elements or the Brezzi-Douglas- Duràn-Fortin (BDDF) elements [11]. We assume that each pair contains at least polynomials of degree r_d and l_d for velocity and pressure, respectively, where $l_d = r_d$ or $l_d = r_d - 1$. We also consider a special mixed element method called the multipoint flux mixed finite element (MFMFE) method for efficient discretizations of Darcy flow on irregular grids [55, 29, 54]. The method employs the lowest order BDM_1 space on simplices or quadrilaterals or an enhanced BDDF_1 space on hexahedra. These spaces have the property that on each element edge of face with s vertices, the velocity space has s normal degrees of freedom, one associated with each vertex. This allows for the velocity to be eliminated locally around each vertex in terms of neighboring pressures through the use of an appropriate quadrature rule, resulting in a cell-centered system for the pressure. The mixed finite element spaces in Darcy are defined on a reference element $\hat{E}$ and via a bijection mapping $F_E : \hat{E} \to E$ on the physical elements as

$$\mathbf{V}_h(E) = \frac{1}{J_E} DF_E \hat{\mathbf{V}}(\hat{E}) \circ F_E^{-1}, \quad W_h(E) = \hat{W}(\hat{E}) \circ F_E^{-1},$$

where the Piola transformation is used to preserve normal components of the velocity. Here DF_E and $J_E = |\det(DF_E)|$ are the Jacobian matrix and its determinant, respectively. In the MFMFE method, we employ the quadrature rule on an element E for the local velocity elimination as

$$(K^{-1}\mathbf{q},\mathbf{v})_{Q,E} \equiv (\mathcal{K}^{-1}\hat{\mathbf{q}},\hat{\mathbf{v}})_{\hat{Q},\hat{E}} \equiv \frac{|\hat{E}|}{s}\sum_{i=1}^{s}\mathcal{K}^{-1}(\hat{\mathbf{r}}_i)\hat{\mathbf{q}}(\hat{\mathbf{r}}_i)\cdot\hat{\mathbf{v}}(\hat{\mathbf{r}}_i), \quad \text{where} \quad \mathcal{K} = JDF^{-1}\hat{K}(DF^{-1})^T.$$

Note that this the trapezoidal quadrature rule on the reference element. It localizes the interactions of the velocity degrees of freedom and gives a block diagonal velocity mass matrix with blocks associated with mesh vertices. It is then inexpensive to eliminate the velocities resulting in a positive definite pressure system. The global finite element space are $X^h := \oplus_{i=1}^N X_i^h$, $W^h := \oplus_{i=1}^N W_i^h \cap L_0^2(\Omega)$. On each interface, let Λ_{ij}^H be a finite element space associated with $\mathcal{T}_{ij}^H$ consisting of continuous or discontinuous piecewise polynomials of degree at least r_{ss} on Γ_{ss}, r_{dd} on Γ_{dd}, and r_{sd} on Γ_{sd}. The global mortar finite element space is $\Lambda^H := \bigoplus \Lambda_{ij}^H$.

The multiscale mortar finite element discretization for the Stokes-Darcy system is given by: find $(\mathbf{u}^h, p^h, \boldsymbol{\lambda}^H) \in X^h \times W^h \times \Lambda^H$ such that

$$\forall\, \mathbf{v}^h \in X^h,\ a_h(\mathbf{u}^h,\mathbf{v}^h) + b(\mathbf{v}^h,p^h) + b_\Gamma(\mathbf{v}^h,\boldsymbol{\lambda}^H) = \int_\Omega \mathbf{f}\cdot\mathbf{v}^h, \tag{3.2.1}$$

$$\forall\, w^h \in W^h,\ b(\mathbf{u}^h,w^h) = -\int_{\Omega_d} w^h\, q_d, \tag{3.2.2}$$

$$\forall\, \boldsymbol{\mu}^H \in \Lambda^H,\ b_\Gamma(\mathbf{u}^h,\boldsymbol{\mu}^H) = 0, \tag{3.2.3}$$

where $a_h(\cdot,\cdot) = a(\cdot,\cdot)$ in Ω_s and Ω_d, when standard mixed finite element discretizations are used, and it is an approximation to $a(\cdot,\cdot)$ in Ω_d based on the quadrature rule in the case of the MFMFE method.

Remark 3.2.1. *To handle domains with curved non-matching grid interfaces, the continuity condition (3.2.3) is imposed by mapping the subdomain and mortar grids to reference grids with flat interfaces. On Stokes-Darcy and Darcy-Darcy interfaces, we employ the Piola transformation for the velocity, which preserves the normal component of the vector:* $\mathbf{u}\cdot\mathbf{n}|e| = \hat{\mathbf{u}}\cdot\hat{\mathbf{n}}|\hat{e}|$. *The matching condition* $\langle[\mathbf{u}^h\cdot\mathbf{n}],\mu^H\rangle = 0$ *is imposed on the reference grid configuration by projecting the normal component on each side onto the reference mortar*

grid. On Stokes-Stokes interfaces, the grids are also mapped to reference grids to impose $\langle [\mathbf{u}^h], \mu^H \rangle = 0$. *Since full vector continuity is imposed, the standard change of variables is used to map the velocity space in this case.*

The following convergence result has been shown in [27, 46].

Theorem 3.2.1. *Assuming sufficient smoothness of the solution, there exists a positive constant* C *independent of* h *and* H *such that*

$$\|\mathbf{u} - \mathbf{u}^h\|_V + \|p - p^h\|_W \leq C(h^{r_s} + h^{r_d+1} + h^{l_d+1} + H^{r_{ss}+1/2} + H^{r_{dd}+1/2} + H^{r_{sd}+1/2}).$$

3.3 A NON-OVERLAPPING DOMAIN DECOMPOSITION ALGORITHM

In this section, we present a non-overlapping domain decomposition algorithm [50]. We show that the algebraic system (3.2.1)–(3.2.3) can be reduced to a mortar interface problem for λ^H that can be solved by a Krylov space iterative method. Each iteration requires computing the action of the interface operator, which is done by solving subdomain problems of either Stokes or Darcy type in parallel.

Following [28], each local problem can be split into two parts. One part has specified normal stress in Stokes or pressure in Darcy on the interface and zero source term and boundary conditions. The other part is the complementary problem with zero normal stress or pressure on the interface and the given source term and boundary conditions. In the Darcy subdomains Ω_i, $N_S + 1 \leq i \leq N$, given pressure λ_n on Γ_{ij}, the first problem is: find $(\mathbf{u}_i^*(\lambda_n), p_i^*(\lambda_n)) \in X_{d,i}^h \times W_{d,i}^h$ such that

$$a_i(\mathbf{u}_i^*(\lambda_n), \mathbf{v}_i) + b_i(\mathbf{v}_i, p_i^*(\lambda_n)) = -\langle \lambda_n, \mathbf{v}_i \cdot \mathbf{n}_i \rangle_{\partial\Omega_i \setminus \partial\Omega}, \quad \mathbf{v}_i \in X_{d,i}^h, \tag{3.3.1}$$

$$b_i(\mathbf{u}_i^*(\lambda_n), w_i) = 0, \quad w_i \in W_{d,i}^h, \tag{3.3.2}$$

and the corresponding complementary problem is: find $(\bar{\mathbf{u}}_i, \bar{p}_i) \in X_{h,i}^D \times W_{h,i}^D$ such that

$$a_i(\bar{\mathbf{u}}_i, \mathbf{v}_i) + b_i(\mathbf{v}_i, \bar{p}_i) = (\mathbf{f}_i, \mathbf{v}_i)_{\Omega_i}, \quad \mathbf{v}_i \in X_{d,i}^h,$$

$$b_i(\bar{\mathbf{u}}_i, w_i) = -(q_i, w_i)_{\Omega_i}, \quad w_i \in W_{d,i}^h.$$

In the Stokes subdomains Ω_i, $1 \le i \le N_S$, given normal stress $\boldsymbol{\lambda} = (\lambda_n, \boldsymbol{\lambda}_\tau)$, where λ_n is specifies on $\partial\Omega_i \setminus \partial\Omega$ and $\boldsymbol{\lambda}_\tau = (\lambda_\tau^1, \ldots, \lambda_\tau^{d-1})$ on Γ_{ss}, the first problems is: find $(\mathbf{u}_i^*(\boldsymbol{\lambda}), p_i^*(\boldsymbol{\lambda})) \in X_{s,i}^h \times W_{s,i}^h$ such that

$$a_i(\mathbf{u}_i^*(\boldsymbol{\lambda}), \mathbf{v}_i) + b_i(\mathbf{v}_i, p_i^*(\boldsymbol{\lambda})) = -\langle \lambda_n, \mathbf{v}_i \cdot \mathbf{n}_i \rangle_{\partial\Omega_i \setminus \partial\Omega} - \sum_{l=1}^{d-1} \langle \lambda_\tau^l, \mathbf{v}_i \cdot \boldsymbol{\tau}_i^l \rangle_{\partial\Omega_i \cap \Gamma_{ss}}, \quad \mathbf{v}_i \in X_{s,i}^h,$$

$$b_i(\mathbf{u}_i^*(\boldsymbol{\lambda}), w_i) = 0, \quad w_i \in W_{s,i}^h,$$

and the corresponding complementary problem is: find $(\bar{\mathbf{u}}_i, \bar{p}_i) \in X_{s,i}^h \times W_{s,i}^h$ such that

$$a_i(\bar{\mathbf{u}}_i, \mathbf{v}_i) + b_i(\mathbf{v}_i, \bar{p}_i) = (\mathbf{f}_i, \mathbf{v}_i)_{\Omega_i}, \quad \mathbf{v}_i \in X_{s,i}^h, \tag{3.3.3}$$

$$b_i(\bar{\mathbf{u}}_i, w_i) = 0, \quad w_i \in W_{s,i}^h. \tag{3.3.4}$$

Note that the first type problem has boundary conditions on the interfaces

$$-(\mathbf{T}\mathbf{n}_i) \cdot \mathbf{n}_i = \lambda_n, \quad -(\mathbf{T}\mathbf{n}_i) \cdot \boldsymbol{\tau}_i^l = \lambda_\tau^l, \quad 1 \le l \le d-1, \quad 1 \le i \le N_S, \quad \text{on } \Gamma_{ss},$$

and

$$-(\mathbf{T}\mathbf{n}_i) \cdot \mathbf{n}_i = \lambda_n, \quad -(\mathbf{T}\mathbf{n}_i) \cdot \boldsymbol{\tau}_i^l - \frac{\mu_s \alpha_0}{\sqrt{K_l}} \mathbf{u}_i \cdot \boldsymbol{\tau}_i^l = 0, \quad 1 \le l \le d-1, \quad 1 \le i \le N_S, \text{ on } \Gamma_{sd}.$$

It is easy to see that solving (3.2.1)–(3.2.3) is equivalent to solving the interface problem: find $\boldsymbol{\lambda}^H \in \Lambda^h$ such that

$$s(\boldsymbol{\lambda}^H, \boldsymbol{\mu}^H) \equiv -b_\Gamma(\mathbf{u}^*(\boldsymbol{\lambda}^H), \boldsymbol{\mu}^H) = b_\Gamma(\bar{\mathbf{u}}, \boldsymbol{\mu}^H), \quad \boldsymbol{\mu}^H \in \Lambda^H. \tag{3.3.5}$$

After solving interface problems, one can recover the global velocity and pressure by $\mathbf{u}^h = \mathbf{u}^*(\boldsymbol{\lambda}^H) + \bar{\mathbf{u}}$, $p^h = p^*(\boldsymbol{\lambda}^H) + \bar{p}$.

Let us introduce the Steklov–Poincaré type operator $S : \Lambda_H \to \Lambda_H$,

$$\forall\ \boldsymbol{\lambda}^H \in \Lambda^H, \quad (S\boldsymbol{\lambda}^H, \boldsymbol{\mu}^H) = s(\boldsymbol{\lambda}^H, \boldsymbol{\mu}^H) \quad \forall\ \boldsymbol{\mu}^H \in \Lambda^H.$$

Then the interface problem (3.3.5) can be written as: find $\boldsymbol{\lambda}^H \in \Lambda^H$ such that

$$S\boldsymbol{\lambda}^H = b, \tag{3.3.6}$$

where $b : \Lambda^H \to \mathbb{R}$, $b(\boldsymbol{\mu}^H) = b_\Gamma(\bar{\mathbf{u}}_h, \boldsymbol{\mu}^H)$, $\forall\, \boldsymbol{\mu}^H \in \Lambda^H$.

The matrix form of the above method is as follows. We use u, p, and λ to represent the degrees of freedom for velocity, pressure, and Lagrange multipliers, respectively. The discrete right hand side functions in the coupled system are denoted by F and Q. The linear system arising in (3.2.1)–(3.2.3) is of the form

$$\begin{pmatrix} A & B & C \\ B^t & 0 & 0 \\ C^t & 0 & 0 \end{pmatrix} \begin{pmatrix} u \\ p \\ \lambda \end{pmatrix} = \begin{pmatrix} F \\ Q \\ 0 \end{pmatrix} \quad \Leftrightarrow \quad \begin{pmatrix} R & \tilde{C} \\ \tilde{C}^t & 0 \end{pmatrix} \begin{pmatrix} x \\ \lambda \end{pmatrix} = \begin{pmatrix} \eta \\ 0 \end{pmatrix},$$

where $x = (u, p)^t$ is the vector of subdomain unknowns and $\eta = (F, Q)^t$. Then the matrix form of the interface problem (3.3.6) corresponds to the Schur complement system

$$\tilde{C}^t R^{-1} \tilde{C} \lambda = \tilde{C}^t R^{-1} \eta. \tag{3.3.7}$$

Note that a Krylov space iterative method for solving (3.3.7) requires at each iteration computing the action of

$$R^{-1} = \begin{pmatrix} R_1^{-1} & & \\ & \ddots & \\ & & R_N^{-1} \end{pmatrix},$$

which is achieved by solving local subdomain problems in parallel. The following result on the properties of the interface operator has been shown in [50] for the case $H = O(h)$.

Theorem 3.3.1. *The bilinear form $s(\cdot, \cdot)$ is symmetric and positive definite on $\Lambda^H \setminus \mathbb{R}$. Moreover, there exist positive constants C_1 and C_2 independent of h and H such that*

$$C_1 \min\left\{h, \frac{K_{\min}^2}{K_{\max}}\right\} \leq \frac{s(\boldsymbol{\lambda}, \boldsymbol{\lambda})}{\|\boldsymbol{\lambda}\|_\Gamma^2} \leq C_2 \max\left\{1, \frac{K_{\max}}{h}\right\}, \quad \forall \boldsymbol{\lambda} \in \Lambda^H \setminus \mathbb{R}, \tag{3.3.8}$$

where $K_{\min}$ and $K_{\max}$ are the smallest and largest eigenvalues of $\mathbf{K}$, respectively.

The above result implies that the Conjugate Gradient method can be employed for the solution of the interface problem (3.3.5). The condition number of the interface operator is $O(h^{-2})$. Efficient interface preconditioners such as balancing [14, 42] can be employed to speed up the iteration. Another possibility is to employ a multiscale flux basis [22] to reduce the cost of each interface iterations.

3.4 NUMERICAL RESULTS

In this section, we present three numerical examples to study the behavior of the method. In the numerical tests we consider the case $\mathbf{T}(\mathbf{u}_s, p_s) = -p_s\mathbf{I} + \nu\nabla\mathbf{u}_s$ in Ω_s. In the first two examples we take $\mathbf{K} = K\mathbf{I}$ in Ω_d, where K is a positive constant. In the last example we test heterogeneous permeability. In the first example, we test the numerical convergence and the condition number of the interface algebraic system. The analytical solution is as in the numerical tests in [27]. It is designed to satisfy the interface conditions (1.1.4)–(1.1.6). The computational domain $\overline{\Omega} = \overline{\Omega}_s \cup \overline{\Omega}_d$ is a smooth map of the reference domain $\hat{\Omega}$, where $\hat{\Omega}_s = (0,2) \times (\frac{1}{2}, 1)$ and $\hat{\Omega}_d = (0,2) \times (0, \frac{1}{2})$. The boundary conditions are defined as follows. In the Darcy region, the pressure is specified on the left, right, and bottom boundaries, while in the Stokes region, the velocity is specified on the left and top boundaries, and normal and tangential stress are specified on the right boundary. We split the domain into eight subdomains, four in Stokes and four in Darcy. The subdomain girds are non-matching on the interfaces. We use the lowest order Taylor–Hood triangular finite elements ($r_s = 2$) to discretize the Stokes subdomains and the MFMFE method on quadrilaterals ($r_d = l_d = 0$) to discretize the Darcy subdomains. Discontinuous piecewise linear mortar finite elements are used on all interfaces ($r_{ss} = r_{sd} = r_{dd} = 1$). To test convergence, we run a sequence of nested grid refinements. The coarsest level girds are alternating 3×4 and 2×3 and $H = 2h$. The computed vertical velocity and its numerical error on the second level are shown in Figure 3.4.1. Note that the vertical velocity, which is normal to the Stokes-Darcy interface is continuous. The numerical errors and convergence rates are reported in Tables 9 and 10, where l denotes the grid level. We observe convergence for the Stokes velocity and pressure of order between $h^{3/2}$ and h^2, as well as first order convergence for the Darcy velocity and pressure. The optimal convergence rates for stand alone discretizations are second order for Stokes and first order for Darcy. The reduction in the Stokes convergence in the coupled case is expected, due to the coupling with the lower order Darcy discretization and the effect of the non-matching grids error, see Theorem 3.2.1. In Table 11 we report the extreme eigenvalues and condition number of the interface operator and the number of CG iterations on all grid levels. We confirm that smallest eigenvalue is $O(h)$ and the largest eigenvalue is

$O(h^{-1})$, leading to condition number is $O(h^{-2})$, as predicted by Theorem 3.3.1.

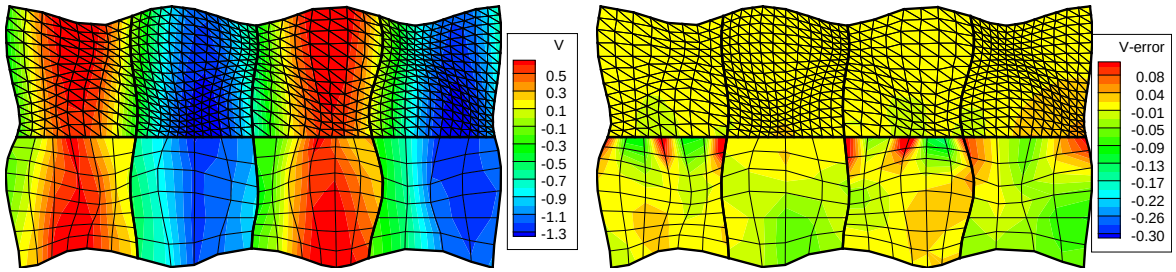

Figure 3.4.1: Computed vertical velocity (left) and error (right) on subdomain grids 4×6 and 6×8 in Example 1.

l	$\|\mathbf{u}_s - \mathbf{u}_{s,h}\|_{1,\Omega_s}$	*rate*	$\|p - p_{s,h}\|_{\Omega_s}$	*rate*
1	5.89e-01		4.58e-02	
2	1.49e-01	1.98	1.15e-02	1.99
3	3.66e-02	2.03	2.82e-03	2.03
4	9.65e-03	1.92	7.61e-04	1.89
5	2.96e-03	1.70	2.43e-04	1.65

Table 9: Numerical errors and convergence rates in Ω_s for Example 1.

In Example 2, we present a more realistic geometry domain, see Figure 3.4.2. In the Stokes region we specify inflow condition on the the left boundary and zero stress on the right boundary. On the top surface boundary of the Stokes region, a combination of horizontal velocity and zero normal stress is specified. In the Darcy region, we specify no flow condition on the left and right boundaries and Dirichlet pressure condition on the bottom boundary. There are no external forces. In this example we study the effect of changing the permeability on the interface condition number. We run three tests with $K = 1.0, 0.1, 0.01$ on the same sequence of grid refinements as in Example 1. The results are presented in Tables 12–14. In all three cases the smallest eigenvalue is approximately a constant, which indicates that the constant term on the left in (3.3.8) is dominant. In the case $K = 1.0$, the largest eigenvalue is

l	$\|\mathbf{u}_d - \mathbf{u}_{d,h}\|_{H(\mathrm{div},\Omega_d)}$	*rate*	$\|p - p_{d,h}\|_{\Omega_d}$	*rate*
1	7.20e-01		1.51e-01	
2	3.61e-01	1.00	7.50e-02	1.01
3	1.81e-01	1.00	3.76e-02	1.00
4	9.04e-02	1.00	1.88e-02	1.00
5	4.51e-02	1.00	9.40e-03	1.00

Table 10: Numerical errors and convergence rates in Ω_d for Example 1.

$O(h^{-1})$ as expected by the theory. In the cases $K = 0.1$ and $K = 0.01$, the largest eigenvalue is approximately constant, which indicates that for small enough permeability the constant term on the right in (3.3.8) is dominant. We also observe that the largest eigenvalue scales with K, which is consistent with the right inequality in (3.3.8).

The final example is a simulation of coupled surface water and ground water flows using the realistic geometry from Example 2 and heterogeneous permeability K given by a single realization of a stochastic permeability field. A Karhunen-Loève (KL) expansion for the log permeability $Y = \ln(K)$ (a scalar quantity) is computed from the specified covariance function

$$C_Y(\mathbf{x}, \bar{\mathbf{x}}) = \sigma_Y^2 \exp\left[\frac{-|x_1 - \bar{x}_1|}{\eta_1} - \frac{|x_2 - \bar{x}_2|}{\eta_2}\right].$$

The parameters used for this test are mean value 1.0, correlation lengths $\eta_1 = 0.1$, $\eta_2 = 0.05$, and variance $\sigma_Y = 2.1$. The series is truncated after 400 terms. The permeability is shown in Figure 3.4.3. The boundary conditions are as in Example 2, except that no flow is specified on the right boundary in Stokes. The grids are as in Example 2, except that they have been refined by 2 in the x-direction. The computed solution on the second refinement level is plotted in Figure 4.3.14. The eigenvalues and condition number of the interface operator are presented in Table 15. Since $K_{\min}$ is approximately 0.1 and $K_{\max}$ is approximately 10, the term $\frac{K_{\min}^2}{K_{\max}}$ is dominant on the left inequality in (3.3.8) and the term $\frac{K_{\max}}{h}$ is dominant in the right inequality, resulting in smallest eigenvalue $O(1)$ an largest eigenvalue $O(h^{-1})$.

l	$eig.min.$	$eig.max.$	$cond(S_h)$	$iter.num.$
1	0.546	18.639	34.2	30
2	0.200	36.441	182.2	69
3	8.237e-02	90.086	1093.7	153
4	3.423e-02	158.217	4622.0	279
5	1.511e-02	318.619	21087.7	585

Table 11: Interface condition number and number of CG iterations in Example 1.

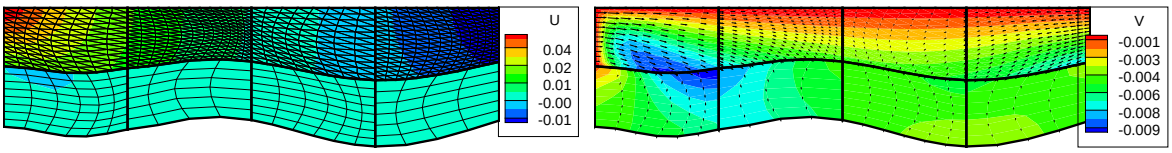

Figure 3.4.2: Computed horizontal (left) and vertical velocity (right) on subdomain grids 4×6 and 6×8 in Example 2.

l	$eig.min.$	$eig.max.$	$cond(S_h)$	$iter.num.$
1	0.313	16.515	52.8	36
2	0.11	33.886	288.0	64
3	8.243e-02	62.297	755.8	101
4	5.836e-02	115.363	1976.7	135
5	7.878e-02	222.677	2826.6	179

Table 12: Interface condition number and number of CG iterations in Example 2: $K = 1.0$.

l	$eig.min.$	$eig.max.$	$cond(S_h)$	$iter.num.$
1	0.297	21.685	73.0	43
2	9.406e-02	15.654	166.4	53
3	4.604e-02	17.664	383.6	72
4	4.038e-02	15.324	379.5	71
5	3.472e-02	21.074	607.0	86

Table 13: Interface condition number and number of CG iterations in Example 2: $K = 0.1$.

l	$eig.min.$	$eig.max.$	$cond(S_h)$	$iter.num.$
1	2.443e-02	341.748	13990.2	165
2	6.697e-02	258.815	3864.5	137
3	3.788e-02	255.276	6739.1	150
4	2.867e-02	220.372	7685.4	176
5	2.243e-02	236.620	10550.8	158

Table 14: Interface condition number and number of CG iterations in Example 2:$K = 0.01$.

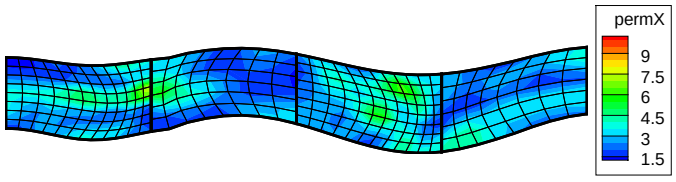

Figure 3.4.3: Permeability in Example 3.

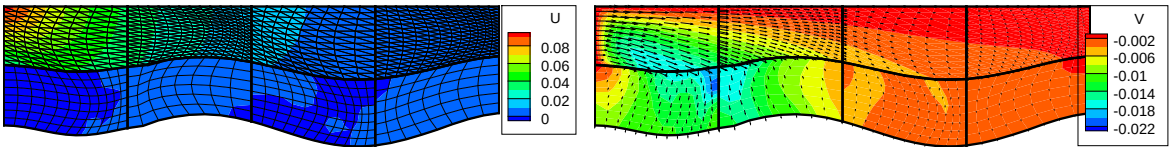

Figure 3.4.4: Computed horizontal (left) and vertical velocity (right) on subdomain grids 8×6 and 12×8 in Example 3.

l	$eig.min.$	$eig.max.$	$cond(S_h)$	$iter.num.$
1	0.317	98.914	312.3	65
2	0.115	182.041	1585.2	127
3	6.705e-02	427.515	6375.8	191
4	8.180e-02	937.411	11459.3	268
5	9.633e-02	2863.566	29725.9	398

Table 15: Interface condition number and number of CG iterations in Example 3.

4.0 COUPLING STOKES-DARCY FLOW WITH TRANSPORT ON IRREGULAR GRIDS

In this chapter, We employ the Local Discontin Galerkin (LDG) mortar method to discretize transport equation which is based on [49, 35]. The method is locally mass conservative and due to a built-in upwinding mechanism it accurately approximates sharp fronts. The LDG mortar method can be formulated on general unstructured grids and allows one to vary the degree of the approximating polynomials from element to element. The LDG mortar method combines ideas from the DG and the mortar MFE methods, since it approximates both the concentration and the diffusive flux using functions, which are discontinuous across the inter-element boundaries.

In the method, the subdomain grids need not match and the mortar grid may be much coarser, giving a two-scale method. We weakly impose the boundary condition on the inflow part of the interface and the Dirichlet boundary condition on the elliptic part of the interface via Lagrange multipliers, for subdomain problems. We provide the matching condition on the interface by weakly imposing the continuity of the total flux on the interface and the continuity of the solution on the elliptic part of the interface via mortar finite elements. The (discrete) problem is now solvable in each subdomain in terms of Lagrange multipliers and the resulting algorithm is easily parallelizable. By using a higher order mortar approximation, we are able to compensate for the coarseness of the grid scale and maintain good(fine scale) overall accuracy.When the interface is not resolved well while the subdomain scales are fine enough, our approach also makes it easy to improve global accuracy by simply refining the local mortar grid where needed. We also extend previous LDG tranport analysis [13, 12]to nondivergence free velocity.

4.1 LDG MORTAR METHOD FOR TRANSPORT

The Stokes-Darcy flow system is coupled with transport equation on $\Omega = \Omega_1 \cup \Omega_2$. We rewrite the transport equation in a mixed form by introducing the diffusive flux:

$$\boldsymbol{z} = -\boldsymbol{D}\nabla c \tag{4.1.1}$$

The original system is equivalent to

$$\phi c_t + \nabla \cdot (c\mathbf{u} + \boldsymbol{z}) = \phi s \quad \forall (\mathbf{x}, t) \in \Omega \times (0, T), \tag{4.1.2}$$

where $c(\mathbf{x}, t)$ is the concentration of some chemical component, $0 < \phi_* \leq \phi(\mathbf{x}) \leq \phi^*$ is the porosity of the medium in Ω_2, $\mathbf{D}(\mathbf{x}, t)$ is the diffusion/dispersion tensor assumed to be symmetric and positive definite with smallest and largest eigenvalues D_* and D^*, respectively, $s(\mathbf{x}, t)$ is a source term, and $\mathbf{u}$ is the velocity feild defined by $\mathbf{u}|_{\Omega_i} = \mathbf{u}_i$, $i = 1, 2$. The model is completed by the initial condition

$$c(\mathbf{x}, 0) = c^0(\mathbf{x}), \quad \forall \mathbf{x} \in \Omega \tag{4.1.3}$$

and the boundary conditions

$$(c\mathbf{u} + \boldsymbol{z}) \cdot \mathbf{n} = (c_{in}\mathbf{u}) \cdot \mathbf{n} \quad \text{on} \quad \Gamma_{in}, \tag{4.1.4}$$

$$\boldsymbol{z} \cdot \mathbf{n} = 0 \quad \text{on} \quad \Gamma_{out}, \tag{4.1.5}$$

Here, $\Gamma_{in} := \{\mathbf{x} \in \partial\Omega : \mathbf{u} \cdot \mathbf{n} < 0\}$, $\Gamma_{out} := \{\mathbf{x} \in \partial\Omega : \mathbf{u} \cdot \mathbf{n} \geq 0\}$, and $\mathbf{n}$ is the unit outward normal vector to $\partial\Omega$. The set of all interior edges (2d) or faces (3d) is denoted by $\Gamma_h(\Omega_i)$. Let $\Gamma_h = \Gamma_h(\Omega_1) \cup \Gamma_h(\Omega_2)$ and $\partial\Omega_i$ denote the boundaries of Ω_i, $\quad i = 1, 2$. $\Gamma_{12} = \partial\Omega_1 \cap \partial\Omega_2$.

We define averages and jumps by

$$\{\phi\} = \frac{1}{2}(\phi^- + \phi^+), \quad [\phi] = \phi^-\mathbf{n}^- + \phi^+\mathbf{n}^+$$

. Let $W_E = H^1(E), \mathbf{V}_E = (W_E)^d$.

Then we define bilinear forms and linear functionals for the LDG mortar method in $\Omega_i, \quad i = 1, 2$:

$$\begin{aligned} B_i^1(\mathbf{z}, \mathbf{v}) = &\sum_{E \in \varepsilon_h(\Omega_i)} \int_E \mathbf{D}^{-1}\mathbf{z}\mathbf{v} - \sum_{E \in \varepsilon_h(\Omega_i)} \int_E c\nabla \cdot \mathbf{v} + \sum_{\gamma \in \Gamma_h(\Omega_i)} \int_\gamma \bar{c}\mathbf{v}^- \cdot \mathbf{n} d\sigma \\ &+ \sum_{\gamma \in \partial\Omega_i \setminus \Gamma_{12}} \int_\gamma c^- \mathbf{v}^- \cdot \mathbf{n}_{\Omega_i} \end{aligned} \tag{4.1.6}$$

$$\begin{aligned} B_i^2(c, \mathbf{z}; \omega) = &\sum_{E \in \varepsilon_h(\Omega_i)} \int_E \phi c_t \omega dx - \sum_{E \in \varepsilon_h(\Omega_i)} \int_E (c\mathbf{u} + \mathbf{z}) \cdot \nabla \omega dx \\ &+ \sum_{\gamma \in \Gamma_h(\Omega_i)} \int_\gamma (c^u \mathbf{u} + \bar{\mathbf{z}}) \cdot \mathbf{n}_{\Omega_i} \omega^-|_{\Omega_i} d\sigma + \sum_{\gamma \in \Gamma_{out} \setminus \Gamma_{12}} \int_\gamma c^- \mathbf{u} \cdot \mathbf{n}_{\Omega_i} \omega^-|_{\Omega_i} d\sigma \end{aligned} \tag{4.1.7}$$

$$L_i^1(\mathbf{v}, \lambda) = -\sum_{\tau \in \Gamma_H} \int_{\tau \cap \Gamma_{12}} \lambda \mathbf{v}^- \cdot \mathbf{n}_{\Omega_i} \tag{4.1.8}$$

$$\begin{aligned} L_i^2(\omega, \mu) = &\sum_{E \in \varepsilon_h(\Omega_i)} \int_E \phi s \omega dx - \sum_{\gamma \in \Gamma_{in} \setminus \Gamma_{12}} \int_\gamma c_{in} \omega^-|_{\Omega_i} \mathbf{u} \cdot \boldsymbol{n}_{\Omega_i} d\sigma \\ &- \sum_{\tau \in \Gamma_H} \int_{\tau \cap \Gamma_{12}} (c^u \mathbf{u} + \bar{\mathbf{z}}) \cdot \mathbf{n}_{\Omega_i} \mu d\sigma \end{aligned} \tag{4.1.9}$$

Then the semidiscrete LDG mortar scheme to approximate the solution to (4.1.1)–(4.1.5) is then to find $c(\cdot, t) \in L^2(\Omega)$ such that $c(\cdot, t)|_{\Omega_i} \in X(\Omega_i)$ for $i = 1, 2$ and $\lambda \in \Lambda$ such that

$$B_i^1(\mathbf{z}, \mathbf{v}) = L_i^1(\mathbf{v}, \lambda) \quad i = 1, 2, \quad t \in [0, T) \quad \forall \mathbf{v} \in \mathbf{V}_E \tag{4.1.10}$$

$$B_i^2(c, \mathbf{z}; \omega) = L_i^2(\omega, \mu) \quad i = 1, 2, \quad t \in [0, T) \quad \forall \omega \in W_E \forall \mu \in \Lambda \tag{4.1.11}$$

$$\sum_{i=1,2} \sum_{\tau \in \Gamma_H} \int_{\tau \cap \Gamma_{12}} [\mathbf{z}] \mu d\sigma = 0 \quad \forall \mu \in \Lambda. \tag{4.1.12}$$

$$c(\cdot, 0) = c^0 \tag{4.1.13}$$

where $V := L^2(\Omega)^d$,$\mathbf{X}(\Omega_i) = \{q \in L^2(\Omega_i) : \forall E \in \varepsilon_h(\Omega_i), q|_E \in H^s(E)\}, \quad s > 3/2, \quad i = 1, 2$ and $\Lambda = H^{1/2}(\Gamma_{12})$.

4.2 FINITE ELEMENT DISCRETIZATION

4.2.1 LDG mortar finite element method

For the LDG discretization we will use the finite element spaces:

$$X_h(\Omega_i) = \{q_h \in L^2(\Omega_i) : \forall E \in \varepsilon_h(\Omega_i), q_h|_E \in P_r(E)\}, \quad i = 1, 2, r \geq 1.$$

$$\boldsymbol{V}_h(\Omega_i) = \{\mathbf{v}_h \in (L^2(\Omega_i))^d : \forall E \in \varepsilon_h(\Omega_i), \mathbf{v}_h|_E \in (P_r(E))^d\}, \quad i = 1, 2, r \geq 1.$$

where $P_r(E)$ is the space of all polynomials of degree $\leq r$ on E.

On the interface we will use a mortar finite elment space to approximate c and weakly impose continuity of flux and c :

$$\Lambda_H = \{\mu_H \in L^2(\Gamma_{12}) : \forall \tau \in \Gamma_H, \mu_h|_\tau \in P_{\bar{r}}(\tau)\}, \quad \bar{(}r) \geq 1.$$

$$\begin{aligned} B^1_{i,h}(\mathbf{Z}, \mathbf{v}) = &\sum_{E \in \varepsilon_h(\Omega_i)} \int_E \mathbf{D}^{-1}\mathbf{Z}\mathbf{v} - \sum_{E \in \varepsilon_h(\Omega_i)} \int_E C\nabla \cdot \mathbf{v} + \sum_{\gamma \in \Gamma_h(\Omega_i)} \int_\gamma \bar{C}\mathbf{v}^- \cdot \mathbf{n} d\sigma \\ &+ \sum_{\gamma \in \partial\Omega_i \setminus \Gamma_{12}} \int_\gamma C^- \mathbf{v}^- \cdot \mathbf{n}_{\Omega_i} \end{aligned} \tag{4.2.1}$$

$$\begin{aligned} B^2_{i,h}(C, \mathbf{Z}; \omega) = &\sum_{E \in \varepsilon_h(\Omega_i)} \int_E \phi C_t \omega dx - \sum_{E \in \varepsilon_h(\Omega_i)} \int_E (C\mathbf{U} + \mathbf{Z}) \cdot \nabla\omega dx \\ &+ \sum_{\gamma \in \Gamma_h(\Omega_i)} \int_\gamma (C^u \mathbf{U} + \bar{\mathbf{Z}}) \cdot \mathbf{n}_{\Omega_i} d\sigma + \sum_{\gamma \in \Gamma_{out} \setminus \Gamma_{12}} \int_\gamma C^- \mathbf{U} \cdot \mathbf{n}_{\Omega_i} \omega^-|_{\Omega_i} d\sigma \\ &+ \sum_{E \in \varepsilon_h(\Omega_i)} \frac{1}{2} \int_E C\nabla \cdot (\mathbf{u} - \boldsymbol{U})\omega + \sum_{\gamma \in \Gamma_{out} \setminus \Gamma_{12}} \frac{1}{2} \int_\gamma C^-(\mathbf{u} - \boldsymbol{U}) \cdot \boldsymbol{n}_{\Omega_i} \omega^- d\sigma \\ &- \sum_{\gamma \in \Gamma_{in} \setminus \Gamma_{12}} \frac{1}{2} \int_\gamma C^-(\mathbf{u} - \boldsymbol{U}) \cdot \boldsymbol{n}_{\Omega_i} \omega^- d\sigma \end{aligned} \tag{4.2.2}$$

$$L^1_{i,h}(\mathbf{v}, \lambda) = -\sum_{\tau \in \Gamma_H} \int_{\tau \cap \Gamma_{12}} \lambda \mathbf{v}^- \cdot \mathbf{n}_{\Omega_i} \tag{4.2.3}$$

$$L^2_{i,h}(\omega,\mu) = \sum_{E\in\varepsilon_h(\Omega_i)}\int_E \phi s\omega dx - \sum_{\gamma\in\Gamma_{in}\setminus\Gamma_{12}}\int_\gamma c_{in}\omega^-|_{\Omega_i}\mathbf{u}\cdot\boldsymbol{n}_{\Omega_i}d\sigma \\ - \sum_{\tau\in\Gamma_H}\int_{\tau\cap\Gamma_{12}}(C^u\mathbf{U}+\bar{\mathbf{Z}})\cdot\mathbf{n}_{\Omega_i}\mu d\sigma \tag{4.2.4}$$

Then the semidiscrete LDG mortar scheme to approximate the solution to (4.1.1)–(4.1.5) is then to find $C(\cdot,t)\in L^2(\Omega)$ such that $C(\cdot,t)|_{\Omega_i}\in X(\Omega_i)$ for $i=1,2$ and $\lambda\in\Lambda$ such that

$$B^1_{i,h}(\mathbf{Z},\mathbf{v}) = L^1_{i,h}(\mathbf{v},\lambda) \quad i=1,2, \quad t\in[0,T) \tag{4.2.5}$$

$$B^2_{i,h}(C,\mathbf{Z};\omega) = L^2_{i,h}(\omega,\mu) \quad i=1,2, \quad t\in[0,T) \tag{4.2.6}$$

$$\sum_{i=1,2}\sum_{\tau\in\Gamma_H}\int_{\tau\cap\Gamma_{12}}[\mathbf{Z}]\mu d\sigma = 0 \quad \forall\mu\in\Lambda. \tag{4.2.7}$$

$$C(\cdot,0) = C^0 \tag{4.2.8}$$

4.2.2 Stability of the LDG mortar finite element method

We present a stability analysis with matching grids over a LDG motar schemes. In this case C^u will canceled when sum over two neighboring domain edges Γ_{12}.Then the rest proof will be almost same as in [49]. By adding (4.2.5) and (4.2.6), using integration by parts, summing over the two subdomain Ω_1 and Ω_2, and integrating over t, we obtain the equivalent formulation

$$B_U(C,\mathbf{Z};\omega,\mathbf{v};\lambda,\mu) = -\int_0^T \langle c_{in}\mathbf{u}\cdot\mathbf{n},\omega^-\rangle_{\Gamma_{in}\setminus\Gamma_{12}}dt + \int_0^T \sum_{i=1,2}\sum_{E\in\varepsilon_h(\Omega_i)} (\phi s,\omega)_E dt \tag{4.2.9}$$

where

$$\begin{aligned} B_U(C,\mathbf{Z};\omega,\mathbf{v};\lambda,\mu) := \int_0^T \{ & \sum_{i=1,2}\sum_{E\in\varepsilon_h(\Omega_i)} \{(\phi C_t,\omega)_E - (C\mathbf{U}+\mathbf{Z},\nabla\omega)_E + \langle C^-\mathbf{U}\cdot\mathbf{n}_E,\omega^-\rangle_{\partial E\cap\Gamma_{out}} \\ & + \langle (C^u\mathbf{U}+\bar{\mathbf{Z}})\cdot\mathbf{n}_E,\omega^-\rangle_{\partial E\setminus\Gamma} + (\mathbf{D}^{-1}\mathbf{Z},\mathbf{v})_E - (C,\nabla\cdot\mathbf{v})_E + \langle \bar{C},\mathbf{v}^-\cdot\mathbf{n}_E\rangle_{\partial E\setminus\Gamma} \\ & + \langle C^-,\mathbf{v}^-\cdot\mathbf{n}_E\rangle_{\partial E\cap\Gamma} + \frac{1}{2}(\nabla\cdot(\mathbf{u}-\mathbf{U})C,\omega)_E + \frac{1}{2}(C^-(\mathbf{u}-\mathbf{U})\cdot\mathbf{n}_E,\omega^-)_{\partial E\cap\Gamma_{out}} \\ & - \frac{1}{2}(C^-(\mathbf{u}-\mathbf{U})\cdot\mathbf{n}_E,\omega^-)_{\partial E\cap\Gamma_{in}}\} + \sum_{i=1,2}\sum_{\tau\in\Gamma_H}\int_{\tau\cap\Gamma_{12}}\lambda_H[\mathbf{v}]d\sigma \\ & + \sum_{i=1,2}\sum_{\tau\in\Gamma_H}\int_{\tau\cap\Gamma_{12}}[C\mathbf{U}+\mathbf{Z}]\mu d\sigma\}\ dt. \end{aligned} \tag{4.2.10}$$

Taking $\omega = C$, $\mathbf{v} = \mathbf{Z}$,$\mu = \lambda$ and using (4.2.7) and (4.2.8) we have

$$B_U(C,\mathbf{Z};C,\mathbf{Z}) = \Theta_1 + \Theta_2 + \Theta_3 \tag{4.2.11}$$

where

$$\Theta_1 = \int_0^T \sum_E \{(\phi C_t,C)_E + (\mathbf{D}^{-1}\mathbf{Z},\mathbf{Z})_E\}dt$$

$$\begin{aligned} \Theta_2 = \int_0^T \sum_E \{ & -(C\mathbf{U},\nabla C)_E + \langle C^u\mathbf{U}\cdot\mathbf{n}_E,C^-\rangle_{\partial E\setminus\Gamma}\langle C^-\mathbf{U}\cdot\mathbf{n}_E,C^-\rangle_{\partial E\cap\Gamma_{out}} \\ & + \frac{1}{2}(C\nabla\cdot(\mathbf{u}-\mathbf{U}),C)_E + \frac{1}{2}(C^-(\mathbf{u}-\mathbf{U})\cdot\mathbf{n}_E,C^-)_{\partial E\cap\Gamma_{out}} \\ & - \frac{1}{2}(C^-(\mathbf{u}-\mathbf{U})\cdot\mathbf{n}_E,C^-)_{\partial E\cap\Gamma_{in}}\}dt \end{aligned}$$

$$\Theta_3 = \int_0^T \sum_E \{-(\mathbf{Z}, \nabla C)_E + \langle \bar{\mathbf{Z}} \cdot \mathbf{n}_E, C^- \rangle_{\partial E \setminus \Gamma} - (C, \nabla \cdot \mathbf{Z})_E$$
$$+ \langle \bar{C}, \mathbf{Z}^- \cdot \mathbf{n}_E \rangle_{\partial E \setminus \Gamma} + \langle C^-, \mathbf{Z}^- \cdot \mathbf{n}_E \rangle_{\partial E \cap \Gamma} \} dt$$

Then the rest argument is same as in [49], we obtain following stability result.

Theorem 4.2.1. *The solution to the semidiscrete LDG method* (4.2.5) – (4.2.8) *satisfies*

$$|||(C, \mathbf{Z})||| \leq e^{LT/2}(\phi^* \|c^0\|^2 + \int_0^T \langle |\mathbf{u} \cdot \mathbf{n}|, (c_{in}^2) \rangle_{\Gamma_{in}} dt)^{1/2} + e^{LT} \int_0^T \|\phi^{1/2} s\| dt, \qquad (4.2.12)$$

where $L := \|\phi^{-1}(\nabla \cdot \mathbf{u})_-\|_{0,\infty}$

4.3 NUMERICAL RESULTS

4.3.1 Convergence tests

In this section, we will present several convergence tables to confirm our theories. In all these convergence tests we use both forward Euler and second-order RungeKutta method to discretize the transport equation in time. he final time is $T = 2$, and the time step is $\Delta t = 10^{-3}$, all numbers being dimensionless. The time step is chosen small enough so that the time discretization error is smaller than the spatial discretization error even for the finest grids used. In all test cases, we choose $\phi = 1$.

In the all convergence tests, the true velocity field is:

$$\mathbf{u}_1 = \begin{bmatrix} (2-x)(1.5-y)(y-\xi) \\ -\frac{y^3}{3} + \frac{y^2}{2}(\xi + 1.5) - 1.5\xi y - 0.5 + \sin(\omega x) \end{bmatrix},$$
$$\mathbf{u}_2 = \begin{bmatrix} \omega \cos(\omega x) y \\ \chi(y + 0.5) + \sin(\omega x) \end{bmatrix},$$
$$p_1 = -\frac{\sin(\omega x) + \chi}{2K} + \mu(0.5 - \xi) + \cos(\pi y),$$
$$p_2 = -\frac{\chi}{K}\frac{(y+0.5)^2}{2} - \frac{\sin(\omega x) y}{K},$$

$mesh$	$\|c - C\|_{L^2(L^2)}$	$rate$	$\|c - C\|_{L^\infty(L^2)}$	$rate$
4x4	1.49e-05		2.11e-04	
8x8	3.99e-06	1.90	5.64e-05	1.90
16x16	1.03e-06	1.95	1.46e-05	1.95
32x32	2.61e-07	1.98	3.69e-06	1.98

Table 16: Convergence table for concentration using forward euler with Final time = 0.01 time step =0.01 in two Darcy region with $\boldsymbol{D} = 10^{-3}\mathbf{I}$

The true concentration of the transport equation is

$$c(x, y, t) = t(cos(\pi x) + cos(\pi y))/\pi.$$

The computed concentraion and error is shown in Figure 4.3.1. The convergence rates for the transport equation are studied by solving the coupled flow-transport system on several levels of grid refinement. The numerical errors and convergence rates for the all tests are reported in following tables. In all test cases we observe experimental convergence of order for the concentration error in $O(h^2)$ for the concentraion error in $L^\infty(0, T; L^2(\Omega))$ and approaching $O(h)$ for the diffusive flux error in $L^2(0, T; L^2(\Omega))$. Theoretical results predicted $O(h)$ for both variables. In our case, there are additional terms contributing to the transport numerical error that are coming from the discretization error in the StokesDarcy velocity. For our particular choice of flow discretization these terms are $O(h^2)$from Stokes and $O(h)$from Darcy. The observed second-order convergence of the concentration may be due to the superconvergence of the RaviartThomas velocity at the edge midpoints, which are used to obtain the bilinear velocity for the transport scheme. Further theoretical investigation of this phenomenon will be a topic of future work.

mesh	$\|\boldsymbol{z}-\boldsymbol{Z}\|_{L^2(L^2)}$	*rate*	$\|\boldsymbol{z}-\boldsymbol{Z}\|_{L^\infty(L^2)}$	*rate*
4x4	1.65e-07		2.33e-06	
8x8	8.50e-08	0.96	1.20e-06	0.96
16x16	4.31e-08	0.98	6.09e-07	0.98
32x32	2.16e-08	1.00	3.05e-07	1.00

Table 17: Convergence table for flux using forward euler with Final time = 0.01 time step =0.01 in two Darcy region with $\boldsymbol{D} = 10^{-3}\mathbf{I}$

mesh	$\|c-C\|_{L^2(L^2)}$	*rate*	$\|c-C\|_{L^\infty(L^2)}$	*rate*
4x4	1.83e-05		2.59e-04	
8x8	6.68e-06	1.45	9.44e-05	1.45
16x16	2.84e-06	1.23	4.01e-05	1.24
32x32	1.34e-06	1.08	1.90e-05	1.07

Table 18: Convergence table for concentration using RK2 with Final time = 0.01 time step =0.01 in two Darcy region with $\boldsymbol{D} = 10^{-3}\mathbf{I}$

mesh	$\|\boldsymbol{z}-\boldsymbol{Z}\|_{L^2(L^2)}$	*rate*	$\|\boldsymbol{z}-\boldsymbol{Z}\|_{L^\infty(L^2)}$	*rate*
4x4	2.08e-07		2.94e-06	
8x8	1.57e-07	0.41	2.22e-06	0.41
16x16	1.03e-07	0.61	1.45e-06	0.61
32x32	6.29e-08	0.71	8.90e-07	0.70

Table 19: Convergence table for flux using RK2 with Final time = 0.01 time step =0.01 in two Darcy region with $\boldsymbol{D} = 10^{-3}\mathbf{I}$

$mesh$	$\|c - C\|_{L^2(L^2)}$	$rate$	$\|c - C\|_{L^\infty(L^2)}$	$rate$
4x4	1.35e-05		2.46e-04	
8x8	4.15e-06	1.70	7.94e-05	1.63
16x16	1.31e-06	1.66	2.57e-05	1.63
32x32	4.24e-07	1.62	8.36e-06	1.62

Table 20: Convergence table for concentration using forward euler with Final time = 0.01 time step =0.001 in two Darcy region with $\boldsymbol{D} = 10^{-3}\mathbf{I}$

$mesh$	$\|\boldsymbol{z} - \boldsymbol{Z}\|_{L^2(L^2)}$	$rate$	$\|\boldsymbol{z} - \boldsymbol{Z}\|_{L^\infty(L^2)}$	$rate$
4x4	1.51e-07		2.80e-06	
8x8	9.51e-08	0.67	1.87e-06	0.58
16x16	5.03e-08	0.92	9.77e-07	0.94
32x32	2.42e-08	1.06	4.61e-07	1.08

Table 21: Convergence table for flux using forward euler with Final time = 0.01 time step =0.001 in two Darcy region with $\boldsymbol{D} = 10^{-3}\mathbf{I}$

$mesh$	$\|c - C\|_{L^2(L^2)}$	$rate$	$\|c - C\|_{L^\infty(L^2)}$	$rate$
4x4	1.38e-05		2.52e-04	
8x8	4.31e-06	1.68	8.22e-05	1.61
16x16	1.36e-06	1.66	2.65e-05	1.63
32x32	4.41e-07	1.62	8.60e-06	1.62

Table 22: Convergence table for concentration using RK2 with Final time = 0.01 time step =0.001 in two Darcy region with $\boldsymbol{D} = 10^{-3}\mathbf{I}$

mesh	$\|\boldsymbol{z}-\boldsymbol{Z}\|_{L^2(L^2)}$	*rate*	$\|\boldsymbol{z}-\boldsymbol{Z}\|_{L^\infty(L^2)}$	*rate*
4x4	1.55e-07		2.89e-06	
8x8	9.98e-08	0.64	1.95e-06	0.56
16x16	5.23e-08	0.93	1.01e-06	0.95
32x32	2.50e-08	1.06	4.76e-07	1.09

Table 23: Convergence table for flux using RK2 with Final time = 0.01 time step =0.001 in two Darcy region with $\boldsymbol{D} = 10^{-3}\mathbf{I}$

mesh	$\|c-C\|_{L^2(L^2)}$	*rate*	$\|c-C\|_{L^\infty(L^2)}$	*rate*
4x4	1.37e-05		2.52e-04	
8x8	4.27e-06	1.68	8.19e-05	1.62
16x16	1.35e-06	1.66	2.64e-05	1.63

Table 24: Convergence table for concentration using forward euler with Final time = 0.01 time step =0.0001 in two Darcy region with $\boldsymbol{D} = 10^{-3}\mathbf{I}$

mesh	$\|\boldsymbol{z}-\boldsymbol{Z}\|_{L^2(L^2)}$	*rate*	$\|\boldsymbol{z}-\boldsymbol{Z}\|_{L^\infty(L^2)}$	*rate*
4x4	1.55e-07		2.88e-06	
8x8	9.88e-08	0.65	1.94e-06	0.57
16x16	5.18e-08	0.93	1.01e-07	0.94

Table 25: Convergence table for flux using forward euler with Final time = 0.01 time step =0.0001 in two Darcy region with $\boldsymbol{D} = 10^{-3}\mathbf{I}$

mesh	$\|c - C\|_{L^2(L^2)}$	*rate*	$\|c - C\|_{L^\infty(L^2)}$	*rate*
4x4	1.37e-05		2.52e-04	
8x8	4.29e-06	1.68	8.22e-05	1.61
16x16	1.35e-06	1.67	2.64e-05	1.64

Table 26: Convergence table for concentration using RK2 with Final time = 0.01 time step =0.0001 in two Darcy region with $\boldsymbol{D} = 10^{-3}\mathbf{I}$

mesh	$\|\boldsymbol{z} - \boldsymbol{Z}\|_{L^2(L^2)}$	*rate*	$\|\boldsymbol{z} - \boldsymbol{Z}\|_{L^\infty(L^2)}$	*rate*
4x4	1.55e-07		2.89e-06	
8x8	9.92e-08	0.64	1.95e-06	0.56
16x16	5.20e-08	0.93	1.01e-06	0.95

Table 27: Convergence table for flux using RK2 with Final time = 0.01 time step =0.0001 in two Darcy region with $\boldsymbol{D} = 10^{-3}\mathbf{I}$

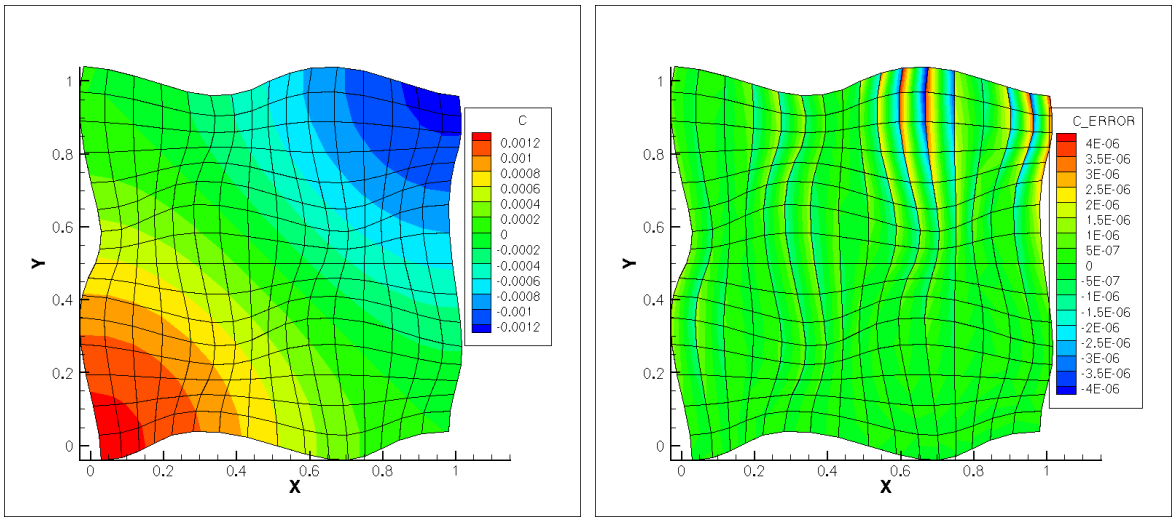

Figure 4.3.1: Computed concentraion (left) and err (right)

4.3.2 Contaminant transport examples

In this section, we present two realistic simulation examples: Example 1 is that circle contaminant simulation originated at the top Stokes region(surface water region) and then transported into Darcy region(porous media region). Example 2 is that inflow of the contaminant is specified on part of the left boundary in the surface water region. The contaminant front eventually reaches and penetrates into the subsurface water region. In all these simulations, the computational domain is taken to be $\Omega = \Omega_1 \cup \Omega_2$where $\Omega_1 = [0,1] \times [\frac{1}{2}, 1]$ represents Stokes region and $\Omega_2 = [0,1] \times [0, \frac{1}{2}]$ represents Darcy region.The flow equations are solved via domain decomposition using the TaylorHood triangular finite elements in Ω_1 and the lowest order RaviartThomas rectangular finite elements in Ω_2. We present two simulations of coupled surface and subsurface flow and contaminant transport. The Stokes region Ω_1 represents a lake or a river, which interacts with an aquifer occupying the Darcy region Ω_2. The porous medium is heterogeneous with permeability varying approximately two orders of magnitude.

In both examples, we use the following flow boundary conditions. In the Stokes region we set parabolic inflow on the left boundary, no normal flow and zero tangential stress on the top boundary, and zero normal and tangential stress on the right (out- flow) boundary. In the Darcy region we set no flow on the left and right boundaries and specify pressure on the bottom boundary to simulate a gravity force.

In example 1, the plume stays compact while in the surface water region. When it reaches the groundwater region, it starts to spread due to the heterogeneity of the porous media. The discontinuity in the tangential velocity along the interface causes some of the contaminant to lag behind and even move in the opposite direction. Similar behavior is observed in example 2, where the contaminant front maintains a relatively flat interface in the surface water region and spreads nonuniformly in the porous media.

We also compared simulations of transport on two different grids (Figure 4.3.4 – Figure 4.3.8). One is on rectangular grids and one is on quads. As you can see, They are almost same. But it makes more sense by using the irregular grids. We also simulate two tranport senarios: one has a unit circle concentration at Stokes region then move into Darcy region;

One has a intial plume concentraion at the left boundary of Stokes region. All these cases used irregular grids and slope limiter to reserves sharp discontinuities in the concentration without numerical oscillations.

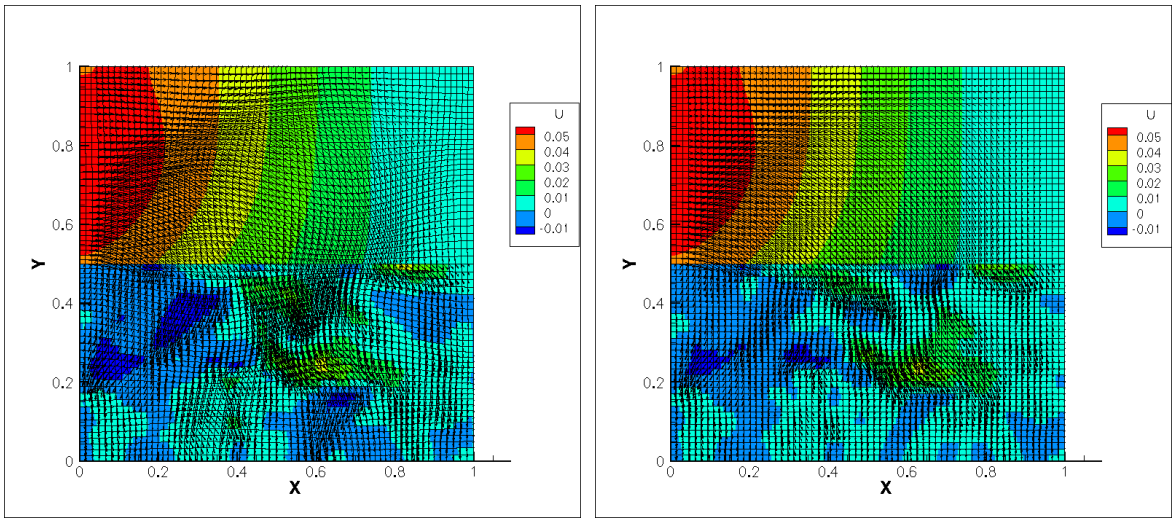

Figure 4.3.2: Transport simulation horizontal velocity feild with map (left) and without map (right)

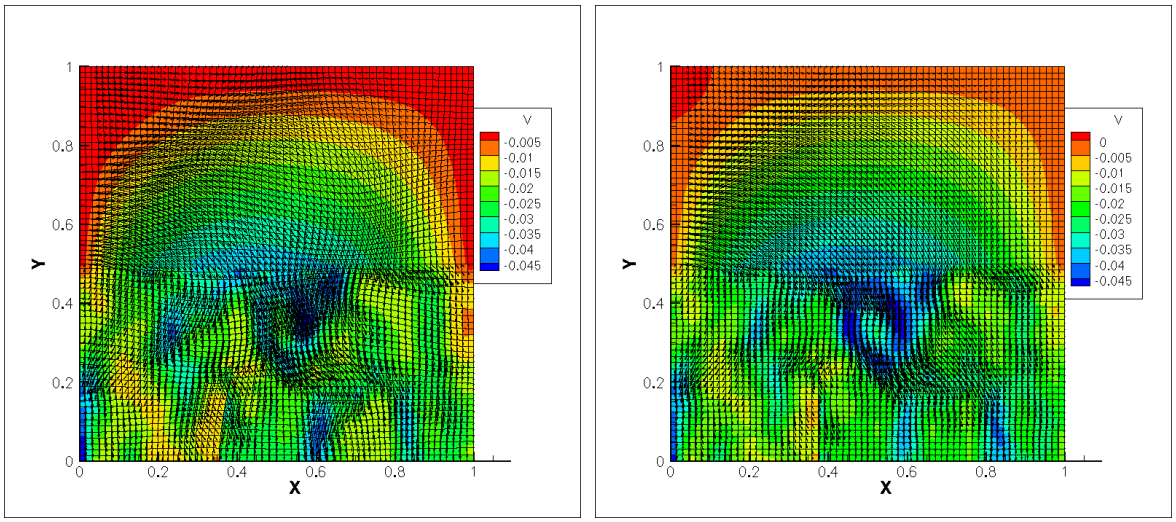

Figure 4.3.3: Transport simulation vertical velocity feild with map (left) and without map (right)

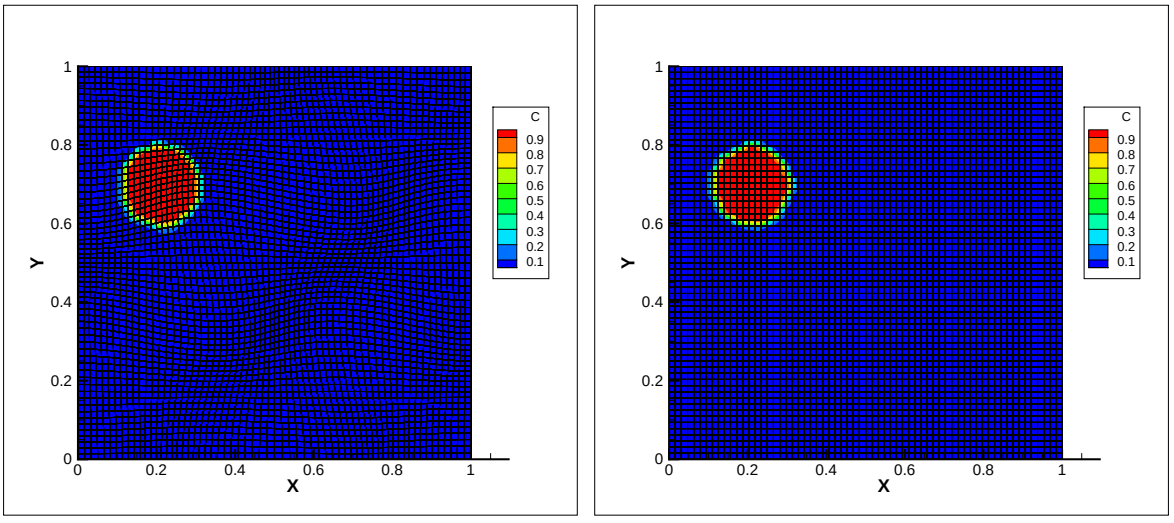

Figure 4.3.4: Transport simulation with map (left) and without map (right) on time = 0.2

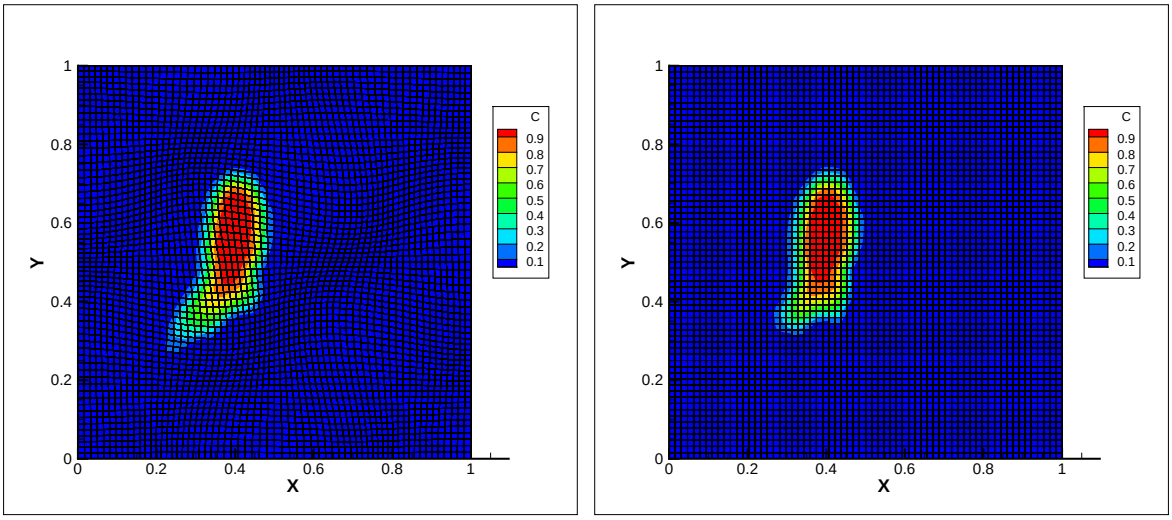

Figure 4.3.5: Transport simulation with map (left) and without map (right) on time = 5.025

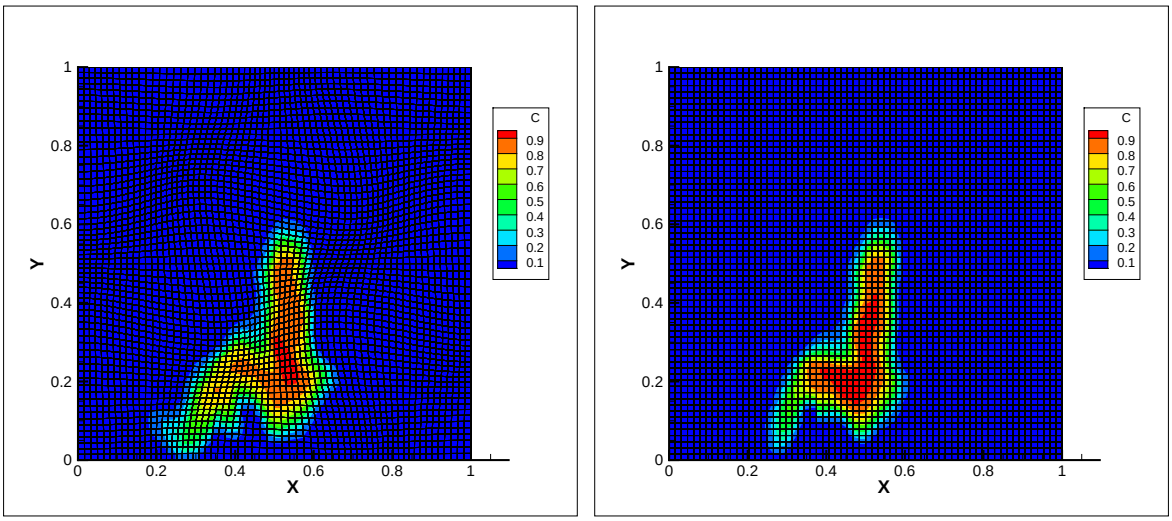

Figure 4.3.6: Transport simulation with map (left) and without map (right) on time = 9.849

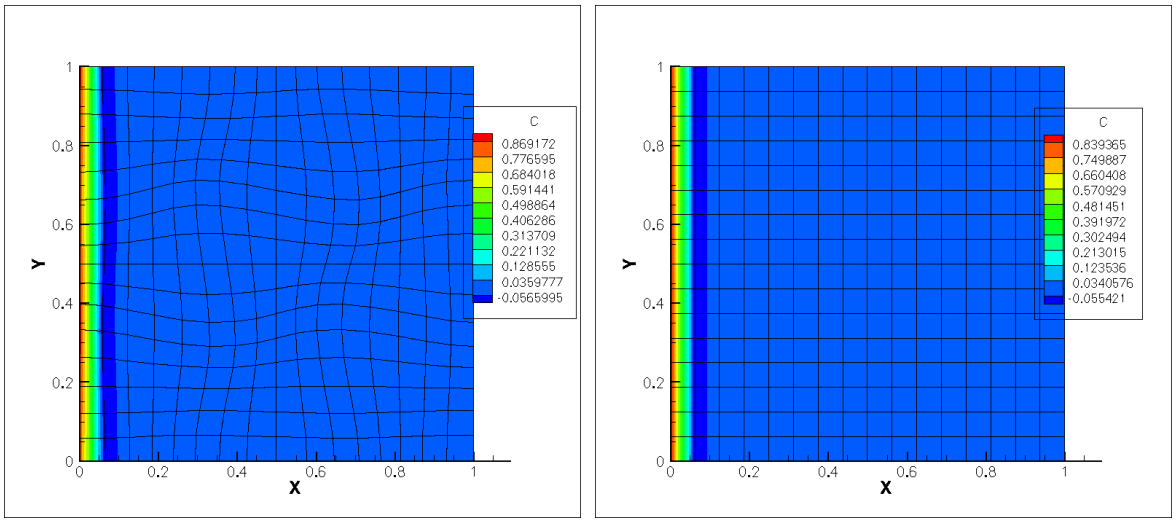

Figure 4.3.7: Transport simulation of moving front with map (left) and without map (right) on time = 0.11

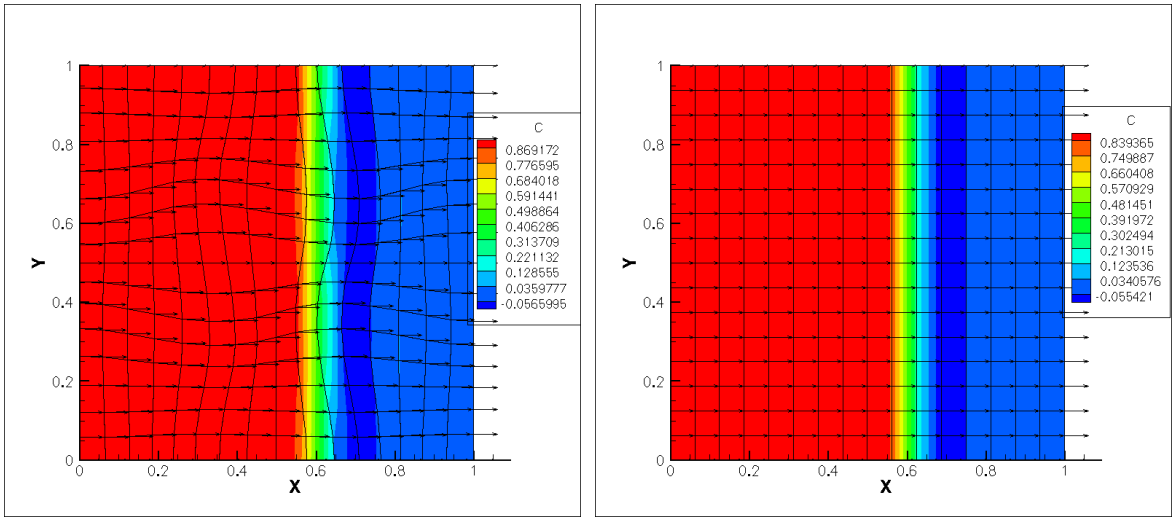

Figure 4.3.8: Transport simulation of moving front and velocity feild with map (left) and without map (right) on time = 2.97

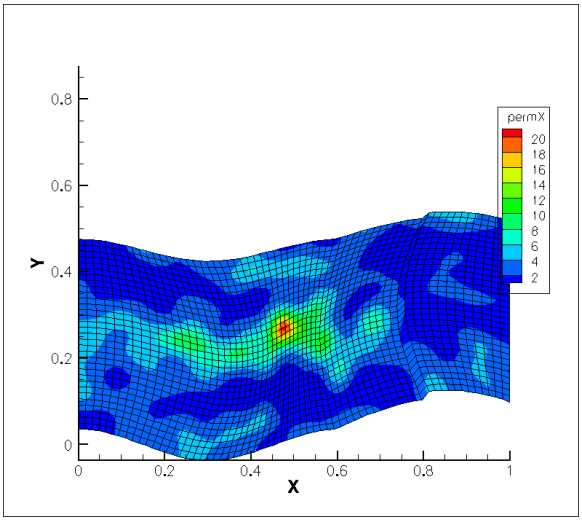

Figure 4.3.9: Permeability in example 1

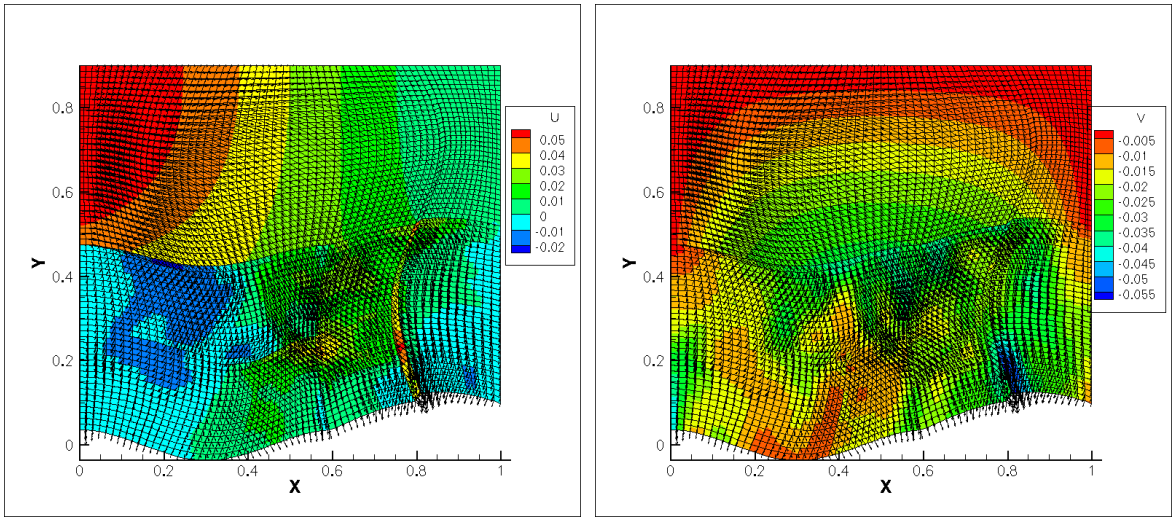

Figure 4.3.10: Horizontal velocity(left) and vertical velocity(right) in example 1

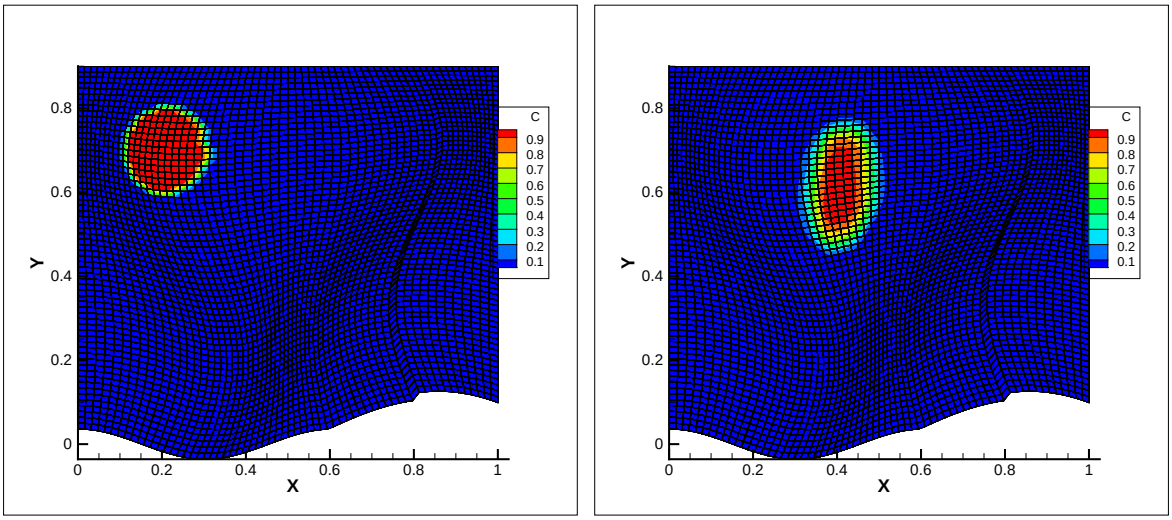

Figure 4.3.11: Transport simulation with map at time = 0.201(left) and at time = 5.025 (right) in example 1

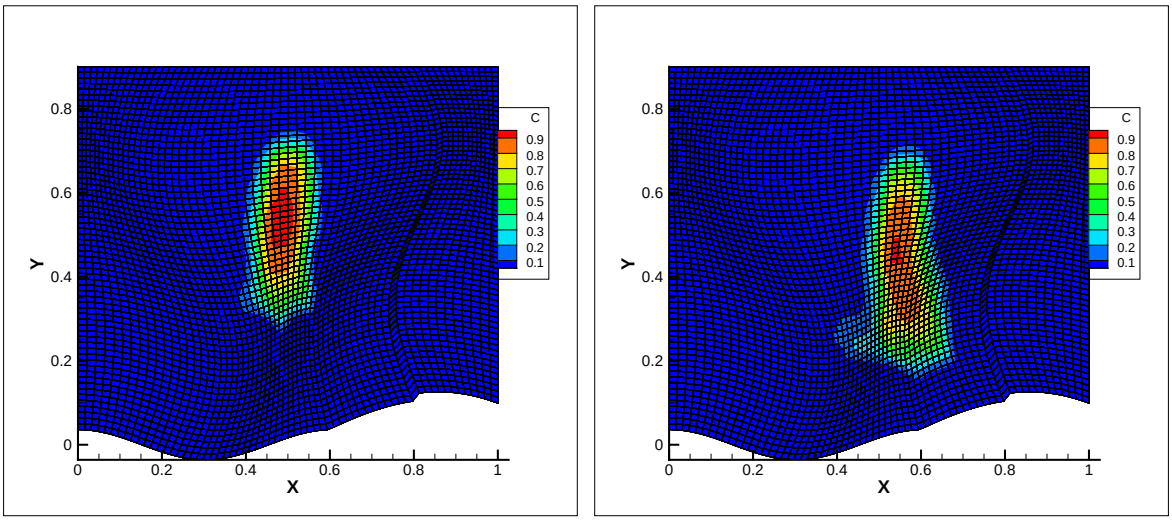

Figure 4.3.12: Transport simulation with map at time = 7.638(left) and at time = 9.849 (right) in example 1

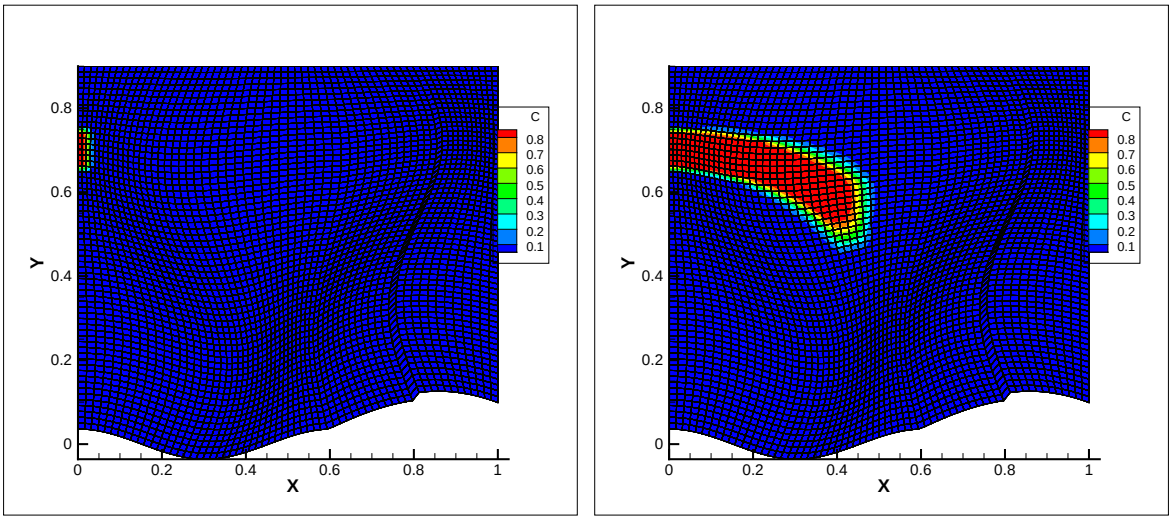

Figure 4.3.13: Transport simulation with map at time = 0.401(left) and at time = 10.02 (right) in example 2

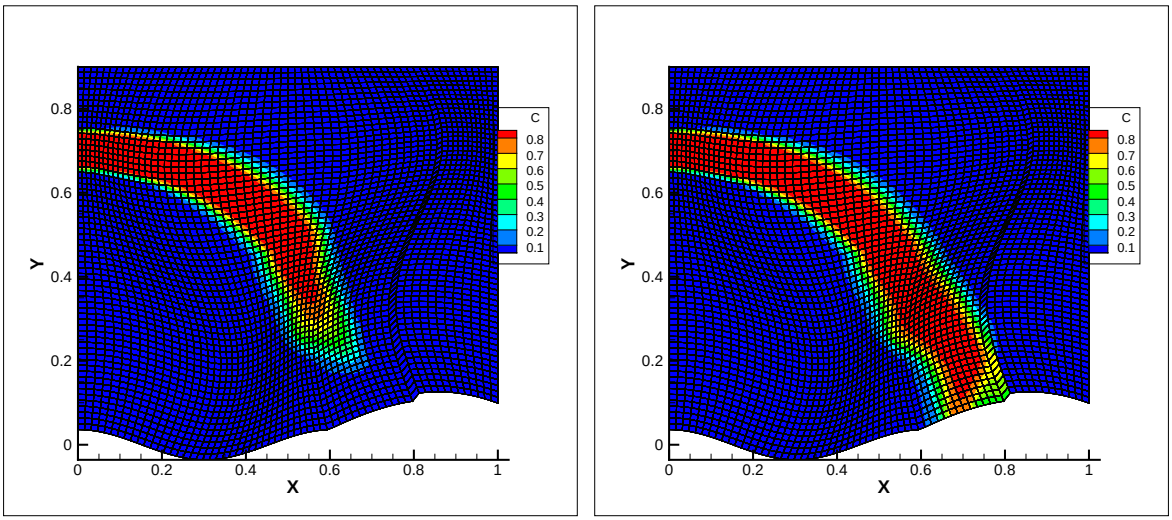

Figure 4.3.14: Transport simulation with map at time = 14.84(left) and at time = 19.65 (right) in example 2

5.0 CONCLUSION AND FUTURE WORKS

In chapter 2, We mainly focused on studying steady state Stokes-Darcy model on irregular domains. We applied a new mixed finite element method called Multi-point Flux Mixed Finite Element (MFMFE) method to handle Darcy flow in irregular porous media regions [29, 55]. This method reduces to a cell-centered finite difference scheme for the scalar variable and is accurate for discontinuous full tensor coefficients on h^2-perturbed parallelograms, simplicial grids, and h^2-perturbed parallelepipeds. Cell-centered discretizations are very efficient and widely used for modeling complex multiphase multicomponent fluid flows in porous media, since multiscale spatial variability of the material properties often necessitate millions of cells for accurate approximations [47, 52]. This method has a symmetric and a non-symmetric version. The symmetric method can handle h^2-perturbed parallelograms, simplicial grids, and h^2-perturbed parallelepipeds, while the non-symmetric method can deal with more general quadrilaterals and hexahedra. This is a typical grid encountered in geological models. Furthermore, hexahedral grids can represent highly irregular geometries with significantly reduced number of elements compared to tetrahedral grids. This is especially important in computationally intensive applications such as carbon sequestration in saline aquifers. The symmetric MFMFE method has been designed to be a cell-centered pressure scheme that is accurate for both smooth and discontinuous full tensor permeability, but unfortunately it is not accurate on general hexahedral grids. As in the non-symmetric MPFA method on quadrilaterals, a coercivity condition needs to be satisfied for the well-posedness of the non-symmetric MFMFE method. The condition depends on the element distortion and permeability anisotropy. Although the non-symmetric method converges on rough grids, where the convergence of the symmetric method deteriorates, for some highly anisotropic problems, the non-symmetric method loses coercivity, while the symmetric method still works.

Therefore one or the other method may be preferable, depending on the properties of the grids and the permeability coefficient. This choice can be made element by element. In Stokes flow, we use a traditional stable Galerkin finite element method on triangular mesh. We proved stability of the scheme and derived error analysis for both symmetric and non-symmetric MFMFE method by assuming suitable compatibility and inf-sup conditions for mortar functions [46]. The stability and convergence analysis relies on the construction of a bounded global interpolant in the space of weakly continuous velocities that also preserves the velocity divergence in the usual discrete sense. This is done in two steps, starting from suitable local interpolants and correcting them to satisfy the interface matching conditions. The correction step requires the existence of bounded mortar interpolants. This is a very general condition that can be easily satisfied in practice. We present two examples in 2-D and one example in 3-D that satisfy this solvability condition. Our error analysis shows that the global velocity and pressure errors are bounded by the fine scale local approximation error and the coarse scale non-conforming error. Since the polynomial degrees on subdomains and interfaces may differ, one can choose higher order mortar polynomials to balance the fine scale and the coarse scale error terms and obtain fine scale asymptotic convergence. The dependence of the stability and convergence constants on the subdomain size is explicitly determined. In particular, the stability and fine scale convergence constants do not depend on the size of subdomains, while the coarse scale non-conforming error constants deteriorate when the subdomain size goes to zero. This is to be expected, as the relative effect of the non-conforming error becomes more significant in such regime. However, this dependence can be made negligible by choosing higher order mortar polynomials, as mentioned above. Our multiscale Stokes-Darcy formulation can be viewed as an extension of the mortar multiscale mixed finite element (MMMFE) method for Darcy. The MMMFE method provides an alternative to other multiscale methods in the literature such as the variational multiscale method and the multiscale finite element method [2, 54]. All three methods utilize a divide and conquer approach: solve relatively small fine scale subdomain problems that are only coupled on the coarse scale through a reduced number of degrees of freedom. The mortar multiscale approach is more flexible as it allows for employment of a posteriori error estimation to adaptively refine the mortar grids where necessary to improve

the global accuracy. Following the non-overlapping domain decomposition approach, it can be shown that the global Stokes-Darcy problem can be reduced to a positive definite coarse scale interface problem. The latter can be solved using a preconditioned Krylov space solver requiring Stokes or Darcy subdomain solves at each iteration. Sub-domain problems can be solved in parallel for efficiency[51].

We implemented the curved interfaces problems by mapping them back to a reference domain with straight interfaces and performing all the calculations there. On the physical domain we approximate the curved interfaces with piecewise linear segments. Although other references utilize blending elements to get a perfect approximation to the the curved interfaces, the idea of the implementation for the curved interfaces is still the same as ours and our methods are much cheaper and easier to implement.

In chapter 3, We also presented domain decomposition method for the coupled Stoke-Darcy flow with curved interfaces. The effectiveness of the domain decomposition depends on the rate at which the interface iterations converge. The latter is characterized by the condition number of the algebraic problem. We investigated the dependence of the condition number on the subdomain mesh size, permeability and the interface type. The number of subdomains also has effect on the convergence. Due to the lack of global information exchange between the subdomains the condition number increases rapidly as the number of subdomain increases. Therefore, in order to be able to solve in parallel a large scale problem by employing a large number of processors, one for each subdomain, we need a suitable preconditioning technique. Numerical results were presented to confirm theories.

In chapter 4, We developed a LDG mortar method to discretize transport equation which will allow for non-matching grids on neighboring subdomains. We developed stability analysis and also presented several numerical simulations under irregular gemotery with matching grids.

We will develop convergence analysis for the concentration and diffusive flux on non-matching grids. The numerical error may be a combination of the DG discretization error, mortar error and the error from the discretization of the Stokes-Darcy velocity. The main difficulties here are the implementation of our method on non-matching grids and convergence analysis of the scheme. Then, we can consider the complete coupled problem where

the velocity from Stokes-Darcy flow impacts the concentration and the change of concentration influences the Stokes-Darcy velocity. For the current results, we pre-compute the Stokes-Darcy velocity and plug it into the transport equation as a known flow field. After the implementation of transport on irregular grids with non-matching grids and convergence analysis for the method on non-matching grids, we may consider this challenging problem in the near future.

BIBLIOGRAPHY

[1] T. Arbogast, L. C. Cowsar, M. F. Wheeler, and I. Yotov. Mixed finite element methods on non-matching multiblock grids. *SIAM J. Numer. Anal.*, 37:1295–1315, 2000.

[2] T. Arbogast, G. Pencheva, M. F. Wheeler, and I. Yotov. A multiscale mortar mixed finite element method. *Multiscale Model. Simul.*, 6(1):319–346, 2007.

[3] Todd Arbogast, Clint N. Dawson, Philip T. Keenan, Mary F. Wheeler, and Ivan Yotov. Enhanced cell-centered finite differences for elliptic equations on general geometry. *SIAM J. Sci. Comput.*, 19(2):404–425, 1998.

[4] Todd Arbogast, Mary F. Wheeler, and Ivan Yotov. Mixed finite elements for elliptic problems with tensor coefficients as cell-centered finite differences. *SIAM J. Numer. Anal.*, 34(2):828–852, 1997.

[5] G. S. Beavers and D. D. Joseph. Boundary conditions at a naturally impermeable wall. *J. Fluid. Mech*, 30:197–207, 1967.

[6] Faker Ben Belgacem. The mixed mortar finite element method for the incompressible Stokes problem: convergence analysis. *SIAM J. Numer. Anal.*, 37(4):1085–1100 (electronic), 2000.

[7] Faker Ben Belgacem. A stabilized domain decomposition method with nonmatching grids for the Stokes problem in three dimensions. *SIAM J. Numer. Anal.*, 42(2):667–685 (electronic), 2004.

[8] Christine Bernardi, Tomás Chacón Rebollo, Frédéric Hecht, and Zoubida Mghazli. Mortar finite element discretization of a model coupling Darcy and Stokes equations. *M2AN Math. Model. Numer. Anal.*, 42(3):375–410, 2008.

[9] S. C. Brenner. Poincaré–Friedrichs inequalities for piecewise H^1 functions. *SIAM J. Numer. Anal.*, 41:306–324, 2003.

[10] S. C. Brenner. Korn's inequalities for piecewise H^1 vector fields. *Math. Comp.*, 73:1067–1087, 2004.

[11] F. Brezzi and M. Fortin. *Mixed and hybrid finite element methods.* Springer-Verlag, New York, 1991.

[12] Z. Chen and J. Douglas, Jr. Prismatic mixed finite elements for second order elliptic problems. *Calcolo*, 26:135–148, 1989.

[13] Bernardo Cockburn and Chi-Wang Shu. The local discontinuous Galerkin method for time-dependent convection-diffusion systems. *SIAM J. Numer. Anal.*, 35(6):2440–2463, 1998.

[14] L. C. Cowsar, J. Mandel, and M. F. Wheeler. Balancing domain decomposition for mixed finite elements. *Mathematics of Computation*, 64:989–1015, 1995.

[15] D. Boffi D. N. Arnold and R. S. Falk. Quadrilateral h(div) finite elements. *SIAM J. Numer. Anal.*, 42:2429–2451, 2005.

[16] Carlo D'Angelo and Paolo Zunino. Robust numerical approximation of coupled Stokes' and Darcy's flows applied to vascular hemodynamics and biochemical transport. *ESAIM Math. Model. Numer. Anal.*, 45(3):447–476, 2011.

[17] Marco Discacciati, Edie Miglio, and Alfio Quarteroni. Mathematical and numerical models for coupling surface and groundwater flows. *Appl. Numer. Math.*, 43(1-2):57–74, 2002. 19th Dundee Biennial Conference on Numerical Analysis (2001).

[18] V. J. Ervin, E. W. Jenkins, and S. Sun. Coupled generalized nonlinear Stokes flow with flow through a porous medium. *SIAM J. Numer. Anal.*, 47(2):929–952, 2009.

[19] J.Douglas F.Brezzi and L.D.Marini. Two families of mixed finite elements finite elements for second order elliptic problems. *Numer.Math.*, (47):217–235, 1985.

[20] R.Duran F.Brezzi, J.Douglas and M.Fortin. Mixed finite elements for second order elliptic problems in three variables. *Numer.Math.*, (51):237–250, 1987.

[21] Juan Galvis and Marcus Sarkis. Non-matching mortar discretization analysis for the coupling Stokes-Darcy equations. *Electron. Trans. Numer. Anal.*, 26:350–384, 2007.

[22] B. Ganis and I. Yotov. Implementation of a mortar mixed finite element method using a multiscale flux basis. *Comput. Methods Appl. Mech. Eng.*, 198(49-52):3989–3998, 2009.

[23] Gabriel N. Gatica, Salim Meddahi, and Ricardo Oyarzúa. A conforming mixed finite-element method for the coupling of fluid flow with porous media flow. *IMA J. Numer. Anal.*, 29(1):86–108, 2009.

[24] Gabriel N. Gatica, Ricardo Oyarzúa, and Francisco-Javier Sayas. Analysis of fully-mixed finite element methods for the Stokes-Darcy coupled problem. *Math. Comp.*, 80(276):1911–1948, 2011.

[25] V. Girault and P.-A. Raviart. *Finite Element Methods for Navier-Stokes Equations.* Number 5 in Springer series in Computational Mathematics. Springer-Verlag, Berlin, Heidelberg, New York, Tokyo, 1986.

[26] V. Girault and L. R. Scott. A quasi-local interpolation operator preserving the discrete divergence. *Calcolo*, (40):1–19, 2003.

[27] V. Girault, D. Vassilev, and I. Yotov. Mortar multiscale finite element method for Stokes and Darcy flows. Technical Report TR-MATH 12-06, Department of Mathematics, University of Pittsburgh, 2012.

[28] R. Glowinski and M. F. Wheeler. Domain decomposition and mixed finite element methods for elliptic problems. In R. Glowinski, G. H. Golub, G. A. Meurant, and J. Periaux, editors, *First International Symposium on Domain Decomposition Methods for Partial Differential Equations*, pages 144–172. SIAM, Philadelphia, 1988.

[29] R. Ingram, M. F. Wheeler, and I. Yotov. A multipoint flux mixed finite element method on hexahedra. *SIAM J. Numer. Anal.*, 48:1281–1312, 2010.

[30] Ross Ingram, Mary F. Wheeler, and Ivan Yotov. A multipoint flux mixed finite element method on hexahedra. *SIAM J. Numer. Anal.*, 48(4):1281–1312, 2010.

[31] J.C.Nedelec. Mixed finite elements in r^3. *Numer.Math*, 35:315–341, 1980.

[32] J.E.Roberts and J.M.Thomas. *Mixed and hybrid methods,in Handbook of Numerical Analysis,P.G.Ciarlet and J.Lions,eds.*, volume 2. Elsevier Science Publishers B.V., 1991.

[33] J.Wang and T.P.Mathew. *Mixed finite element method over quadrilaterals,in Conference on Advances in Numerical Methods and Applications, I.T.Dimov,B.Sendov, and P.Vassilevski,eds.* World Scientific, River Edge, NJ, 1994.

[34] G. Kanschat and B. Rivière. A strongly conservative finite element method for the coupling of Stokes and Darcy flow. *J. Comput. Phys.*, 229(17):5933–5943, 2010.

[35] Mi-Young Kim and Mary F. Wheeler. A multiscale discontinuous Galerkin method for convection-diffusion-reaction problems. *Comput. Math. Appl.*, 68(12, part B):2251–2261, 2014.

[36] W. J. Layton, F. Schieweck, and I. Yotov. Coupling fluid flow with porous media flow. *SIAM J. Numer. Anal.*, 40(6):2195–2218, 2003.

[37] Konstantin Lipnikov, Mikhail Shashkov, and Ivan Yotov. Local flux mimetic finite difference methods. *Numer. Math.*, 112(1):115–152, 2009.

[38] T. P. Mathew. *Domain decomposition and iterative refinement methods for mixed finite element discretizations of elliptic problems*. PhD thesis, Courant Institute of Mathematical Sciences, New York University, 1989. Tech. Rep. 463.

[39] Mo Mu and Jinchao Xu. A two-grid method of a mixed Stokes-Darcy model for coupling fluid flow with porous media flow. *SIAM J. Numer. Anal.*, 45(5):1801–1813, 2007.

[40] J. Nečas. *Les Méthodes directes en théorie des équations elliptiques*. Masson, Paris, 1967.

[41] P.A.Raviart and J.Thomas. *A mixed finite element method for 2-nd order elliptic problems,in Mathematical aspects of the Finite Element Method, I. galligani and E.Magenes,eds.*

[42] G. Pencheva and I. Yotov. Balancing domain decomposition for mortar mixed finite element methods. *Numer. Linear Algebra Appl*, 10:159–180, 2003.

[43] A. Quarteroni and A. Valli. *Domain Decomposition Methods for Partial Differential equations*. Clarendon Press, Oxford, 1999.

[44] B. Rivière and I. Yotov. Locally conservative coupling of Stokes and Darcy flows. *SIAM J. Numer. Anal.*, 42(5):1959–1977, 2005.

[45] P. G. Saffman. On the boundary condition at the surface of a porous media. *Stud. Appl. Math., L*, (2):93–101, 1971.

[46] P. Song and I. Yotov. Multiscale mortar finite elements for coupled Stokes and Darcy flows on irregular geometry domains. Preprint.

[47] P. Song and I. Yotov. Coupling surface and subsurface flows with curved interfaces. In *proceedings of the 8th International Conference on Scientific Computing and Applications*. Contemporary Mathematics, 2012.

[48] A. Toselli and O. Widlund. *Domain Decomposition Methods - Algorithms and Theory*. Springer-Verlag Berlin Heidelberg, 2005.

[49] D. Vassilev and I. Yotov. Coupling Stokes-Darcy flow with transport. *SIAM J. Sci. Comput.*, 31(5):3661–3684, 2009.

[50] Danail Vassilev, ChangQing Wang, and Ivan Yotov. Domain decomposition for coupled Stokes and Darcy flows. *Comput. Methods Appl. Mech. Engrg.*, 268:264–283, 2014.

[51] P. Song C.Q. Wang and I. Yotov. Domain decomposition for Stokes-Darcy flows with curved interfaces. volume 18, pages 1077–1086. Procedia Computer Science, 2013.

[52] M. F. Wheeler, G. Xue, and I. Yotov. Accurate Cell-Centered Discretizations for Modeling Multiphase Flow in Porous Media on General Hexahedral and Simplicial Grids. *SPE Journal*, 17(3):779–793, 2012.

[53] M. F. Wheeler, G. Xue, and I. Yotov. A multipoint flux mixed finite element method on distorted quadrilaterals and hexahedra. *Numer.Math.*, 121:165–204, 2012.

[54] M. F. Wheeler, G. Xue, and I. Yotov. A multiscale mortar multipoint flux mixed finite element method. *ESAIM: Mathematical Modelling and Numerical Analysis (M2AN)*, 46(4):759–796, 2012.

[55] M. F. Wheeler and I. Yotov. A multipoint flux mixed finite element method. *SIAM J. Numer. Anal.*, 44(5):2082–2106, 2006.

[56] Mary Wheeler, Guangri Xue, and Ivan Yotov. A multipoint flux mixed finite element method on distorted quadrilaterals and hexahedra. *Numer. Math.*, 121(1):165–204, 2012.

[57] Mary F. Wheeler and Ivan Yotov. A multipoint flux mixed finite element method. *SIAM J. Numer. Anal.*, 44(5):2082–2106, 2006.

[58] I. Yotov. *Mixed finite element methods for flow in porous media.* PhD thesis, Rice University, Houston, Texas, 1996. TR96-09, Dept. Comp. Appl. Math., Rice University and TICAM report 96-23, University of Texas at Austin.